

Bypass transition experiments in subsonic boundary layers

Citation for published version (APA):

Schook, R. (2000). *Bypass transition experiments in subsonic boundary layers*. [Phd Thesis 1 (Research TU/e / Graduation TU/e), Mechanical Engineering]. Technische Universiteit Eindhoven.
<https://doi.org/10.6100/IR535851>

DOI:

[10.6100/IR535851](https://doi.org/10.6100/IR535851)

Document status and date:

Published: 01/01/2000

Document Version:

Publisher's PDF, also known as Version of Record (includes final page, issue and volume numbers)

Please check the document version of this publication:

- A submitted manuscript is the version of the article upon submission and before peer-review. There can be important differences between the submitted version and the official published version of record. People interested in the research are advised to contact the author for the final version of the publication, or visit the DOI to the publisher's website.
- The final author version and the galley proof are versions of the publication after peer review.
- The final published version features the final layout of the paper including the volume, issue and page numbers.

[Link to publication](#)

General rights

Copyright and moral rights for the publications made accessible in the public portal are retained by the authors and/or other copyright owners and it is a condition of accessing publications that users recognise and abide by the legal requirements associated with these rights.

- Users may download and print one copy of any publication from the public portal for the purpose of private study or research.
- You may not further distribute the material or use it for any profit-making activity or commercial gain
- You may freely distribute the URL identifying the publication in the public portal.

If the publication is distributed under the terms of Article 25fa of the Dutch Copyright Act, indicated by the "Taverne" license above, please follow below link for the End User Agreement:

www.tue.nl/taverne

Take down policy

If you believe that this document breaches copyright please contact us at:

openaccess@tue.nl

providing details and we will investigate your claim.

Bypass Transition Experiments in Subsonic Boundary Layers

PROEFSCHRIFT

ter verkrijging van de graad van doctor aan de
Technische Universiteit Eindhoven, op gezag van de
Rector Magnificus, prof.dr. M. Rem, voor een
commissie aangewezen door het College voor
Promoties in het openbaar te verdedigen op
donderdag 26 oktober 2000 om 16.00 uur

door

Robert Schook
geboren te Rotterdam.

Dit proefschrift is goedgekeurd door de promotoren:

prof.dr.ir. A.A. van Steenhoven
en
prof.dr.ir. M.E.H. van Dongen

Copromotor:

dr.ir. H.C. de Lange

CIP-DATA LIBRARY TECHNISCHE UNIVERSITEIT EINDHOVEN

Schook, Robert

Bypass transition experiments in subsonic boundary layers / by
Robert Schook. - Eindhoven: Technische Universiteit Eindhoven,
2000. - Proefschrift. - ISBN 90-386-3001-8

Eindhoven University Press Facilities, the Netherlands.

Copyright ©2000 by R. Schook

All rights reserved.

No part of the material protected by this copyright notice may be reproduced or utilized in any form or by any means, electronic or mechanical, including photocopying, recording or by any information storage and retrieval system, without permission from the publisher.

Contents

1	Introduction	1
1.1	Background	1
1.2	Thesis overview	5
2	Transition models	7
2.1	Turbulent spot approach	7
2.2	Empirical relations	15
2.2.1	Turbulence effects	15
2.2.2	Pressure gradient effects	17
2.2.3	Compressibility effects	19
2.2.4	Minimum transition length theory	19
2.3	Unsteady transition	22
2.3.1	The space-time diagram	23
2.3.2	Turbulent band model	24
2.3.3	Narrow wake (moving source) model	24
2.3.4	Wide wake (fixed source) model	26
2.3.5	Model modifications	28
2.4	Conclusions	31
3	Experimental techniques	33
3.1	Introduction	33
3.2	Ludwig tube	34
3.3	Steady-state test section	37
3.3.1	Pressure measurements	38
3.3.2	Error estimation	38
3.4	Turbulence generating grids	39
3.5	Heat flux measurements	42
3.6	Unsteady-state test section	48
3.6.1	Rotating cylinder cascade wake generator	49
3.6.2	Rotating wheel wake generator	50
3.6.3	Moving-belt wake generator	51
3.7	Conclusions	55
4	Steady transition measurements	57
4.1	Heat flux measurements	57
4.2	Intermittency calculation	59
4.3	Stanton number and intermittency distributions	61

4.3.1	Low turbulence levels	62
4.3.2	Turbulent spots	65
4.3.3	High turbulence levels	67
4.3.4	Intermediate turbulence levels	68
4.4	Transition start and length	70
4.5	Cross correlations	72
4.6	Length scale analysis	73
4.7	Overview of intermittency distributions	76
4.8	Mach number influence	78
4.9	Conclusions	78
5	Unsteady transition measurements	81
5.1	Wake induced heat transfer measurements	81
5.1.1	Unsteady transition initiated by strong wakes	82
5.1.2	Unsteady transition initiated by weak wakes	83
5.2	Combined heat transfer measurement	87
5.3	Hot-wire measurements	87
5.4	Comparison of observations with literature	91
5.5	Heat flux levels	94
5.5.1	Mean heat flux	94
5.5.2	Heat flux extrema	96
5.6	Intermittency distributions	98
5.6.1	Wake induced transition (no grid included)	98
5.6.2	Combined transition	101
5.7	Conclusions	102
6	Conclusions	103
	Bibliography	107
A	Derivation of intermittency	113
B	Ludwig tube set-up	119
C	Length scales	123
	Nomenclature	125
	Summary	128
	Samenvatting	129
	Nawoord	130
	Curriculum vitae	131

Chapter 1

Introduction

1.1 Background

In 1928 Frank Whittle published his theory concerning gas turbines, resulting in the first successful airplane flight with this type of propulsion in 1939. After this, the development of turbines went very fast. Nowadays, the gas turbine is used for a lot of applications in both industry and aviation. Generation of electricity is mainly performed by large stationary turbines with a shaft power generation up to hundreds of megawatts. In military and civil aviation the gas turbine is the main power source. For military purposes often so turbojet or small bypass engines are used, while for civil planes the large bypass multi-spool turbines are applied. The latter engine type is constructed of two or three separated shafts, making it possible for the low pressure and the high pressure section to run at different speeds.

The gas turbine consists of three main parts, the compressor, the combustion chamber and the turbine itself (*Cohen et al.* [1996]). Air is compressed in several stages by the compressor which in most cases is of the axial flow type. The working fluid, which often is ambient air, is accelerated by the rotor blades implying an increase of kinetic energy. A conversion of kinetic energy to static pressure is achieved by the stator blades. This process is repeated in each individual stage. Pressure ratios up to 30:1 can be achieved by modern compressors with a large number of stages.

In the combustion chamber, fuel is injected in the compressed air. This mixture is burnt which results in an enthalpy increase of the fluid. Finally, the hot air is expanded in the turbine.

In a multi-spool engine, several turbine stages are situated. The first stages of the turbine, denoted by the high pressure section, give just enough energy that the compressor can be driven. The remaining energy is extracted from the gas by a low pressure turbine. This turbine propels a shaft connected to a generator, in the case of power generation, or the fan in the case of a turbine for civil

airplanes. In a turbojet engine, the remaining energy is not expanded in a low pressure section but in a nozzle, which directly propels the plane.

For obtaining an acceptable efficiency the temperature of the gas entering the turbine should be as high as possible. Modern gas turbines have a turbine inlet temperature of more than 1600°C . This high temperature combined with the enormous force due to their rotation, needs special demands concerning the rotor blades. To regulate the rotor temperature, which is limited due to the high thermal and mechanical loading, an accurate knowledge of the heat flux from the hot gas to the blades is required.

Due to the combustion process, a lot of disturbances are introduced in the mainstream. Therefore, different flow phenomena occur when this gas flows along the blades. These are the appearances of horse shoe vortices, tip flow and secondary flow, boundary layer separation and boundary layer transition (*Simoneau and Simon [1993]*). The latter, laminar to turbulent transition, has a large effect on the heat flux from the gas to the blades. In a turbulent boundary layer the flux can reach values which are three times larger compared to a laminar boundary layer. Therefore, it is essential to know the influence of several parameters on transition. Examples are effects of turbulence level, turbulence length scales, pressure gradient, Reynolds number, compressibility, surface roughness and surface curvature (*Narasimha [1985], Mayle [1991]*).

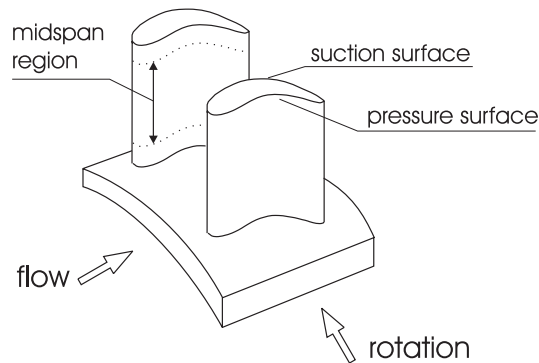


Figure 1.1: Schematic picture of two turbine rotor blades.

It is not the heat transfer which plays an important role in pumps and fans. For these turbomachines the blade friction and/or boundary layer separation determine the flow and thus the efficiency. As friction and heat transfer are coupled, heat transfer experiments can be transformed directly to data which describe the friction processes in these machines. So, knowledge of the effects of boundary layer transition on heat transfer also can improve the efficiency in pumps and

other low velocity turbomachines. Examples of the flow in pumps can be found in *van Esch* [1997].

In describing the transition process, a distinction must be made between the transition start and the transition length. In general, the transition start is assumed to be the streamwise position where the boundary layer starts to behave differently compared to a laminar layer. The transition length is the streamwise distance where the boundary layer develops from completely laminar to fully turbulent.

Figure 1.1 schematically shows two rotor blades together with the designation of important terms. These are the suction (convex) and the pressure (concave) surfaces of the blades. In the midspan region, which is about 50 to 75% of the blade span, the flow can be assumed to behave as two dimensional. Depending on the flow, the transition region can cover up to half the blade chord. Therefore, it is meaningful to study the effects of different parameters on laminar to turbulent transition in a two-dimensional flow.

In the case of a flow with constant mean properties in time, i.e. a steady flow, two kinds of boundary layer transition can be distinguished. The first one is 'natural' transition which occurs due to a boundary layer which becomes unstable. The background turbulence in the main flow is small when this type of transition occurs. Wind-tunnel experiments performed by *Schubauer and Skramstad* [1947] for the flow along a flat plate, showed that the boundary layer is laminar when the Reynolds number based on the leading edge distance (Re_x) is less than $2.8 \cdot 10^6$, while it is completely turbulent when Re_x is larger than $3.9 \cdot 10^6$. As a consequence, the flow is 'transitional' in between these values.

A linear stability theory was developed by Tollmien and Schlichting around 1930. This theory describes at which streamwise distance small disturbances in the boundary layer become unstable and thus amplify. As a result so called Tollmien-Schlichting waves start to occur. Agreement with measurements is found when the disturbances in the flow are 'small', i.e. when the turbulence level in the free stream is less than 0.1%.

Unstable waves grow and therefore the linear theory is also not valid far downstream of the place where the first waves start to develop. During the growth of the waves, spanwise distortions and three dimensional non linear interactions are becoming relevant. Finally, areas of turbulence, denoted as turbulent spots, start to develop in streamwise direction. These spots grow in streamwise and spanwise directions until the flow is completely turbulent and thus transition is completed. In figure 1.2 the transition process for natural transition along a flat plate is shown schematically (*Schlichting* [1979]).

The second type of boundary layer transition is called bypass transition. When the turbulence level is higher than 0.4%, it is assumed that this transition type is important (*Mayle* [1999]). The idea behind bypass transition is that the disturbances in the flow cause laminar fluctuations in the boundary layer which initiate spots, or that disturbances are strong enough to enter the boun-

dary layer and initiate turbulent spots immediately. In both cases the occurrence of Tollmien-Schlichting waves, spanwise vorticity and three dimensional breakdown is 'bypassed', which explains the name. Linear stability theory is irrelevant as the turbulent spots are generated more towards the leading edge of a plate (or turbine blade) compared to natural transition.

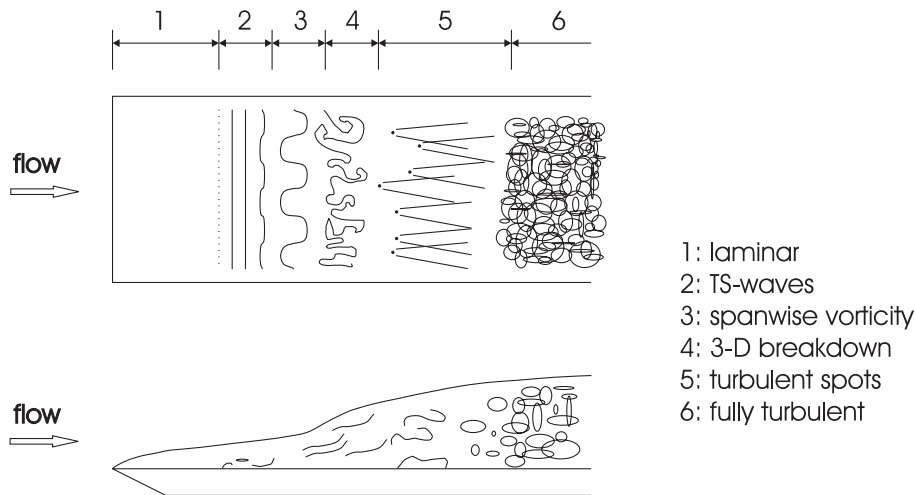


Figure 1.2: The process of natural transition.

In a gas turbine a number of stages are situated behind each other. This holds for both the compressor and the turbine sections. Each stage consists of stator blades having a fixed position, and rotor blades mounted on the rotating shaft. Behind each stator blade a wake is shed which convects downstream with the main flow. The wake influences the boundary layer and as a result the transition process. This flow phenomenon is unsteady as during a certain part of the time the flow along the blades is the flow with the background turbulence, and the remaining part of the time the flow with the wakes. Therefore, transition of this type is denoted as unsteady transition. Another name which can be found in literature is wake induced transition.

The flow between two wakes is denoted here by 'background turbulence'. It should be noted that the corresponding turbulence level is high, especially in the turbine, and thus the transition is of the bypass type. In this thesis the distinction between bypass transition and wake induced transition sometimes will be emphasised by using 'steady' and 'unsteady' transition.

From the discussion thus far it is obvious that bypass transition and wake induced transition have a significant effect on the boundary layer, and thus on the heat transfer, in gas turbines. Both kinds of transition are initiated by large

disturbances in the main flow. For bypass transition this is the high background turbulence level, while for unsteady transition this is the turbulence in the wake which has even larger levels compared to the background turbulence.

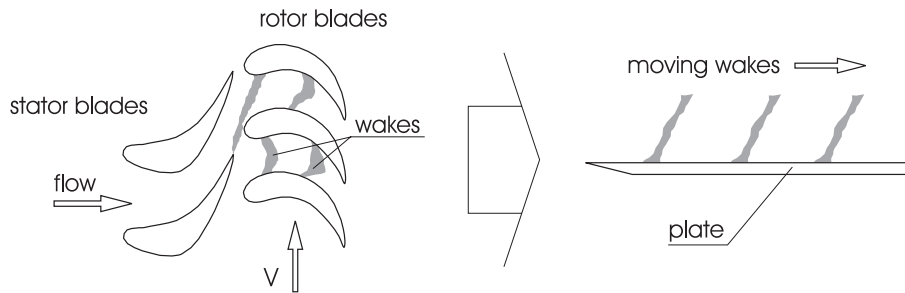


Figure 1.3: Unsteady flow in a gas turbine stage (left), which can be simplified by assuming the flow along a flat plate (right).

1.2 Thesis overview

High levels of turbulence are mainly introduced by the combustion process. As the turbine stage is situated downstream of the combustion chamber, bypass transition is dominant in the turbine section. In contrast to natural transition, the curvature has a minor effect on bypass transition (*Mayle [1991]*). Therefore, an important simplification of the flow problem is justified. Namely, the rotor-stator passage can be modelled as an unsteady flow along a flat plate (figure 1.3).

Now the aim of this thesis can be formulated. The objective is to study the effects of several parameters on both steady and unsteady transition for the flow along a flat plate under gas turbine representative conditions.

Chapter 2 starts with the different 'steady' transition models which can be found in literature. Most of these models are based on a turbulent spot approach. Empirical relations which describe the effect of turbulence, pressure gradients and compressibility on the transition start and the transition length are listed.

After the steady transition models, the unsteady models are treated. From measurements described in literature, it follows that spot based models also perform well for unsteady flows.

In chapter 3 the experimental techniques are explained. For generating a high velocity flow with well known properties, a Ludwig tube set-up is used. The main advantage of using this transient facility, is that the Reynolds number

and the Mach number adjustments can be done independently. A special orifice determines the Mach number while the initial pressure determines the Reynolds number. Background turbulence is generated by means of a static grid. In the test section, hot-wire and pressure measurements are performed to verify the flow conditions. This test section also contains the sensor plate with thin film resistors used for the heat transfer measurements.

To perform unsteady transition experiments, the original test section had to be modified. Attention will be given to several possibilities for generating wakes. The motivation for using a moving belt wake generator and the measurements for determining the flow conditions, are also part of chapter 3. In spite of the differences compared to the original set-up, the new test section appeared to be well suited for performing wake induced transition experiments.

The following part, chapter 4, treats the steady transition measurements. Most important are the heat transfer experiments from which the intermittency distributions are derived. These distributions make it possible to compare different transition cases. It will follow that the original idea behind bypass transition, i.e. the initiation of turbulent spots which grow in streamwise and spanwise directions, is not correct for all the experiments. For high and intermediate turbulence levels, significant deviations compared to low speed experiments, found in literature, are observed. By assuming a modified spot based transition process, the present measurements are described more accurately.

Chapter 5 focuses on the unsteady transition experiments. Wakes which initiate transition at the leading edge, and wakes which cause transition more downstream are generated by the wake generator. The passing wakes cause a significant increase of the heat flux due to the transition. It is found that the peak heat flux in the wakes is dependent on the wake structure. Therefore, the use of a unified 'turbulent' heat flux level is not unambiguous. From this it will follow that transforming data in intermittency distributions is a delicate task.

Finally, in chapter 6 the conclusions and recommendations for further research are given.

Chapter 2

Transition models

2.1 Turbulent spot approach

In the transition zone, which is the area in which the state of the boundary layer changes from laminar to turbulent, a lot of flow characteristics change. A certain point in the transition zone experiences an intermittent flow behaviour. Some part of the time the flow is laminar and some part of the time the flow is turbulent. The fraction of the time in which the flow is turbulent is called the intermittency denoted by γ . The intermittency is zero when the flow is completely laminar and one when it is turbulent. This intermittent behaviour can be explained by the occurrence of 'turbulent spots'. These spots were discovered by *Emmons* [1951] in a water table experiment performed at Harvard University as a student demonstration. Along the table, constructed of glass, water flowed in a thin layer. At random positions in space and time, turbulent 'islands' could be clearly observed. These islands, called the spots, were initiated with irregular shape and grew in streamwise direction during which the initial shape was preserved. The amount and size of the spots could be affected by changing the velocity of the flow or by placing disturbances in the water.

Spot initiation in the 'bypass' mode is assumed to be the mechanism which is important for turbomachinery. In this transition mode, large disturbances in the mainstream enter the boundary layer and generate a small spot. This spot initiation is supposed to be a random phenomenon. As the spot is born, it grows in streamwise direction while the leading edge velocity of the spot is larger than the trailing edge velocity. Also, enlargement in the lateral direction takes place. Due to the growth, the spots start to overlap each other and thus merge until a complete turbulent boundary layer is obtained.

An expression for the fraction of the time during which a certain point P in the transition zone is turbulent can be derived. Assume a turbulent spot which will be initiated at point P_0 with infinitesimal small size. The spot convects in streamwise direction and grows. If the leading edge and the trailing edge velocities

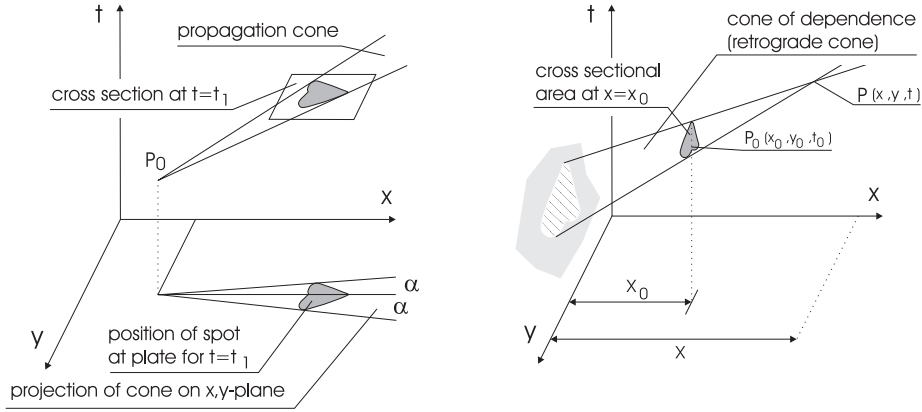


Figure 2.1: Spot propagation in (x, y, t) -space. Figure 2.2: Dependence volume of P (cone of dependence).

are taken constant the spot will cover the marked area in the x, y, t -space (figure 2.1). This area is called the propagation cone and covers all the points which will be turbulent if a spot was generated at P_0 .

Now, we would like to find all the points P_0 which cause P to be turbulent. Therefore, the propagation cone is mirrored, resulting in the so called cone of dependence (figure 2.2). If a spot originates somewhere in this cone, the point P will become turbulent. *Emmons* [1951] derived that the fraction of the time during which a certain point P is turbulent can be expressed by (see also appendix A):

$$\gamma(P) = 1 - \exp\left[-\int_R g(P_0)dV_0\right]. \quad (2.1)$$

In this equation g is the spot production rate and R the cone of dependence. So, the sum of the spot production over all the points P_0 which initiate spots that will move over P are considered by the integral. For the flow along a flat plate with uniform spot production in streamwise direction (g is constant: $g = a$) and a free stream velocity U , *Emmons* [1951] showed that the intermittency can be written as:

$$\gamma(x) = 1 - \exp\left[-\frac{\sigma a(x - x_t)^3}{3U}\right]. \quad (2.2)$$

Transition starts at x_t , the position where the first spots start to appear. In appendix A the derivation of this equation is shown. The spot propagation parameter σ is a measure for the growth of the turbulent spot. The value of the spot propagation parameter approximately has a value of 0.27 (*Schubauer and Klebanoff* [1955]). Often the spot half spreading angle α and the leading and trailing edge velocities (U_{le} and U_{te}) are taken constant. For simplification, the

turbulent spot is supposed to have a triangular shape, which is depicted in figure 2.3.

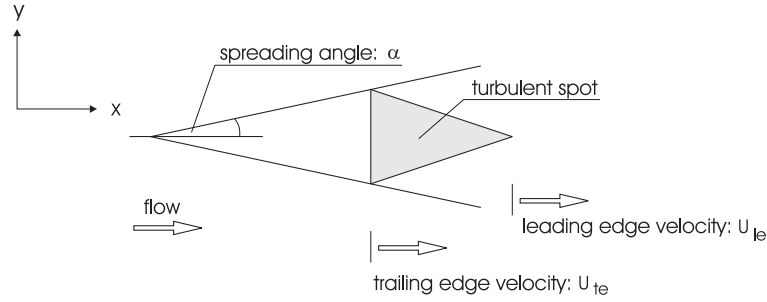


Figure 2.3: Simplified turbulent spot.

In that case, the parameter σ can be denoted in terms of the spot leading and trailing edge velocities (see appendix A):

$$\sigma = \tan(\alpha) \left[\frac{U}{U_{te}} - \frac{U}{U_{le}} \right]. \quad (2.3)$$

To derive equation (2.2) it is assumed that g is constant along the whole plate. This means that the number of turbulent spots which is initiated in streamwise direction is not dependent on the boundary layer conditions. Supposing that at a certain Reynolds number the boundary layer becomes unstable for disturbances, *Narasimha* [1957] argued that it is physically more correct to assume that the spots initiate at one streamwise position x_t , the point where transition starts. An appropriate description of this point like breakdown can be given by incorporating a Dirac delta function ¹ in the spot production parameter:

$$g(x) = n\delta(x - x_t). \quad (2.4)$$

In this equation n is the total amount of spots which is initiated per time per meter span. It therefore has the dimension $\text{m}^{-1}\text{s}^{-1}$. The resulting intermittency distribution, often denoted as the Narasimha distribution, has a quadratic dependence on the streamwise distance:

$$\gamma(x) = 1 - \exp\left[-\frac{\sigma n(x - x_t)^2}{U}\right]. \quad (2.5)$$

It is argued by *Gostelow* [1989] that a Gaussian form of the spot production rate around x_t , is more appropriate. However, this extension is often considered as

¹ $\int_{-\infty}^{\infty} \delta(x) dx = 1$ for $x = 0$, while $\delta(x) = 0$ for $x \neq 0$.

not necessary if the streamwise area in which the spots are initiated is small compared to the transition length.

Johnson and Fashifar [1994] derived the Narasimha distribution in a different way. Assuming a two dimensional boundary layer, the intermittency at a certain streamwise position is the fraction of a spanwise line that is turbulent, at that fixed position. If this definition is used the streamwise variation of the intermittency can be characterized by:

$$\frac{d\gamma}{dx} = N\sigma. \quad (2.6)$$

N is the number of spots per unit length in spanwise direction which are present at a certain streamwise position (i.e. at the line) and σ is the spot propagation parameter. The change in the number of spots can be represented by:

$$\frac{dN}{dx} = \frac{(1-\gamma)n}{U_s} - \frac{N^2\sigma}{(1-\gamma)}. \quad (2.7)$$

The first term of the right-hand side represents the number of spots which reach the present position by convection. The mean spot velocity is U_s . All spots were assumed to originate at x_t with a rate of n per unit time per unit span. A certain number of the spots ($\frac{\gamma n}{U_s}$) disappears due to merging prior to reaching the present position. Also, the turbulent regions on the line are supposed to grow and merge with neighbouring regions with a rate given by the second term of equation (2.7). The reason why *Johnson and Fashifar* [1994] wrote the second term in its present form is unclear.

Equations (2.6) and (2.7) can be combined to an ordinary differential equation describing the intermittency in streamwise direction:

$$(1-\gamma)\frac{d^2\gamma}{dx^2} + \left(\frac{d\gamma}{dx}\right)^2 - \frac{\sigma n}{U_s}(1-\gamma)^2 = 0. \quad (2.8)$$

The solution for the intermittency is:

$$\gamma(x) = 1 - \exp\left[-\frac{\sigma n(x-x_t)^2}{2U_s}\right]. \quad (2.9)$$

This distribution is the same as equation (2.5), the only difference is that the freestream velocity U is replaced by 2 times the spot velocity: $2U_s$.

Another spot production mechanism is derived by *Johnson* [1994]. In this model the assumption that near wall velocity fluctuations are responsible for the initiation of turbulent spots is used. These velocity fluctuations are a result of the pressure fluctuations in the flow. *Johnson* [1994] considered the total pressure in a fluid, which can be represented as a mean part and a fluctuating part:

$$P = \overline{P} + P' = \overline{p} + p' + \frac{1}{2}\rho(\overline{u} + u')^2. \quad (2.10)$$

In this equation an overbar represents the time mean component and a prime the fluctuating component. By subtracting the time mean and non dimensionalizing with the product of freestream velocities $U'_{rms}\bar{U}$ and the density, an expression is obtained for the difference between the total and the static pressure fluctuations:

$$E' = \frac{p' - P'}{\rho U'_{rms}\bar{U}} = -\frac{u'\bar{u}}{U'_{rms}\bar{U}} + \frac{1}{2} \frac{\overline{u'^2} - u'^2}{U'_{rms}\bar{U}}, \quad (2.11)$$

with U'_{rms} the root mean square deviation of the freestream velocity U ($U'_{rms} = \sqrt{U'^2}$). From measurements performed by *Johnson* [1994], it follows that in the near wall region the root mean square of E' is proportional to the distance perpendicular to the wall by:

$$E'_{rms} = \beta Re_\delta^2 Z^2. \quad (2.12)$$

The factor β is a proportionality factor and Z is the dimensionless distance normal to the plate ($Z = \frac{z}{\delta}$), with δ the boundary layer thickness.

Equations (2.10) and (2.12) in combination with the definition of the free stream turbulence level in an isotropic flow ($Tu = \frac{U'_{rms}}{U}$) results in:

$$\bar{u}'_{rms} = \beta U^2 Re_\delta^2 Z^2 Tu. \quad (2.13)$$

For a Blasius boundary layer along a flat plate Re_δ^2 is proportional to Re_x , so it follows that \bar{u}'_{rms} is proportional to the streamwise distance:

$$\bar{u}'_{rms} \sim U^2 Re_x. \quad (2.14)$$

Now it is assumed that when the local velocity has a minimum smaller than some fraction \mathcal{C} of the mean local velocity, a turbulent spot is initiated. This is the case when $u'_m < \mathcal{C}\bar{u}$. From analysing a turbulent signal, *Johnson* [1994] found that the fraction P of velocity minima² that satisfies the criterium of a certain \mathcal{C} (e.g. *Johnson* used $\mathcal{C} = 0.5$) depends on u'_{rms} and u'_m , in which the latter is the local minimum velocity, by:

$$P \sim \frac{u'_{rms}}{u'_m}. \quad (2.15)$$

Applying the above mentioned criterion and using equation (2.15) it follows that:

$$P \sim \frac{u'_{rms}}{\bar{u}}. \quad (2.16)$$

This result, together with equation (2.14) leads to the conclusion that:

$$P \sim Re_x. \quad (2.17)$$

²The total number of velocity minima is counted. The minima which have a value less than a certain level are taken into account.

From this, *Johnson and Fashifar* [1994] derived that the generation of turbulent spots increases linearly with the streamwise direction. Therefore, they assumed that $\frac{\sigma n}{U_s}$ is not constant but a linear function of x :

$$\frac{\sigma n}{U_s} = \zeta(x - x_t). \quad (2.18)$$

When ζ is taken constant, this relation together with equation 2.9 gives for the intermittency distribution:

$$\gamma(x) = 1 - \exp[-\mathcal{J}(x - x_t)^3], \quad (2.19)$$

with \mathcal{J} a constant. This distribution is called the Johnson intermittency distribution throughout this thesis.

Remark on the spot production parameter

The derivation of the Johnson intermittency distribution as given above, is not consistent with the original derivation of *Emmons* [1951]. First recall the Narasimha distribution which assumes a spot production at a fixed streamwise position with an amount of n spots per second per meter span (thus n has dimension $\text{m}^{-1}\text{s}^{-1}$). In this case, the spot production parameter is denoted by: $g(x) = n\delta(x - x_t)$. This spot production results in an intermittency distribution in which the exponent is proportional to x^2 .

In the original theory it is supposed that the spots are not initiated at one streamwise position, but that the spot production is constant along the plate. The resulting exponent of the intermittency distribution is proportional to x^3 .

So, the Johnson distribution (equation (2.19)) equals the intermittency distribution as already proposed by *Emmons* [1951] (equation (2.2)). However, the according spot production parameters are different.

Johnson and Fashifar [1994] concluded from equation (2.17) that the generation of turbulent spots increases linearly with the streamwise direction. This implies that the spot production parameter can be expressed as: $g(x) \sim x$. Now, if equation (2.1) is used, it follows that the exponent of the intermittency distributions is proportional to x^4 instead of x^3 . Despite this contradiction, the Johnson model is assumed to originate from a constant spot production rate along the plate which results in the x^3 distribution.

The Narasimha and Johnson transition model can be transformed in a universal intermittency distribution. For this purpose the non-dimensional streamwise coordinate is introduced:

$$\xi = \frac{Re_x - Re_{xt}}{Re_\lambda} = \frac{x - x_t}{\lambda}, \quad (2.20)$$

with λ the streamwise distance between the points where the intermittency equals 0.25 and 0.75. In terms of ξ the Narasimha distribution becomes:

$$\gamma(\xi) = 1 - \exp(-0.411\xi^2), \quad (2.21)$$

and the Johnson distribution:

$$\gamma(\xi) = 1 - \exp(-0.0941\xi^3). \quad (2.22)$$

Both distributions are shown in figure 2.4.

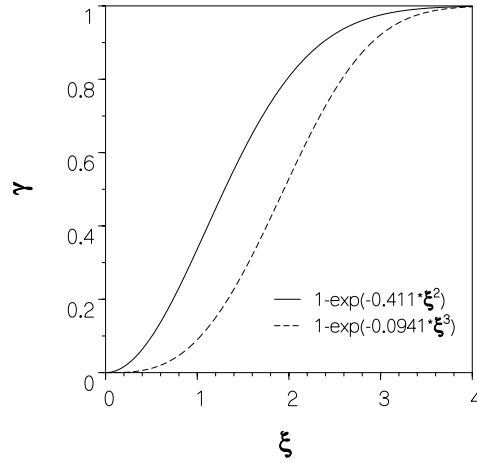


Figure 2.4: Intermittency distributions for the Narasimha model (straight line) and the Johnson model (dashed line).

Recently *Johnson and Ercan* [1999] modified the Johnson model. In a similar way as equation (2.7) is derived, they proposed a new equation for the amount of spots in streamwise direction:

$$\frac{dN}{dx} = \frac{(1 - \gamma)\sigma}{U \tan \alpha} \Lambda - \frac{2N^2 \tan \alpha}{(1 - \gamma)}, \quad (2.23)$$

and for the intermittency:

$$\frac{d\gamma}{dx} = 2N \tan \alpha. \quad (2.24)$$

In equation (2.23), Λ is the number of spots per unit span which was generated upstream. If it is assumed that the freestream turbulence is convected with the main velocity U , the spot generation rate per unit time per unit area is $PU(v/l)^3$,

with P the proportion of minima which will generate a spot and v the number of minima per integral wavelength l . The resulting expression for Λ is:

$$\Lambda = \int_0^x P U \left(\frac{z}{l} \right)^3 dx. \quad (2.25)$$

According to *Johnson and Ercan* [1999] this method of describing the intermittency is consistent with the Narasimha distribution. If a concentrated breakdown is supposed:

$$\Lambda = 0 \text{ for } x < x_t$$

and

$$\Lambda = n \text{ for } x \geq x_t,$$

while α and σ are taken constant, the Narasimha distribution (equation (2.5)) indeed is obtained.

In order to describe the transition by the above formulated model, information is needed to formulate the function Λ . Therefore information about the proportion P and the factor $\frac{z}{l}$ is required.

A way to determine these parameters is described by *Johnson and Ercan* [1999]. They found that the minima of the local velocities u'_m have a distribution:

$$\mathcal{D}\left(\frac{u'_m}{u'_{rms}}\right) = \left(\frac{u'_m}{u'_{rms}}\right)^2 \exp\left[-\frac{1}{2}\left(\frac{u'_m}{u'_{rms}}\right)^2\right]. \quad (2.26)$$

A plausible threshold for the generation of spots according to the authors is half the local velocity. Thus, a spot is generated when $u'_m < 0.5\bar{u}$. Using this, together with the distribution of minima, gives for the proportion of spot initiating minima:

$$P = \frac{1}{4} \sqrt{\frac{1}{2\pi}} \int_0^{\bar{u}/2u'_{rms}} \left(\frac{\bar{u}}{u'_{rms}}\right)^2 \exp\left[-\frac{1}{8}\left(\frac{\bar{u}}{u'_{rms}}\right)^2\right] d\left(\frac{\bar{u}}{u'_{rms}}\right). \quad (2.27)$$

Also a relation is found for the number of minima per integral wavelength:

$$v = 3.2 - 2.5 \exp\left[-0.043\left(\frac{l}{L}\right)\right], \quad (2.28)$$

with L the free stream integral length scale. So, when L is known the ratio $\frac{v}{l}$ can be determined for use in equation (2.25). Now, all the information is available to calculate the intermittency. *Johnson and Fashifar* [1994] and *Johnson and Ercan* [1999] show that the above mentioned model gives better results than the concentrated breakdown hypothesis as used in the Narasimha model.

2.2 Empirical relations

Relations which couple the transition start to the transition length are available in literature. The length λ is defined as the distance between the points where the intermittency is 0.25 and 0.75. *Dhawan and Narasimha* [1958] found a correlation between the Reynolds number based on this length and the transition start:

$$Re_\lambda = 5Re_{xt}^{0.8}. \quad (2.29)$$

On the basis of more experiments this relation is modified to (*Narasimha* [1985]):

$$Re_\lambda = 9Re_{xt}^{0.75}. \quad (2.30)$$

Empirical relations are often based on a dimensionless form of the Narasimha intermittency distribution (equation (2.5)). This distribution can be transformed in an expression including the local Reynolds number ($Re_x = \frac{Ux}{\nu}$). For this purpose the dimensionless spot formation rate, $\hat{n} = \frac{n\nu^2}{U^3}$, is introduced (*Mayle* [1991]). The resulting intermittency distribution is:

$$\gamma = 1 - \exp[-\hat{n}\sigma(Re_x - Re_{xt})^2]. \quad (2.31)$$

The model described by equation (2.31) has two constants. These are the Reynolds number at the start of transition, Re_{xt} , and the product of the dimensionless spot formation rate and the spot propagation parameter, $\hat{n}\sigma$. The first constant determines the position where turbulent spots start to develop, i.e. the transition start, while the latter determines the transition length. In literature, empirical relations can be found which describe the influence of several parameters, for example pressure gradients, turbulence characteristics and compressibility effects, on these model constants. Where possible a distinction between the effect on the transition start and the transition length is made.

Usually, the relations found in literature are expressed in terms of the momentum thickness θ or the displacement thickness δ^* . For a Blasius boundary layer the streamwise position x is related to these thicknesses by (*Schlichting* [1979]):

$$Re_\theta = 0.664\sqrt{Re_x}, \quad (2.32)$$

and

$$Re_{\delta^*} = 1.72\sqrt{Re_x}. \quad (2.33)$$

These transformations are used in the empirical relations in the next section.

2.2.1 Turbulence effects

Effect on the transition start

The effect of turbulence on transition has been subject of many studies. *Abu-Ghannam and Shaw* [1980] found that the transition start is dependent on the

turbulence level (in %) by: ³

$$Re_{\theta t} = 163 + \exp(6.91 - Tu). \quad (2.34)$$

Relation (2.34) implies that the transition start always occurs at a momentum thickness Reynolds number which is 163 or larger. This lower limit originates from the Tollmien-Schlichting stability limit. However, *Mayle* [1991] reasoned that this limit is irrelevant because bypass transition has another transition mechanism than natural transition. A best fit with the data available resulted in the relation ($0.2\% < Tu < 8\%$):

$$Re_{\theta t} = 400 Tu^{-\frac{5}{8}}. \quad (2.35)$$

Both relations are depicted in figure 2.5.

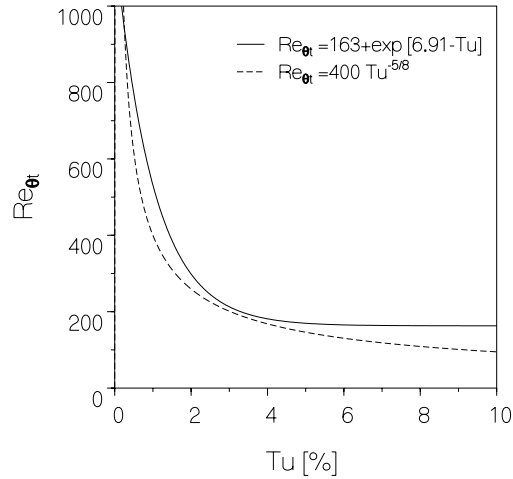


Figure 2.5: Reynolds number based on the momentum thickness at the transition start as a function of the turbulence level.

Effect on the transition length

Also there is an influence of the turbulence on the transition length. When the turbulence level increases, the production of turbulent spots becomes more intense and as a result the transition length decreases. A best fit for the spot production rate, as used in equation (2.31), is (*Mayle* [1991]):

$$\hat{n}\sigma = 1.5 \cdot 10^{-11} Tu^{\frac{7}{4}}. \quad (2.36)$$

³For an incompressible fluid, the turbulence level is defined as: $Tu = \frac{\overline{(u-\bar{u})^2}^{1/2}}{\bar{u}} \cdot 100\%$; this means that Tu characterizes the velocity fluctuations in the flow. However, for our high speed experiments we use the mass fluctuations, in terms of ρu to calculate the turbulence level (see also chapter 3).

Narasimha [1985] used a modified spot production rate \hat{N} . He suggested that this rate, which is defined as $\hat{N} = \hat{n}\sigma Re_{\theta t}^3$, is independent of the turbulence level and always has the value $0.7 \cdot 10^{-3}$. The proposal of introducing \hat{N} suggests that the breakdown rate scales with the boundary layer thickness δ_t and the viscous diffusion time $\frac{\delta_t^2}{\nu}$, which is a physically appealing conclusion according to *Walker* [1993]. However, *Gostelow and Blunden* [1989] found that \hat{N} is proportional to $Tu^{-\frac{1}{8}}$. The use of more data, based on intermittency measurements, resulted in the relation (*Gostelow and Dey* [1991]; *Gostelow et al.* [1994]):

$$\hat{N} = 0.86 \cdot 10^{-3} \exp[-0.546 \ln(Tu)]. \quad (2.37)$$

This equation implies that \hat{N} decreases with increasing turbulence level. *Walker* [1993] compared equation (2.37) with equation (2.36):

$$\hat{n}\sigma = \frac{n\sigma\nu^2}{U^3} = \frac{\hat{N}}{Re_{\theta t}^3} = 1.5 \cdot 10^{-11} Tu^{\frac{7}{4}}. \quad (2.38)$$

He concluded that it is physically unreasonable that the spot production rate n does not involve the local boundary layer thickness. However, when one realizes that there also is a correlation between $Re_{\theta t}$ and Tu (equation (2.35)), *Walker* [1993] suggests that this discrepancy is largely resolved.

A common way to characterize the turbulence is in terms of the turbulence level. However, the turbulence generated by several static grids can give an identical turbulence level while the structure of the turbulence is different. Mostly, the static grids are constructed of rods with a certain diameter placed at a relative distance called the mesh. An effect of the mesh size on the start of transition is found by *Hall and Gibbings* [1972]. They found that for an incompressible flow with zero pressure gradient, the transition start shifts 25% (maximum) towards the trailing edge when the mesh size is enlarged from 1 to 2 inch, while the turbulence level is constant.

2.2.2 Pressure gradient effects

The pressure gradient has a large effect on both the transition start and the transition length. The general trend is that a favourable pressure gradient has a stabilizing effect on the flow, and therefore the transition start is situated more downstream. The trailing edge velocity of the spots is found to be larger compared to the velocity in a zero pressure gradient flow. In combination with the observation that the leading edge velocity remains nearly unchanged, the result is that the transition length becomes larger.

An adverse pressure gradient has a destabilizing effect on the flow. Therefore, the transition start is situated more upstream while the transition length decreases. Very strong adverse pressure gradients might result in boundary layer separation.

It is found in literature (e.g. *Abu-Ghannam and Shaw* [1980]) that for high turbulence levels the effect of the pressure gradient on boundary layer transition diminishes. This also supports the flat plate approach as proposed in the introduction of this thesis.

Characterization of the pressure gradient can be done in terms of the pressure gradient parameter at the onset of transition, defined as:

$$\lambda_{\theta t} = \frac{\theta_t^2}{\nu} \frac{dU}{dx}. \quad (2.39)$$

Effect on the transition start

Abu-Ghannam and Shaw [1980] proposed a correlation with the combined effect of the turbulence level (Tu in %) and the pressure gradient:

$$Re_{\theta t} = 163 + \exp[F(\lambda_{\theta}) - \frac{F(\lambda_{\theta})}{6.91} Tu]. \quad (2.40)$$

The function F is expressed for an adverse pressure gradient ($\lambda_{\theta} \leq 0$) by:

$$F(\lambda_{\theta}) = 6.91 + 12.75\lambda_{\theta} + 63.64\lambda_{\theta}^2, \quad (2.41)$$

while for a favourable pressure gradient ($\lambda_{\theta} \geq 0$):

$$F(\lambda_{\theta}) = 6.91 + 2.48\lambda_{\theta} - 12.27\lambda_{\theta}^2. \quad (2.42)$$

Effect on the transition length

Chen and Thyson [1971] proposed a transition zone model by assuming that the spot velocities are proportional to the free stream velocity, that the spot grows at a constant angle relative to the local external streamline and that concentrated breakdown occurs. On the basis of these assumptions *Cebeci and Smith* [1974] suggested for the intermittency distribution:

$$\gamma = 1 - \exp[-G(x - x_t) \int_{x_t}^x \frac{dx}{U}], \quad (2.43)$$

where the parameter G is estimated from a data fit:

$$G = \frac{1}{1200} \frac{U^3}{\nu^2} Re_{xt}^{-1.34}. \quad (2.44)$$

For a zero pressure gradient this model becomes:

$$Re_{\lambda} = 22 Re_{xt}^{0.67}, \quad (2.45)$$

which gives nearly the same results as equation (2.29) for $Re_{xt} \sim 10^5$. The *Chen and Thyson* [1971] model gives good results for flows with a favourable pressure gradient but fails for flows with an adverse pressure gradient. The reason for this, according to *Walker* [1993], is that the influence of an adverse pressure gradient on the physics is not incorporated in the model.

2.2.3 Compressibility effects

Measurements which study the effect of compressibility on bypass transition are still scarce. From experiments available in literature it follows that the bypass transition mechanism remains unchanged compared to low velocities. The concentrated breakdown hypothesis was confirmed by *Owen and Horstman* [1972]. They showed that the intermittencies obtained agree well with the Narasimha distribution. However, *James* [1958] reported that when the Mach number is increased, also the propagation of the turbulent spots increases but the longitudinal growth rate decreases. *Clark et al.* [1994] performed heat transfer measurements for natural occurring spots and found that the spot spreading angle decreases for higher Mach numbers while the streamwise growth nearly remains unchanged.

Effect on the transition start

Zysina-Molozhen and Kuznetsova [1969] measured that the start of transition delays as a function of the Mach number. From a data fit they proposed the correlation:

$$\frac{Re_{xt}(M)}{Re_{xt}(M=0)} \sim 1 + 0.38M^{0.6}. \quad (2.46)$$

A physical reason for the shift of transition start might be that a compressible boundary layer has a fuller velocity profile and thus is more stable (*Hogendoorn* [1997]).

Effect on the transition length

Chen and Thyson [1971] proposed an empirical relation which correlates the Reynolds number based on the transition length and the Reynolds number at the transition start:

$$Re_{Lt} = A Re_{xt}^{0.67}, \quad (2.47)$$

in which A is dependent on the Mach number:

$$A = 60 + 4.68 M^{1.92}. \quad (2.48)$$

This relation is based on measurements with the Mach number ranging from 0 to 5. When the Mach number is zero, relation (2.44) is obtained. Note the difference between Re_{Lt} and Re_{λ} . The former is based on the transition length which is defined as the streamwise distance where the intermittency ranges from 0.01 to 0.99, while the latter is based on the distance between $\gamma = 0.25$ and $\gamma = 0.75$. For the Narasimha distribution both lengths are related by:

$$L_t = 3.36\lambda. \quad (2.49)$$

2.2.4 Minimum transition length theory

A theory for the minimum possible length of the transition zone was developed by *Walker* [1989]. It is assumed that the transition process is initiated due to

instability of the boundary layer. Therefore Tollmien-Schlichting (TS) waves are responsible for the generation of spots at x_t . In this process it is likely that spots arise with a frequency corresponding to the most amplified TS-wave. Now the minimum transition length is supposed to be the length which is required for the first meeting of adjacent spots. The thus determined length is an underestimation of the real transition length because laminar flow is still available when the first spots start to meet, implying that transition is not completed. Another reason is the assumption that every TS-cycle a spot is generated, which is probably an overestimation of the spot production rate.

For the longitudinal merging of spots a frequency of spot inception is needed. From stability calculations for Falkner-Skan boundary layer profiles (*Obremski et al.* [1969]), it is derived that the circular frequency at which the amplification rate is maximum, can be described by:

$$\frac{\omega \nu}{U^2} = 3.2 Re_{\delta_*}^{-3/2}, \quad (2.50)$$

with Re_{δ_*} the Reynolds number based on the displacement thickness. These frequencies are thought to represent the disturbances which have the maximum amplification ratio and thus are responsible for transition.

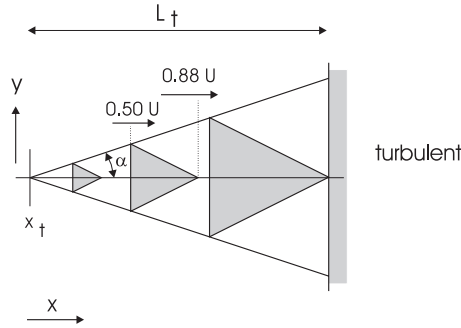


Figure 2.6: Minimum transition length approach.

A simplified spot, as depicted in figure 2.6, with leading edge velocity of $0.88U$ and trailing edge velocity of $0.50U$ results in a transition length of:

$$L_t = 1.16 U T, \quad (2.51)$$

which is the length needed for two succeeding spots, initiated at the same streamwise and spanwise position on the plate, to meet on the spot center-line. This can be verified easily from geometrical considerations. The disturbance period

T , i.e. the time between the initiation of spots, follows directly from equation (2.50):

$$T = \frac{2\pi}{\omega} = 2.0 \frac{\nu}{U^2} Re_{\delta_*}^{3/2}. \quad (2.52)$$

Combination of equations (2.51) and (2.52) gives for the Reynolds number based on the transition length:

$$Re_{Lt} = C_{lo} Re_{\delta_*}^{3/2}. \quad (2.53)$$

The constant C_{lo} has a value of 2.32. For a Blasius boundary layer the relation between the Reynolds number based on the displacement thickness and the Reynolds number based on the streamwise distance is:

$$Re_{\delta_*} = 1.72 Re_x^{1/2}. \quad (2.54)$$

Substitution in equation (2.53) gives for a flow with a zero pressure gradient:

$$Re_{Lt} = 5.23 Re_{xt}^{3/4}. \quad (2.55)$$

Only the longitudinal merging of spots is considered in the derivation so far. However, lateral meeting of spots might be more restrictive. If the disturbance period T is used, combined with the Tollmien-Schlichting phase velocity of C_r , the TS-wavelength becomes:

$$\lambda_{TS} = T C_r = 2.0 \frac{C_r \nu}{U^2} Re_{\delta_*}^{3/2}. \quad (2.56)$$

Assuming that spots are initiated with a spanwise distance of this value, together with a spot spreading angle of 10° , the merging of two spots generated at the same time will occur after a length:

$$Re_{Lt} = 5.6 \frac{C_r}{U} Re_{\delta_*}^{3/2} = C_{la} Re_{\delta_*}^{3/2}. \quad (2.57)$$

According to *Walker* [1989] the value of C_{la} decreases from 2.2 to 1.2 when Re_{δ_*} increases from 600 to 10000 (see also the instability diagram giving $\frac{C_r}{U}$ as a function of Re_{δ_*} in *Schlichting* [1979]). This suggests that lateral merging determines the minimum transition length ($C_{la} \leq C_{lo}$).

By using equation (2.49) which describes the relation between L_t and λ , the Narasimha correlation (2.30) becomes in terms of the transition length:

$$Re_{Lt} = 30.2 Re_{xt}^{3/4}. \quad (2.58)$$

It is seen that there is a large difference (factor of six) between the minimum transition length (equation (2.55)) and the transition length obtained from measurements (equation (2.58)). If lateral merging is used as the actual restriction this factor becomes even higher. Therefore, the minimum transition length theory should be used with care.

2.3 Unsteady transition

A distinction must be made between 'direct' and 'indirect' unsteady transition. Direct transition is known as transition directly caused by the wakes while indirect transition is known as transition caused by velocity fluctuations. *Orth* [1993] prefers to mention 'wake turbulence induced' and 'periodic unsteadiness induced' transition instead of direct and indirect transition.

First, attention will be paid to indirect transition, which was investigated thoroughly by *Miller and Fejer* [1964] and *Obremski and Fejer* [1967]. They studied the transition process in a flow with a periodically changing mainstream velocity:

$$U(t) = U_\infty + \Delta U \sin \omega t, \quad (2.59)$$

with U_∞ a mean velocity component and ΔU the amplitude of the varying mainstream velocity. It was found that the start of transition depends on an unsteady Reynolds number:

$$Re_{ns} = \frac{U_\infty \Delta U}{\nu \omega}. \quad (2.60)$$

If the value of this Reynolds number is larger than approximately 27000, the transition starts with turbulent spots which are produced periodically with the frequency of the main flow. The start of transition is found to be dependent on the amplitude of the external flow and not on the frequency. Therefore, the transition is determined by the velocity fluctuations, i.e. indirect unsteady transition.

When the unsteady Reynolds number is less than 25000 the transition starts at a constant streamwise position which is not dependent on both the amplitude and the frequency of the external flow. In this region, oscillations are not dominant in the transition process.

The unsteady Reynolds number can be rewritten in:

$$Re_{ns} = \frac{U_\infty \Delta U}{\nu \omega} = \frac{U_\infty C}{\nu} \frac{U_\infty \Delta U}{\omega C U_\infty} = Re \frac{1}{k} \frac{\Delta U}{U_\infty}. \quad (2.61)$$

In this equation Re is the Reynolds number based on the chord of a turbine blade and k a reduced frequency. An estimate of characteristic values for turbomachinery are (*Funazaki et al.* [1993]): $Re \sim 10^6$, $k \sim 10$ and $\frac{\Delta U}{U_\infty} \sim 0.1$, resulting in an unsteady Reynolds number of 10^4 . While this unsteady Reynolds number is less ⁴ than 25000, it is concluded that for the flow in turbomachines transition is not likely to be caused by velocity fluctuations in the main flow but by the turbulence in the wake. Hence, we will focus on the wake turbulence itself.

Boundary layer transition in a gas turbine originates from two sources. The first one is steady bypass transition, which is a result of the high background

⁴The chord Reynolds number of 10^6 is relatively high for gas turbines. For example, *Mayle* [1991] mentions a value of roughly $4 \cdot 10^5$. This implies that the unsteady Reynolds number becomes even smaller than 10^4 .

turbulence level, for example initiated in the combustion chamber. A second source is the influence of the wakes which are shed behind the stator blades and flow along the rotor blades. While both phenomena are present simultaneously, it is interesting to know the combined effect on the turbine blades. Only, a small amount of literature on the combined effect of steady and unsteady transition is available. For example, *Mayle and Dullenkopf* [1990] investigated the heat transfer along a turbine blade. They found that the effects of bypass and wake induced transition can be superposed. Flat plate measurements at high velocity and large turbulence levels are unknown.

2.3.1 The space-time diagram

Unsteady transition often is described by means of a space-time diagram (x, t -diagram) (*Pfeil et al.* [1983]). Figure 2.7 shows the simplest form of an x, t -diagram. On the vertical axis the time is depicted and on the horizontal axis the streamwise direction. The wakes are supposed to have a period time T . Due to the influence of a wake (wake turbulence), a turbulent 'patch' starts to develop at a certain streamwise distance from the leading edge. The patch convects along the surface and grows while the leading and trailing edge velocities of the patch are not equal. These patches, which in first approximation are thought to be fully turbulent, are assumed to behave in a comparable way like natural occurring spots.

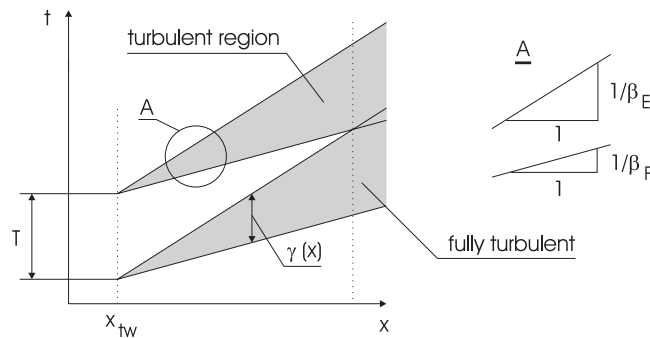


Figure 2.7: Space-time diagram.

Suppose that the leading edge velocity is β_F times the mainstream velocity and the trailing edge velocity β_E times the mainstream velocity. The resulting turbulent region is shown by the gray area in the figure. Now, the intermittency at a certain streamwise position is easily determined by taking the turbulent flow duration divided by the wake period time T . The intermittency resulting from figure 2.7, increases linearly in streamwise direction, until the flow is turbulent.

More complicated space-time diagrams are developed in literature, while the 'simple' diagram, as described above, does not represent measurements well in all transition cases. For example, wake characteristics can be incorporated. This will be treated in section 2.3.5. First three different approaches of modelling wake induced transition will be discussed:

- Turbulent band or turbulent 'patch' model.
- Narrow wake (moving source) model.
- Wide wake (fixed source) model.

2.3.2 Turbulent band model

The turbulent band approach is the most simple way to describe unsteady transition. It is assumed that the wake turbulence causes turbulent patches and that the transition can be described by the space-time diagram as treated before. The flow in a patch is supposed to be fully turbulent. The leading edge velocity of turbulent events is found to be larger than 0.75 times the mainstream velocity for experiments listed by *Hodson et al.* [1992]. Trailing edge velocities ranging from 0.3 up to 0.85, depending on the set-up, are quoted.

In some experiments, the leading edge velocity is found to be nearly one or even larger. This latter case is explained by *Addison and Hodson* [1990a,b]. They argued that transition is most likely to occur near the center-line on the wake as the turbulence at that position is greatest. At first approximation the turbulence level in the wake can be assumed to have a gaussian distribution around the center-line. As the boundary layer grows, it becomes more unstable and as a result it becomes also susceptible for lower turbulence levels. If the wake convects downstream, it is possible that spots are initiated more downstream of the center-line of the wake. In the case of a wake velocity equal to the mainstream velocity the 'apparent' propagation of the patch seems to take place at a velocity which is a bit higher.

The unsteady transition is completed when the trailing edge of a turbulent patch merges with the leading edge of a previous patch. In that case the complete flow is turbulent. This implies that the wake passing frequency has a direct effect on transition. A high frequency results in an early 'meeting' of patches and thus a decrease of the transition length. When the wake passing frequency is high enough the transition is completed before natural turbulent spots start to occur.

2.3.3 Narrow wake (moving source) model

In the turbulent band model, it is assumed that in the patch generated by the wake, the boundary layer is completely turbulent. The narrow wake (moving source) model supposes that not a fully turbulent band exists, but an area in which turbulent spots start to develop (*Hodson et al.* [1992]).

Assume that the wake is a narrow source of turbulent spots which move with the free stream velocity. The source thus moves with approximately the leading edge velocity of the wake generated turbulent events. Until a certain streamwise distance the boundary layer is stable, as is the case for steady boundary layer transition. When this position x_{tw} is reached, turbulent spots are initiated underneath the wake. The position of x_{tw} is likely to depend on the turbulence level at the wake center-line (narrow wake). It also is expected that the production rate of spots is equal to the rate for steady transition. For natural transition the leading edge and the trailing edge velocities are roughly 0.88 and 0.50 times the mainstream velocity, respectively. As stated before, the narrow wake moves with the free stream. Due to the velocity difference between the wake and the spots which are generated, the wake center-line flows along an undisturbed (laminar) boundary layer which is situated downstream of x_{tw} . The boundary layer is susceptible for the disturbances in the wake and as a result new spots start to develop.

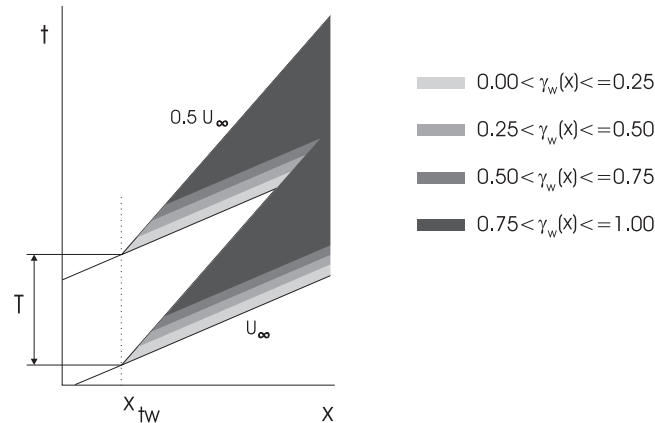


Figure 2.8: Space-time diagram for the narrow wake (moving source) model.

Figure 2.8 shows the space-time diagram for the narrow wake (moving source) model. The 'turbulent' regions, depicted by the gray areas, are not fully turbulent as is the case in the simple space-time diagram depicted earlier (figure 2.7). The turbulence in these areas shows an intermittent behaviour due to the turbulent spots initiated by the wake. Therefore, a local intermittency can be used for describing the wake induced turbulence. The value of this *wake*-intermittency, denoted by $\gamma_w(x)$, is not constant through the induced turbulent part.

Most downstream of the wake (in the lower part of the 'tongue' as depicted in figure 2.8) only a few spots are generated, thus the wake-intermittency is relatively small. In upstream direction, spots are initiated earlier by the wake

and therefore the wake-intermittency is larger.

The fraction of time the flow is turbulent at one streamwise direction, i.e. the intermittency in its original definition, can be estimated by taking into account all the local intermittencies at one x -position in the space-time diagram.

If the spot production rate is very large, this model becomes the turbulent band model. The only difference is that the leading edge velocity of the turbulent patch for both models is different (U_∞ for the narrow wake (moving source) model and approximately $0.85 U_\infty$ for the turbulent band model).

In the case of a narrow wake, the spot production source can be thought as situated on the wake center-line. According to *Hodson et al.* [1992], this latter case is an extension of the concentrated breakdown hypothesis of *Dhawan and Narasimha* [1958] for unsteady transition.

2.3.4 Wide wake (fixed source) model

Mayle and Dullenkopf [1990] based an unsteady transition model on the assumption of the occurrence of turbulent spots. They assumed that the wake is a production source of spots. However, the strength of the wake is so intense that the spots immediately form a turbulent 'strip'. This strip convects and grows along the streamwise surface. The speed of the strip not necessarily equals the mainstream velocity but is a fraction of this; the same assumption which accounts for natural occurring turbulent spots. It is thought that when the strip is formed, the propagation and the growth are independent of the wake itself.

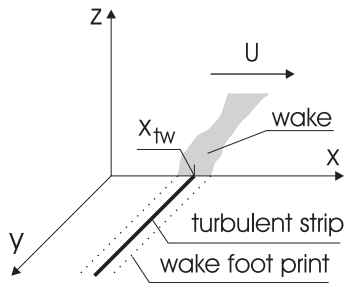


Figure 2.9: Turbulent strip approach; strip is initiated at streamwise position $x = x_{tw}$.

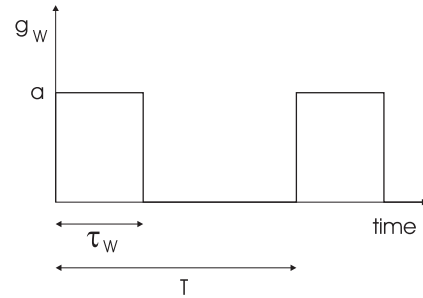


Figure 2.10: Spot production parameter at streamwise position $x = x_{tw}$; ($g = 0$ for $x \neq x_{tw}$).

Suppose that the spot production has two sources, production due to natural (or bypass) transition and production due to passing wakes. The spot production parameter g then can be written as:

$$g = g_n + g_w. \quad (2.62)$$

It is assumed that both g_n (the subscript n means *natural*) and g_w (the subscript w means *wake*) are independent. In reality this might not be true for example due to the influence of the becalmed region. This region is the area just behind the turbulent spot (*Schubauer and Klebanoff* [1955]). In experiments (*Gostelow et al.* [1997]), the flow in the becalmed region is found to be more stable than in a laminar boundary layer due to a fuller velocity profile. Therefore, the initiation of new spots in this region is more difficult than spot generation in a Blasius boundary layer.

Spot production due to wakes is a function of time and spot production due to natural transition is constant in time. The intermittency now can be written in analogy with the *Emmons* [1951] theory:

$$\gamma(P) = 1 - \exp\left[-\int_{R_n} g_n dV_0\right] \exp\left[-\int_{R_w} g_w dV_0\right]. \quad (2.63)$$

In this equation R_n is the volume of dependence for the natural spots and R_w for the wake induced spots. If the wake period is T , the time averaged intermittency becomes:

$$\tilde{\gamma}(x) = \frac{1}{T} \int_{t_1}^{t_1+T} \gamma(P) dt = 1 - [1 - \gamma_n(x)][1 - \tilde{\gamma}_w(x)]. \quad (2.64)$$

In this equation $\gamma_n(x)$ and $\tilde{\gamma}_w(x)$ are:

$$\gamma_n(x) = 1 - \exp\left[-\int_{R_n} g_n dV_0\right], \quad (2.65)$$

$$\tilde{\gamma}_w(x) = 1 - \frac{1}{T} \int_{t_1}^{t_1+T} \exp\left[-\int_{R_w} g_w dV_0\right] dt. \quad (2.66)$$

For natural transition the assumption of point wise breakdown is used (*Dhawan and Narasimha* [1958]). *Mayle and Dullenkopf* [1990] stated that also for wake induced transition there is a most probable location for the transition start, denoted by x_{tw} . In general x_{tw} is not equal to x_t . The wake is assumed to be a switch which starts or stops the production of spots at x_{tw} (figure 2.9). Spots are assumed to be initiated when the 'wake footprint' flows along this position. The time in which spots are produced is thought to be the wake duration τ_w . Therefore, the spot production parameter for the wake induced part, is described by a series of block pulses as shown in figure 2.10.

When the wake is very weak the transition is supposed to be more 'natural' like. This suggests that x_{tw} will approach x_t . It is likely that g_w and x_{tw} are functions of the wake characteristics, like wake strength and wake structure. It was reasoned that there also is an influence of the wake passing frequency because some time is required for the boundary layer to completely respond on the wake *Mayle and Dullenkopf* [1990]. After some algebra, it was shown that equation (2.66) can be transformed in:

$$\tilde{\gamma}_w(x) = 1 - \exp\left[-b\left(\frac{\tau_w}{T}\right)\left(\frac{x - x_{tw}}{U_{st}}\right)\right], \quad (2.67)$$

$$b = 4a \tan \alpha.$$

This equation holds for a constant velocity of the turbulent strip denoted by U_{st} . The parameter α is one-half of the propagation angle of the turbulent strip, a the turbulent strip production strength (comparable to n in the bypass transition case), T the wake period and τ_w the wake duration. Now the expression for the total intermittency, thus due to natural and wake induced transition, becomes:

$$\tilde{\gamma}(x) = 1 - \exp\left[-\frac{\sigma n(x - x_t)^2}{U}\right] \exp\left[-b\left(\frac{\tau_w}{T}\right)\left(\frac{x - x_{tw}}{U_{st}}\right)\right]. \quad (2.68)$$

Mayle and Dullenkopf [1990] compared their theory to the data of *Pfeil and Herbst* [1979] who performed measurements in a rotating cylinder cascade. The theory showed good agreement and a resulting data fit is:

$$\tilde{\gamma}_w(x) = 1 - \exp[-0.733r(x - 0.04)], \quad (2.69)$$

where r is the number of rotating cylinders of the wake generator (see also section 3.6.1). The streamwise distance x_{tw} appeared to be 0.04, which corresponds to the beginning of wake induced transition. In this equation it is supposed that wake induced transition is completed before natural spots start to develop. If it is assumed that $r = 90$ corresponds to a fully turbulent flow, *Mayle and Dullenkopf* [1990] derived that: $\frac{b}{U_{st}} = 66 \text{ m}^{-1}$. It seemed that this factor is nearly constant for several sets of experiments. In a more thorough investigation of the measurements and a dimensional analysis, *Mayle and Dullenkopf* [1991] found an expression for wake induced transition which does not involve the quantity $\frac{b}{U_{st}}$. This resulted in a new relation for the intermittency:

$$\tilde{\gamma}_w(x) = 1 - \exp\left[-1.9\left(\frac{x - x_{tw}}{U T}\right)\right]. \quad (2.70)$$

2.3.5 Model modifications

Funazaki [1996a,b] used the fixed source model, but his experiments (*Funazaki* [1993]) are not described adequately by equation (2.70). Problems occurred at high wake passing frequencies. Comparable deviations were found by *Han et al.* [1993]. Therefore, another model which is based on the evolution of wake induced turbulent spots in a space-time diagram is proposed (similar to that of *Pfeil et al.* [1983]). The wake induced intermittency for the diagram depicted in figure 2.7 can be written as:

$$\gamma_w(x) = \left[\frac{1}{U_E} - \frac{1}{U_F}\right] \frac{x - x_{tw}}{T} = \left[\frac{1}{\beta_E} - \frac{1}{\beta_F}\right] \frac{x - x_{tw}}{L} S, \quad (2.71)$$

with $U_E = \beta_E U_\infty$, $U_F = \beta_F U_\infty$ and S the Strouhal number based on the length L of the plate ($S = \frac{L}{U_\infty T}$). U_E and U_F are the propagation speeds of the preceding

and the following portions of the turbulent patch. Furthermore, it was assumed that $\beta_E = 0.55$ and $\beta_F = 1.0$.

Funazaki [1996a,b] performed heat transfer measurements along a flat plate in a low speed wind-tunnel with a rotating disk wake generator. The rotational speed of the disk was varied between 900 and 1500 rpm, resulting in a cylinder mean speed ranging from 24.5 to 40.8 m/s. He found that there is a dominant effect of the wake passing frequency on wake induced transition. When the disk rotational speed and the number of cylinders are varied such that the frequency (and thus the Strouhal number) remains unchanged, the same heat flux distributions are found. This suggests that the Strouhal number is important and not the velocity of the cylinders. Also an influence of wake characteristics was measured on the heat flux. Increasing the cylinder diameter as well as decreasing the distance between the wake generator and the plate, resulted in an increase of the flux. This implies that the original model of Mayle and Dullenkopf (equation (2.70)), in which it is assumed that the wake only acts as a switch to initiate transition, does not hold for the present measurements.

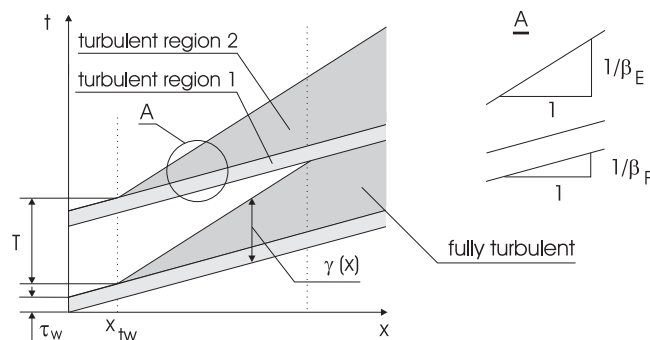


Figure 2.11: Turbulent strip approach; wake width is incorporated.

To resolve this discrepancy *Funazaki* [1996a,b] refers to *Addison and Hodson* [1990 a,b], who mentioned that the time needed for the wake turbulence to diffuse into a laminar boundary layer is very short compared to the wake passing period. So, the boundary layer is immediately activated to become turbulent by the turbulence kinetic energy which enters it rapidly. While the laminar boundary layer thickness is very thin and the velocity gradient is large, a viscous effect is strong enough to dissipate the turbulence kinetic energy quickly, so the boundary layer is supposed to return to laminar when the wake has passed.

The above mentioned theory implies that the turbulent state only lasts for the wake duration. On the basis of this, *Funazaki* modified equation (2.71). Figure 2.11 gives the diagram including a wake which has a duration τ_w . Region 1 is assumed to be the wake turbulence itself and region 2 the turbulence resulting

from the patches. If both regions 1 and 2 are thought to consist of 100 percent turbulent flow, the intermittency can be calculated in an analogous manner as depicted in figure 2.7. The resulting intermittency distribution has a constant value τ_w/T , until the streamwise position x_{tw} is reached. At this position the intermittency starts to increase linearly. The onset of wake induced transition is regarded to be x_{tw} , being the point where patches initiated by wakes start to develop. An expression for the intermittency is:

$$\gamma_w(x) = \min[1, \Gamma(x)] \quad (2.72)$$

$x \geq x_{tw}$:

$$\Gamma(x) = \left(\frac{1}{\beta_E} - \frac{1}{\beta_F}\right) \frac{x - x_{tw}}{U_\infty T} + \frac{\tau_w}{T} = \left(\frac{1}{\beta_E} - \frac{1}{\beta_F}\right) \frac{x - x_{tw}}{L} S + \frac{S}{S_w}$$

$x < x_{tw}$:

$$\Gamma(x) = \frac{S}{S_w},$$

with S and S_w Strouhal numbers defined by:

$$S = \frac{L}{U_\infty T}$$

and

$$S_w = \frac{L}{U_\infty \tau_w}.$$

It is supposed that the leading edge velocity of the patch equals the trailing edge velocity of the wake. Incorporating the spreading of wakes due to diffusion in the mainstream would result in a divergence of the wake turbulence region. However, in the case that both regions are supposed to contain 100% turbulence, wake spreading has no effect on the model if $x > x_{tw}$.

The wake width is incorporated in the model described by equation (2.72). However, no attention is given to the transition start x_{tw} which might be dependent on the wake strength. On the basis of his experiments *Funazaki* [1996a,b] proposed a slightly modified model, which is depicted in figure 2.12.

Assume that underneath the wake, turbulent patches start to occur somewhere at position x_s . In the case of strong wakes, the disturbances at the rear of the wake are such strong that even here patches start to develop. Therefore the distance between x_{tw} and x_s is not very large. An estimation for this location can be made by using the natural transition criterion (2.34), which describes the start of transition as a function of the turbulence level ($Re_{\theta t} = 163 + \exp[6.91 - Tu]$). The minimum momentum thickness Reynolds number at the transition start is 163, so an intense wake probably would cause transition at this position.

In the case of weak wakes, the most probable location for a patch is to occur at the center-line of the wake. The wake is not strong enough to initiate patches

at the rear. Therefore, there is some distance between x_{tw} and x_s which is determined by geometrical consideration of the space-time diagram:

$$x_{tw} = x_s + \frac{U_\infty \tau_w}{2\left(\frac{1}{\beta_E} - \frac{1}{\beta_F}\right)} = x_s + 0.61 U_\infty \tau_w. \quad (2.73)$$

In this equation τ_w is the wake duration, while for the leading and trailing edge velocities the following values are used: $\beta_E = 0.55$ and $\beta_F = 1.0$.

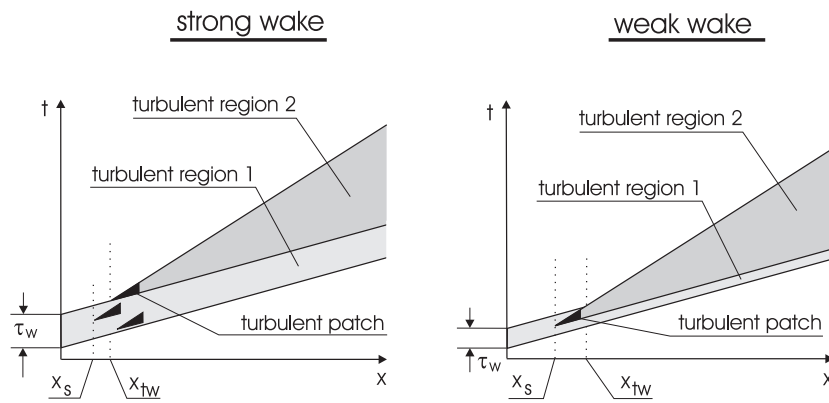


Figure 2.12: Modified space-time diagram according to Funazaki (note that x_s and x_{tw} are situated further downstream for weak wakes).

2.4 Conclusions

This chapter gives an overview of models which can be used for describing steady and unsteady bypass transition. Most of the models are based on the occurrence of turbulent spots. In the case of bypass transition, large disturbances in the mainstream enter the boundary layer and generate a small area of turbulence. These areas (the spots) are assumed to grow in streamwise and spanwise direction while their leading and trailing edge velocities are not equal.

The Narasimha intermittency distribution often is used for the characterization of steady transition. It is supposed that the turbulent spots are initiated with infinitesimal small size at one streamwise position. In dimensionless form the two parameters which determine the Narasimha model are the spot production parameter and the Reynolds number based on the transition start.

A common way to describe the effects of turbulence, pressure gradients and compressibility on transition, is to incorporate the individual influences on the model parameters. The general trend is that increasing the turbulence level, results in an earlier transition start and a shortening of the transition length. Also

the structure of the turbulence plays a role. However, the number of experiments on this effect found in literature is small.

A favourable pressure gradient has a stabilizing effect of the flow. Therefore, a delay of the transition start and an enlargement of the transition length is obtained. An adverse pressure gradient has a destabilizing effect, resulting in an opposite behaviour.

High velocity experiments and measurements which study the effect of compressibility are scarce and not unequivocal. It was found that increasing the Mach number stabilizes the flow, but this is a minor effect compared to influences of turbulence and pressure gradients.

Unsteady transition can be visualized by means of a space-time diagram. Most simple is the diagram obtained from the turbulent band model. It assumes that the wake causes a 'patch' which is completely turbulent. This patch behaves in a similar way as an individual turbulent spot. Therefore, the leading edge velocity is larger than the trailing edge velocity, resulting in a turbulent band which grows linearly in streamwise direction. The flow is fully turbulent when two successive turbulent patches meet each other.

Extension of the turbulent band model is done by assuming a narrow wake (moving source) approach. Not a fully turbulent patch exists underneath the wake, but a small band in which turbulent spots start to develop. This implies that growing regions with an intermittent flow behaviour convect along the surface.

The wide wake (fixed source) model supposes that the wake only acts as a switch which activates the generation of a turbulent strip. This strip can be thought as a region with many turbulent spots. In this approach the wake characteristics are of minor importance because when the strip is formed, the propagation and the growth are independent of the wake itself. The total spot production in this model can thus be described as a superposition of natural and wake induced spots. However, it appeared that not all the wake induced transition experiments can be described adequately by the wide wake (fixed source) model. For this reason, some modifications which take into account wake properties, are applied by several authors.

Chapter 3

Experimental techniques

3.1 Introduction

Hogendoorn [1997] concluded that there is a lack of boundary layer bypass transition data in the subsonic range. He compared the suitability of several set-ups, keeping in mind some specific restrictions. The first one was that as much as flow parameters, like the Mach number, the Reynolds number, free stream turbulence level and pressure gradient, have to be adjusted independently. The second requirement was to initiate a flow with a transition zone which is large enough to perform accurate measurements. Three different facilities were compared, the wind-tunnel, the Isentropic Light Piston Tunnel and the Ludwieg tube. A summary of the study executed by *Hogendoorn* [1997] is given below.

The first possibility is to take an open wind-tunnel. In literature wind-tunnels are often used to perform boundary layer transition research. An advantage of a tunnel is that it can run continuously, so long duration measurements can be performed. However, a major problem with wind-tunnels is that the Reynolds number and the Mach number can not be adjusted independently. The Mach number is defined as the actual velocity U divided by the speed of sound c :

$$M = \frac{U}{c} = \frac{U}{\sqrt{\kappa RT}}. \quad (3.1)$$

The Reynolds number is a measure for the fraction of convective and viscous forces. When not taking into account a length scale one can use the *unit Reynolds number*, which is (dimension m^{-1}):

$$Re_u = \frac{U}{\nu} = \frac{U\rho}{\mu}. \quad (3.2)$$

Neglecting the effect of temperature and using air, so κ and R are not varied, it is easily seen that the only possibility to change the Mach number is to alter the velocity. However, changing the velocity will also change the Reynolds number

as for an open wind-tunnel it is hard to vary the density ρ . From this it can be concluded that the Mach number and the Reynolds number are coupled, so it does not satisfy the first requirement.

A second experimental set-up which can be used is an Isentropic Light Piston Tunnel (ILPT). Isentropically compressed air is pumped through a test section into a dump tank. The test time varies between 70 ms and 300 ms depending on the geometry. Transition measurements are known on cascades (*Consigny and Richards* [1982]) and flat plate geometries (*Clark et al.* [1994]). However, the latter experiments are performed at a low turbulence level (naturally occurring turbulent spots). Disadvantages of this set-up are the large fluctuations in static pressure (3.5%) which result in variations of the Reynolds number and the Mach number. Also the construction of an ILPT is complicated and therefore expensive.

The third facility of interest is a Ludwieg tube. Only a few articles can be found which describe the use of this set-up for boundary layer transition research. An example for film cooling experiments is presented by *Zhang et al.* [1993]. In a Ludwieg tube the Reynolds number and the Mach number can be varied independently. Also the transition zone can be altered such that it is long enough for performing accurate measurements. So, both requirements as listed earlier are satisfied. *Hogendoorn* [1997] decided to study the possibilities of this facility in order to execute bypass transition research. He found that indeed very reliable experiments can be performed in a Ludwieg tube. As a result the same set-up is used for all the measurements described in this thesis. The specific flow conditions and principles will be part of the next section.

3.2 Ludwieg tube

A Ludwieg tube set-up (another name is expansion tube) consists of three main parts. A long tube is connected via a test section to a dump tank. The tank and the test section are separated by a choking orifice and a membrane of Melinex. A schematic diagram of the set-up is given in figure 3.1. The cross section of the tube and the test section is $0.1 \times 0.1 \text{ m}^2$, while the length of the tube is 10 m. In the test section a sensor plate, hot-wire probes and pressure gauges can be mounted. Prior to an experiment the pressure in the dump tank (volume 0.43 m^3) is reduced by a vacuum pump to approximately 500 Pa. The pressure in the tube and thus also in the test section is set to a value which is between 10^3 and 10^5 Pa (\sim atmospheric pressure). Melinex with a thickness of $19 \mu\text{m}$ is sufficient to withstand the initial pressure difference. When the membrane is ruptured by an electrical pulse the experiment starts. A shock wave and contact surface run into the tank while an expansion wave travels from the choking orifice into the tube and test section. The flow is accelerated due to the expansion wave and finally chokes at the choking orifice. When this condition holds the flow in the test section is constant and has a subsonic velocity. The expanded air flows

from the tube and section into the tank. During the time the flow is steady in the test section, which is approximately 40 ms depending on the section, the measurements are performed.

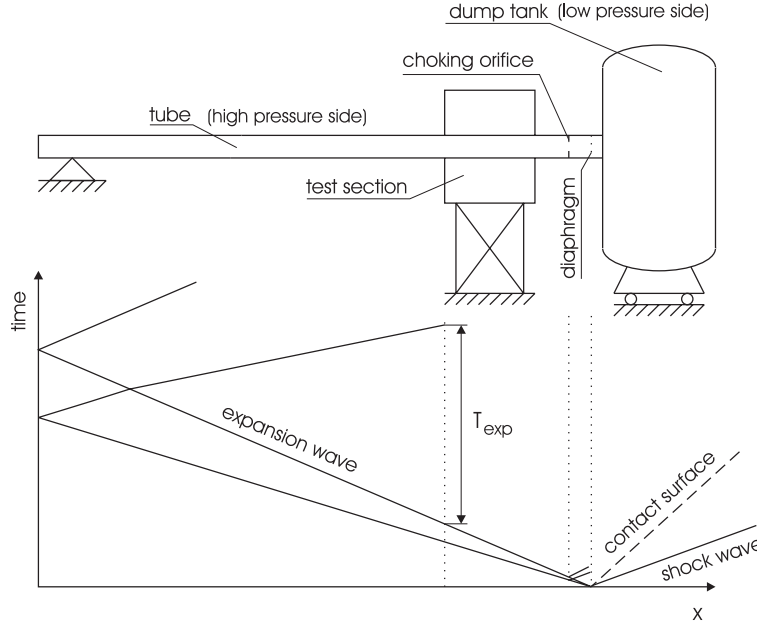


Figure 3.1: Ludwig tube principle.

The Mach number is determined by the ratio of the tube and the choking orifice area, while the Reynolds number is adjusted by setting the initial pressure in the tube. For most experiments ambient air is used. It is also possible to perform experiments with other gases, for example nitrogen. This might be required when the air humidity is very high and therefore the expansion can lead to the formation of water droplets in the test section. However, in all the experiments performed, no problems occurred using ambient air.

The conditions in a Ludwig tube can be calculated by using quasi-one-dimensional gas dynamics (*Owczarek* [1964]). Assuming a quasi-one-dimensional homenergetic flow, it follows that the Mach number in the test section is dependent on the cross sectional area of the tube and the choking orifice:

$$\frac{A}{A^*} = \frac{1}{M_t} \left[\frac{2}{\kappa + 1} \left(1 + \frac{\kappa - 1}{2} M_t^2 \right) \right]^{\frac{\kappa + 1}{2(\kappa - 1)}} \quad (3.3)$$

In this equation κ is the ratio of the specific heats of the gas used for the experiment ($\kappa = \frac{C_p}{C_v} = 1.4$ for air), A the cross sectional area of the tube (incorporating

the blockage of the sensor plate) and A^* the area of the choking orifice, which is $\frac{1}{4}\pi D^2$, as shown in figure 3.2. Equation (3.3) gives an estimate of the Mach number which should be expected above the plate. However, as mentioned earlier, the actual Mach number will deviate due to the influence of the sensor plate. Also, the effective area of the tube will be smaller because of boundary layer formation at the side walls.

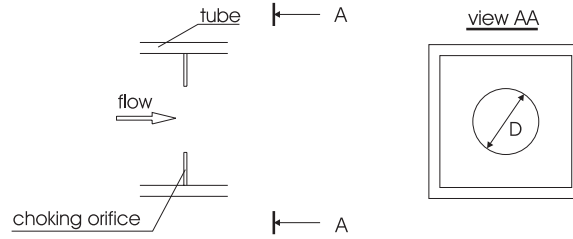


Figure 3.2: Choking orifice.

Therefore, a better way to determine the Mach number should be used. This can be achieved by measuring the ratio of the initial pressure in the tube and the actual pressure during the experiment ($\frac{p_t}{p_i}$). Assuming isentropic flow and a single left running simple wave:

$$\frac{p_t}{p_i} = \left(\frac{c_t}{c_i}\right)^{\frac{2\kappa}{\kappa-1}} \quad (3.4)$$

and

$$u + \frac{2c}{\kappa - 1} = \text{constant}, \quad (3.5)$$

it follows that the Mach number is a function of the pressure ratio:

$$M_t = \frac{2}{\kappa - 1} \left[\left(\frac{p_t}{p_i}\right)^{-\frac{\kappa-1}{2\kappa}} - 1 \right]. \quad (3.6)$$

Now it is possible to calculate all the flow conditions in the Ludwieg tube. The velocity is derived using the definition for the Mach number (equation (3.1)) and the isentropic relation (equation (3.4)). From the relation for the speed of sound ($c = \sqrt{\kappa RT}$) and the ideal gas law ($p = \rho RT$), the static temperature and the density can be estimated. The dynamic viscosity is computed by Sutherland's law (temperature in Kelvin):

$$\mu = 1.458 \cdot 10^{-6} \frac{T^{1.5}}{T + 110.4}. \quad (3.7)$$

Finally, the unit Reynolds number follows from equation (3.2).

3.3 Steady-state test section

The steady transition measurements are performed in a test section which is schematically depicted in figure 3.3. This test section is 780 mm long, made of aluminium with a thickness of 20 mm, and has the same cross section as the tube. In the section, the sensor plate can be mounted such that the plate is positioned just in the middle of the cross section. It also can have a certain angle of incidence to avoid flow separation. The sensor plate has dimensions: length 160 mm, width 85 mm and thickness 3 mm, and is constructed of B-270 glass with well known properties. This plate is pasted on a stainless steel plate with a thickness of 1.5 mm. So, the total front area of both the glass and the steel is approximately 4.5 mm times the width of the tube, which is 100 mm. Due to the thus obtained local reduction of the area (blockage), the Mach number above the plate will be higher than the value in the tube (equation (3.3)).

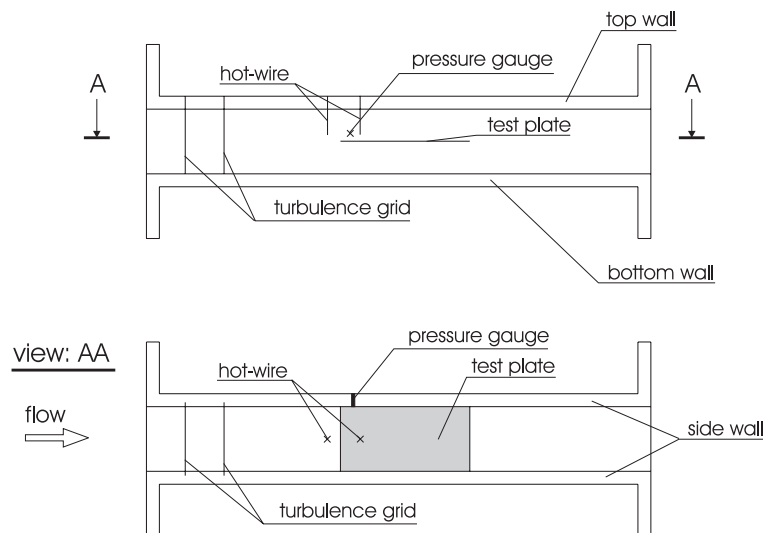


Figure 3.3: Test section for the steady experiments.

A pressure gauge is placed at the side wall, 20 mm behind and 25 mm above the leading edge. Two positions are available for situating a hot-wire. The first position is 27 mm in front of the leading edge while the second position is 30 mm behind the leading edge. The distance of the hot-wire above the plate is in both cases 10 mm (when the angle of incidence is 0°). As a result the boundary layer developing on the sensor plate is not disturbed by the wire. All the positions mentioned are chosen due to constructional reasons. Passive grids are used to generate turbulence in the free stream. These grids can be placed at two positions.

One is situated 167 mm and the second 232 mm in front of the leading edge. The complete test section is sealed, so air leakage is avoided.

3.3.1 Pressure measurements

The conditions in the Ludwieg tube are first tested for a flow in the set-up without a test section. This means that the tube is directly connected to the dump tank. A Sensit pressure gauge was mounted 200 mm upstream of the choking orifice. Figure 3.4 shows the recorded pressure during an experiment. The Mach number is calculated by using equation (3.6) (figure 3.5). It is seen that there is a plateau in the Mach number for about 40 ms. During this time a constant flow is present at the cross section where the pressure gauge is situated. The mean Mach number during the 40 ms is 0.35, as indicated in the figure. Determination of the flow conditions according to equation (3.6) is valid as long as the wave reflected at the downstream end of the tube has not reached the measuring position. This is not the case when $t > 0.060$ s, so the Mach number as drawn, is not correct for the latter part of the expansion.

Also pressure measurements are performed while the test section with the test plate is included. In the latter experiments the gauge is situated 20 mm behind and 25 mm above the leading edge of the plate. The resulting Mach number is found to be 0.34, which is assumed to be the actual number for this set-up configuration. Differences between the measurements *with* and *without* the test section might be explained by blockage of the choking orifice by the sensor plate. The relative decrease of the choking orifice area by blockage is larger than the relative decrease of the tube cross section. If this is the case, equation (3.3) predicts that the Mach number indeed will be lower.

The influence of the unit Reynolds number is studied by performing measurements in the range: $1.5 \cdot 10^6 \text{ m}^{-1} < Re_u < 4.0 \cdot 10^6 \text{ m}^{-1}$. The Mach number is constant within 0.4%; thus as expected, there is no influence of the Reynolds number. This proves one of the major advantages of the Ludwieg tube set-up, the fact that Reynolds number and Mach number adjustments can be done independently.

3.3.2 Error estimation

Variation of the flow conditions together with the reproducibility of experiments performed in a Ludwieg tube were studied by *Hogendoorn* [1997]. While the ambient temperature can be estimated with an accuracy of 0.1 K, an error of maximum 0.02% is expected in the unit Reynolds number and Mach number, due to temperature effects. The ambient pressure can be determined within 130 Pa and the initial pressure difference in the test section within 70 Pa. Therefore, the maximum error in the initial pressure is 200 Pa. *Hogendoorn* [1997] found that the inaccuracy of both the pressure and the temperature effects is smaller than

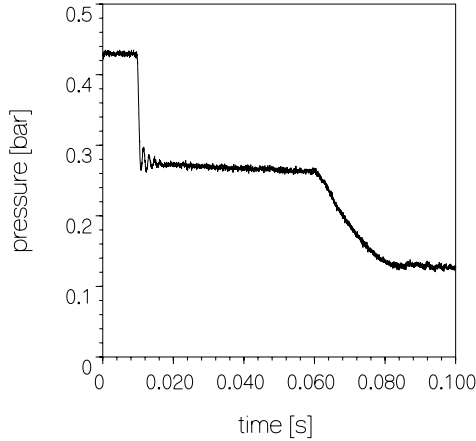


Figure 3.4: Pressure signal recorded in the steady-state test section ($Re_u = 2.4 \cdot 10^6 \text{ m}^{-1}$).

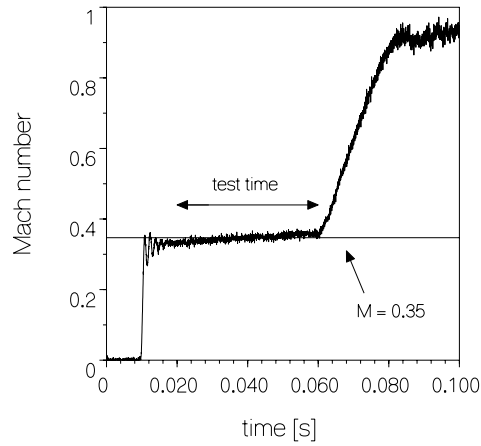


Figure 3.5: Calculated Mach number ($Re_u = 2.4 \cdot 10^6 \text{ m}^{-1}$); the test time is 40 ms.

0.8%. This value holds for the most inaccurate combination, low unit Reynolds number and high Mach number. If the unit Reynolds number increases and/or the Mach number decreases, *Hogendoorn* [1997] determined that the total error also decreases. Therefore, it is concluded that the reproducibility of the flow conditions is very good. Accurate measurements can be performed with the Ludwig tube facility.

3.4 Turbulence generating grids

Turbulence in the main flow is generated by means of static grids which can be mounted at two positions in the test section. These positions are 167 mm (denoted by 'H') and 232 mm (denoted by 'L') in front of the leading edge of the sensor plate. The grids are constructed of cylindrical rods with a diameter d , placed in a square mesh pattern. Figure 3.6 schematically shows the grid. In this figure, the center to center distance between two successive rods is the mesh size. Both the diameter and the mesh determine the structure of the turbulence. Four different grids are used in the present experiments. The values of the bar diameters and the mesh sizes are given in table 3.1.

Hot-wire measurements are performed to characterize the turbulence. A tungsten wire, placed perpendicular to the main flow, is heated. The heat transfer from this wire towards the flow is used to determine mass fluctuations and thus the turbulence level.

When the aspect ratio of the hot-wire (l/d) is larger than 250, the heat trans-

grid	d	mesh
[-]	[mm]	[mm]
4H/4L	4	20
3H/3L	3	18
2H/2L	2	10
1H/1L	1	12.5

Table 3.1: Turbulence grid parameters.

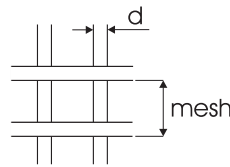


Figure 3.6: Turbulence grid dimensions.

fer to the supports can be neglected (*Bruun* [1995]). In our situation the wire diameter is $2.5 \mu\text{m}$ and the length 0.6 mm , so with a value of 240 this requirement is almost fulfilled. When the wire temperature is kept constant during an experiment (CTA-operation mode), a balance between heat production in the wire and the convective heat loss to the flow is present. The hot-wire is part of a Wheatstone bridge with a bridge voltage V_0 . An electronic device regulates this voltage such that the wire temperature, and thus the resistance, remains constant. Now, the heat production in the wire is dependent on the voltage:

$$P_{prod} \sim V_0^2. \quad (3.8)$$

The convective heat transfer from the heated wire towards the flow is given by:

$$P_{conv} = \pi k l (T_w - T_r) Nu, \quad (3.9)$$

with k the conductivity of the fluid flowing along the wire, l the wire length, T_w the wire temperature, and T_r the recovery temperature. Nu is the Nusselt number which is a function of the Reynolds number for the present experiments. An often used relation to describe this Reynolds number dependence, is King's law:

$$Nu = A_1 + B_1 Re^n. \quad (3.10)$$

In this equation A_1 and B_1 are calibration constants while the exponent has a value between 0.45 and 0.55 (*Bruun* [1995]). A constant gas temperature results

in a constant dynamic viscosity, and thus the Reynolds number is proportional to the mass flux ρU , with U the main flow velocity. The balance between heat production in the wire (equation (3.8)) and the convective heat transfer to the flow (equations (3.9) and (3.10)) results in:

$$V_0^2 = A + B Re^n. \quad (3.11)$$

A and B are again calibration constants while n is taken 0.5. This equation is used for calibrating the hot-wire.

Experiments at four different unit Reynolds numbers are performed with an overheat ratio ¹ of 1.5 (sampling frequency 400 kHz). Measurements for the 3H turbulence grid are depicted in figure 3.7. Figure 3.8 shows the bridge voltage squared as a function of the mass flux. This voltage is calculated during the time there is a constant flow in the test section. To determine the constants A and B a least square fit is used. Good reproducibility of the values is found.

Finally, the actual mean turbulence level during one experiment is calculated by:

$$Tu = \frac{\overline{(\rho U - \overline{\rho U})^2}}{\overline{\rho U}}^{1/2} \cdot 100\%. \quad (3.12)$$

Table 3.2 shows the turbulence levels measured for several turbulence grids. The addition Tu₁ or Tu₂ indicates the position of the hot-wire during the experiment. These positions are respectively 27 mm upstream and 30 mm downstream of the leading edge.

grid	Re_u	Tu ₁	Tu ₂	$M_{crit.}$
[-]	[m ⁻¹]	[%]	[%]	[-]
4H	$1.5 \cdot 10^6$	3.49	2.39	0.46
4L	$2.4 \cdot 10^6$	2.65	2.42	0.46
3H	$1.5 \cdot 10^6$	2.28	2.04	0.48
3L	$2.4 \cdot 10^6$	2.16	1.93	0.48
2H	$3.0 \cdot 10^6$	1.66	1.30	0.43
2L	$4.0 \cdot 10^6$	1.37	1.22	0.43
1H	$3.0 \cdot 10^6$	1.15	1.03	0.63
1L	$5.0 \cdot 10^6$	1.25	0.95	0.63
-	-	0.25	0.25	-

Table 3.2: Turbulence level and critical Mach number for the static grids.

¹The overheat ratio is defined as R_w/R_g , in which R_w is the resistance of the hot-wire when it is heated, while R_g is the hot-wire resistance at the initial temperature (ambient temperature). The value of the overheat ratio is chosen such that the signal-noise ratio is high enough, while the wire temperature is limited to avoid early damage.

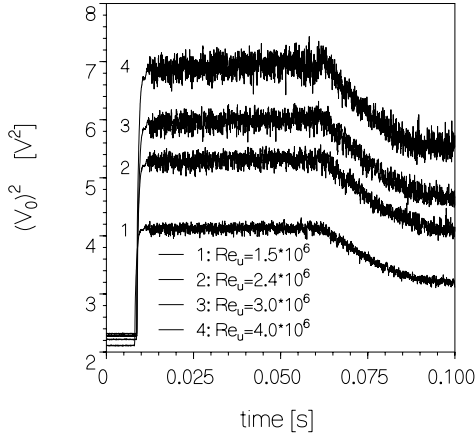


Figure 3.7: Hot-wire signals for the 3H turbulence grid.

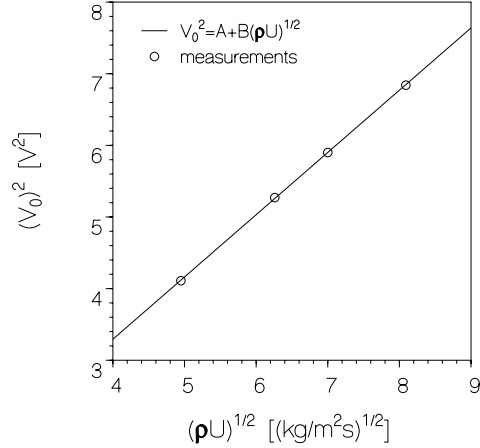


Figure 3.8: Hot-wire calibration for the 3H turbulence grid.

One important remark must be made concerning the blockage of the turbulence grids. To justify the flow conditions in the test section as calculated by using the quasi-one-dimensional gas dynamics described in section 3.2, the flow should choke at the choking orifice and not at the turbulence grid. For this reason the solidity of the grids must be smaller than the solidity of the choking orifice (solidity = blocked area divided by the tube cross sectional area). A critical Mach number, M_{crit} , for each grid is calculated using equation (3.3). These values are listed in table 3.2. As can be seen the critical Mach numbers are larger than 0.40. All the experiments described in this thesis are smaller than this value, so no problems are expected.

3.5 Heat flux measurements

The heat flux in a boundary layer changes significantly when transition occurs. Many experimental techniques are available for determining the transition characteristics, however for our purpose we would like to determine the heat flux as direct as possible. Several methods can be used for measuring the flux from the gas to the wall, or in our case from the wall to the gas as we are dealing with a cooled gas flow (due to the expansion). One of the major requirements is that the heat flux gauges have a fast response time because of the high velocity in the tube and the small size of the turbulent spots. Therefore, the minimum response frequency was set to be 30 kHz (*Hogendoorn* [1997]). Also the sensors should not disturb the boundary layer, which gives a limitation for the height of the gauges.

The former restrictions resulted in the use of a thin film technique. The

principle of thin films is as follows. A thin (titanium) resistor is evaporated on an electrical isolating substrate (figure 3.9 gives a side view of the sensor and substrate). The sensor dimensions are: length: 3 mm, width: 20 μm and height: 70 nm. In streamwise direction twenty-seven sensors with a spacing of 5 mm are available. The first sensor is positioned 2 mm behind the leading edge. A top view of the sensor geometry is given in figure 3.10.

The substrate is pasted on a 1 mm thick metal layer which acts as a heat sink. During the experiment the temperature of this plate is assumed to at remain its initial value.

When the temperature of the film changes, for example due to the change of temperature from the gas which flows along the sensor, the resistance will alter. From the measured resistance the temperature is derived. Finally, the heat flux in the substrate is reconstructed from the temperature history (in time) of the sensor (e.g. *Hogendoorn et al.* [1998]).

Two manners of operating the sensors can be distinguished. The first is using the sensor as a hot film device. In this mode the sensor is heated to approximately 200°C. A disadvantage of this technique is that due to the high sensor temperature the flow might be influenced. A second possibility is to use the sensors as a cold film. It has not the disadvantage as mentioned above and is often used in transient facilities (*Schultz et al.* [1980]).

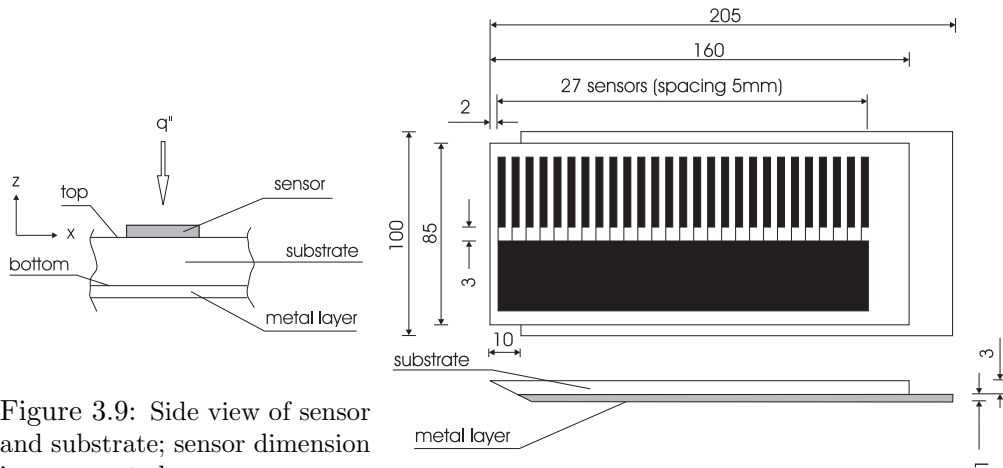


Figure 3.9: Side view of sensor and substrate; sensor dimension is exaggerated.

Figure 3.10: Sensor plate geometry; top view and side view are depicted.

The resistance of a thin film gauge is dependent on the temperature. For small temperature differences a linear approach can be used:

$$R_g = R_0[1 + \alpha_0(T_g - T_0)]. \tag{3.13}$$

In this equation α is the temperature coefficient and the index 0 refers to the reference temperature which is taken to be 20°C . All sensors are calibrated individually, with the temperature ranging from -3.0°C to 20°C . Typical values of R_0 and α_0 are $1.2\text{ k}\Omega$ and $2.2 \cdot 10^{-3}\text{ K}^{-1}$, respectively.

Measuring the sensor resistance during an experiment is possible in two ways. The first one is by using a constant current technique. During the whole experiment the current through the sensors is kept constant. The change of resistance results in a voltage change across the sensor which is:

$$\Delta V = V_g - V_0 = i(R_g - R_0) = V_0\alpha_0(T_g - T_0). \quad (3.14)$$

V_0 is the initial voltage across the sensor and i the current which remains constant. Some experiments were performed using the constant current technique. A simple N-FET electronic circuit was used for generating the current. However, it appeared that there were relatively large current fluctuations. As a result the signal-noise ratio was not high enough to detect individual turbulent spots. For that reason this technique is not used for the experiments described in this thesis.

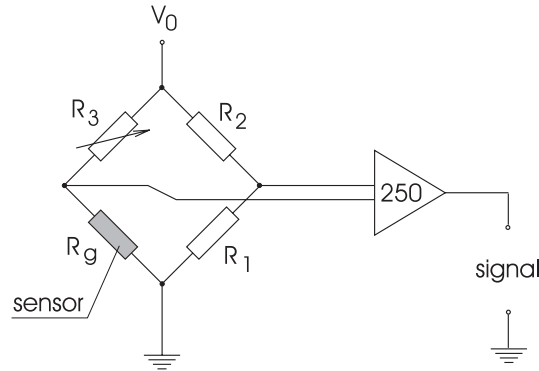


Figure 3.11: Wheatstone bridge.

Another possibility to measure the sensor resistance is to incorporate the sensor in a Wheatstone bridge (figure 3.11). Both the current through and the voltage across the sensor vary during the experiment. The sensor output can be written as (when $R_0\alpha_0(T_g - T_0) \ll R_1 + R_0$):

$$\Delta V = V_0\alpha_0(T_g - T_0) \frac{R_g}{R_g + R_3} \left(1 - \frac{R_g}{R_g + R_3}\right). \quad (3.15)$$

The value of V_0 is set to 10.0 V in all the measurements performed. With values of $R_1 = 270\text{ k}\Omega$ and $R_2 = 680\text{ k}\Omega$ and a balanced Wheatstone bridge, the sensor voltage is 3.0 V and the resulting sensor current is approximately 1.5 mA . When

the sensor temperature changes, also the sensor resistance changes and the bridge becomes unbalanced. The signal is amplified 250 times by an operational amplifier and recorded in a personal computer by means of an AT-MIO-16E interface board. For the data-acquisition, sixteen channels are available. All the flux experiments are triggered on the pressure signal, so the output of fifteen sensors can be recorded during one measurement. An advantage of triggering on the pressure, and not on a temperature signal, is the fast decay of the pressure when the membrane is ruptured. This implies that the start of the test time, for a certain Mach number, is determined unambiguously and thus independent of the flux obtained.

The heat flux resulting from the temperature difference between the expanded gas and the sensor plate, is assumed to be one dimensional. It is shown by *Schultz et al.* [1980] that this assumption is justified. For reconstruction of the heat flux, the one dimensional heat conduction equation perpendicular to the sensor plate surface is solved (z-direction):

$$\rho c \frac{\partial T}{\partial t} = \frac{\partial}{\partial z} \left(k \frac{\partial T}{\partial z} \right). \quad (3.16)$$

In this equation ρ , c and k are the substrate density, heat capacity and conductivity. These properties are well known ($\rho = 2550 \text{ kg/m}^3$, $c = 860 \text{ J/kgK}$ and $k = 0.92 \text{ W/mK}$). The boundary conditions used are the sensor temperature, which is determined by equation (3.13), and the bottom temperature of the plate, which is assumed to be constant during the experiment:

top:

$$T_s(t) = T_g(t) - T_0, \quad (3.17)$$

bottom:

$$T_b(t) = \text{constant} = 0. \quad (3.18)$$

The latter boundary condition is justified as the thermal front of the expansion does not reach the bottom of the plate in the duration of the experiment. *Diller* [1993] showed that this time equals:

$$t = \frac{\rho c D^2}{16k}, \quad (3.19)$$

where D is the substrate thickness. Using the properties for B-270 glass results in a required time of 1.3 s. As the complete expansion takes approximately 0.1 s, no problems occur.

A second order accurate finite volume method, with first order time integration, is used for solving equation (3.16) numerically. The computational domain is divided in 30 elements with grid refinement at the surface. When the temperature distribution is known as a function of time, the surface heat flux can be

calculated by solving Fourier's law:

$$q''(t) = k \frac{T_s(t) - T_{2nd}(t)}{\Delta z}. \quad (3.20)$$

The size of the first element in the numerical domain is Δz and the temperature at the first internal node (2nd nodal point) is T_{2nd} . This method of flux reconstruction is first order and the heat storage in the first element is neglected. *Hogendoorn* [1997] analysed the error by comparing the numerical solution with the analytical solution for a test case with a flux step function. He found that the deviation was less than 0.5%, so the present method is sufficiently accurate.

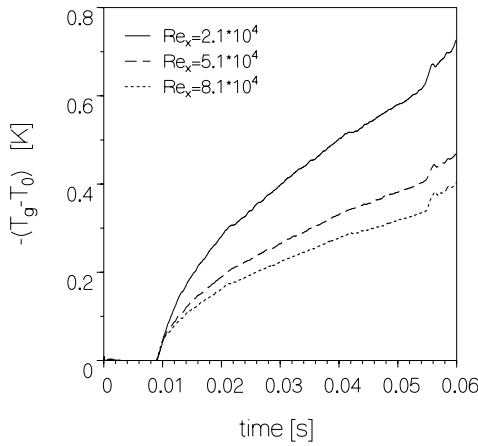


Figure 3.12: Temperature signal of three gauges at different streamwise positions (laminar flow).

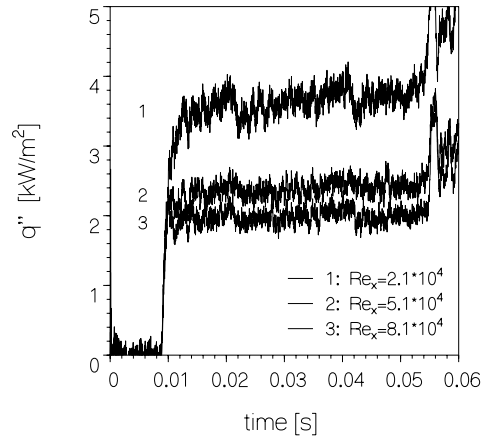


Figure 3.13: Reconstructed heat flux of three gauges at different streamwise positions.

An example of a temperature signal and the resulting heat flux is given in figures 3.12 and 3.13. No turbulence generating grid is used in this experiment, so the flow along the test plate is laminar. The outputs for three sensors at different positions in streamwise direction are depicted. It is seen that, when ignoring the noise, a nearly constant flux level is obtained during the test time.

To check the accuracy of the heat flux sensors, a series of laminar flow measurements is performed at several unit Reynolds numbers. As mentioned earlier, the maximum amount of sensors which can be recorded during a test run is fifteen. However, the number of sensors available is twenty-seven. For that reason two successive experiments are performed. The first run is taken with the odd numbered sensors, while the second experiment is done under the same conditions, but with the even numbered sensors connected. Afterwards, both measurements are combined. The result for $Re_u = 1.5 \cdot 10^6 \text{ m}^{-1}$ is depicted in figure 3.14. Also

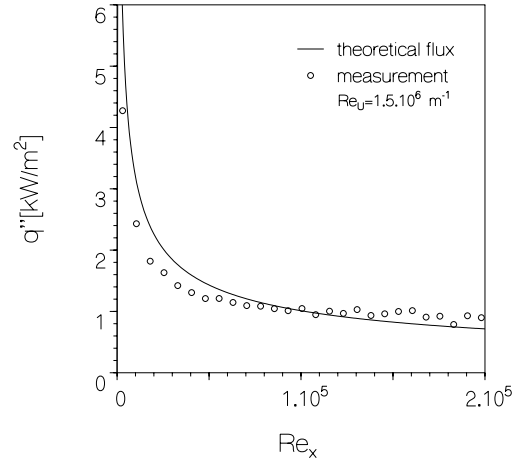


Figure 3.14: Laminar heat flux ($Re_u = 1.5 \cdot 10^6 \text{ m}^{-1}$).

the expected Blasius flux is shown:

$$q_l''(x) = 0.322 \frac{k}{x} (T_w - T_r) Re_x^{\frac{1}{2}} Pr^{\frac{1}{3}}. \quad (3.21)$$

T_r is the recovery temperature², which is a function of the Mach number:

$$T_r = T_\infty \left(1 + \frac{1}{2} (\kappa - 1) M^2 \sqrt{Pr} \right). \quad (3.22)$$

It is seen that the data have a slight deviation compared to the theoretical values. The two main reasons for this discrepancy are:

- Boundary layer start

The theoretical curve starts at the leading edge of the plate, i.e. it is assumed that the boundary layer has zero thickness at this position. However, when the initial value of the boundary layer is not zero, the start of the layer can be thought to be situated slightly before the leading edge. If this is the case the theoretical curve shifts somewhat to the left, and better agreement between measurements and theory is obtained.

- Pressure gradient

To avoid flow separation at the leading edge, the plate is mounted with

²In the case of an adiabatic flow along a surface, the wall temperature is expected to be the stagnation temperature. However, this temperature is somewhat smaller, denoted by the factor \sqrt{Pr} . The value of b is 2 for a laminar, and 3 for a turbulent boundary layer (*Lin* [1959]).

an angle of attack (2.4°) in the test section. For that reason there is a small favourable pressure gradient present in streamwise direction ($\frac{dp}{dx} < 0$; for subsonic flow). This gradient will accelerate the flow, resulting in an increase of the heat flux. The systematic increase is indeed visible in figure 3.14.

The aim of this thesis is to perform bypass transition research, i.e. how does the boundary layer react on large disturbances in the main flow? This means, for example, that it is required to distinguish between measurements *without* and *with* turbulence generating grids. To make an accurate distinction possible, a correction technique is applied. The assumption is that, for a certain unit Reynolds number, the heat flux corresponds to the expected Blasius curve. Deviations between the expected value and the measured value are removed by means of an in-situ calibration. Therefore, a correction factor for each individual sensor is introduced:

$$\mathcal{F} = \frac{q''_{measured}(sensor, Re_u)}{q''_{Blasius}}. \quad (3.23)$$

The heat flux measured in a transitional experiment is divided by \mathcal{F} . Using this method results in a heat flux which follows the Blasius solution in the laminar zone exactly. Now, the transition start can be recognized as a deviation from this curve. Point of discussion might be the fact that a multiplication factor is used to correct the data, and not for example, a certain value which is added or subtracted from the flux measured. The reason for this is that the present method gives the best results.

3.6 Unsteady-state test section

As seen before, it is possible to generate a flow with well-known properties in a Ludwig tube. The next step is to develop a test section to study wake induced transition. For this purpose a wake generator must be incorporated in the set-up. This paragraph describes the development of the new section. First several options for the generation of wakes will be treated. This results in the choice of the device as used for the unsteady transition measurements. The flow conditions differ compared to the original test section. Pressure and hot-wire measurements are performed to quantify these deviations.

Wakes can be generated by moving cylinders in perpendicular direction of the main flow. When this flow has a velocity U and the cylinder speed is V , a flow coefficient Φ can be calculated to characterize the wake:

$$\Phi = \frac{V}{U}. \quad (3.24)$$

Φ determines the angle ($\arctan \Phi$) between the wake and the test plate. If $\Phi = 0$, the flow behind a non-moving cylinder is obtained which is comparable

to turbulence generated by static grids. The latter case is steady instead of unsteady, so Φ must be large enough to obtain an unsteady situation.

In a turbomachine Φ has a value of about 1 (*Cohen et al.* [1996]). Due to the high mainstream velocity in the Ludwig tube, it is not possible to realize this value of Φ in the new set-up. Therefore, we state that Φ must reach values up to 0.3. If the same Mach number is used as for the steady-state experiments ($M = 0.34$; $U \sim 110$ m/s), the cylinder velocity should be 35 m/s, which is relatively high for a mechanical device.

By varying the diameter of a cylinder it is expected that the 'strength' of the wake can be regulated; large diameters result in strong wakes, while small diameters result in weak wakes. To study the influence of different wake types, it is required that the diameter can be altered easily ³.

The initial pressure regulates the unit Reynolds number in the Ludwig tube. In general this pressure is lower than the ambient value. Therefore, the wake generator must be incorporated in the test section.

From the arguments mentioned above, it follows that the main requirements for the wake generator are:

1. The flow coefficient must reach values up to 0.3.
2. There must be a possibility to change the cylinder diameter.
3. The complete wake generator must be incorporated in the test section due to the initial pressure desired.

3.6.1 Rotating cylinder cascade wake generator

A first wake generator of interest is a rotating cylinder cascade wake generator (sometimes denoted as 'rotating squirrel cage' wake generator). Measurements with this generator type are performed by *Pfeil and Herbst* [1979] and more recently by *Liu and Rodi* [1991] and *Orth* [1993]. Two rotating discs are placed at the side walls of a wind-tunnel. Between these discs, cylinders are mounted which move in front of the test plate (figure 3.15). To avoid disturbances, the rotating discs are screened from the tunnel by non-rotating plates. An advantage of this type of wake generator is that the manufacturing is not too difficult. Also, the incorporation in a test section is possible, while the size of the generator is mainly determined by the diameter of the discs. The cross sectional area of our Ludwig tube is 100×100 mm², resulting in a maximum disc diameter of approximately 95 mm and an 'effective' diameter of 90 mm. To obtain the

³It appeared that cylinders with $d = 5$ mm cause transition which starts at the leading edge, while cylinders with $d = 0.6$ mm cause transition which starts somewhere between the leading edge and the point where natural transition takes place. This implies that the appropriate diameter range lies between 0.6 mm and 5 mm.

required cylinder velocity, the rotational speed should be 7500 rpm, which is a rather high, but not an impossible demand.

There are two main disadvantages concerning the generated wakes. Due to the rotation, the cylinders do not move linearly across the main flow in the region where θ exceeds a certain value (see figure 3.15). According to *Liu and Rodi* [1991], this drawback is not critical, while the diameter of the rotating discs is much larger than the zone of interest, which is a few times the boundary layer thickness. So, the cylinders can be assumed to move perpendicular to the main flow.

The second disadvantage of a rotating squirrel wake generator is that strong and weak wakes are generated during one run. The strong wakes, are shed from the downwards moving cylinders, while the weak wakes are shed from the upwards moving cylinders, which are positioned more upstream. Orientation of the strong wakes is correct, whereas the weak wakes are mirrored due to the upward cylinder movement. Both types of wakes interact, resulting in a flow which is unrealistic for turbomachinery. The wake movement along the plate is depicted in figure 3.15. Wakes underneath the plate, i.e. at the pressure surface, are not drawn.

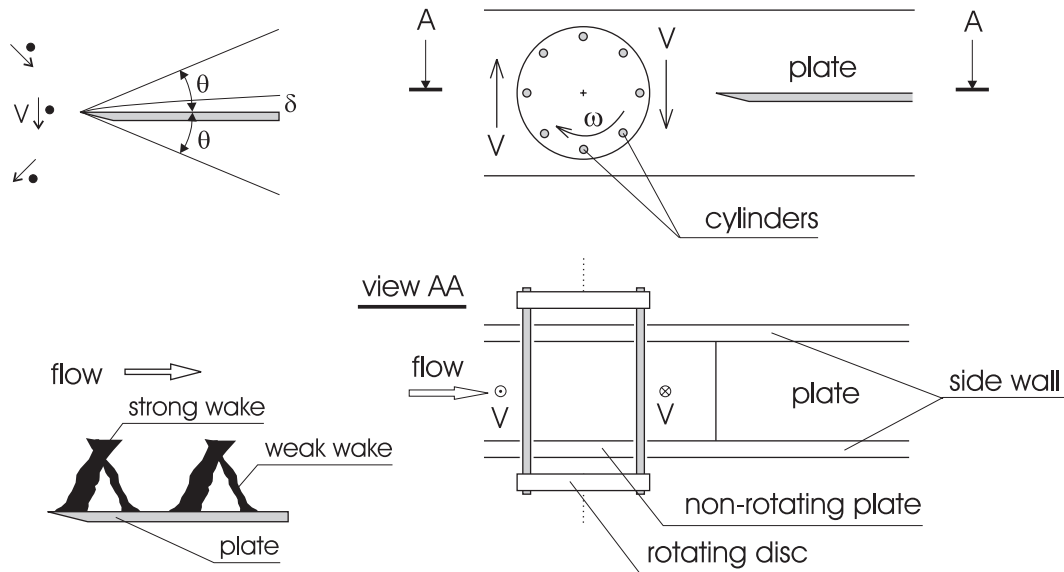


Figure 3.15: Rotating cylinder cascade wake generator.

3.6.2 Rotating wheel wake generator

Another possibility to generate wakes is by using a rotating wheel wake generator. Experiments with this apparatus along a plate are performed by *Funazaki*

[1996a,b], while high velocity cascade measurements are done by *O'Brien and Capp* [1989] and *Doorly* [1987]. The principle of this generator is a wheel with cylinders placed in radial direction (spokes). Figure 3.16 shows this set-up schematically. To create the required cylinder movement, the wheel is positioned outside the test section. The wake initiation is not ideal due to the rotation, i.e. the cylinders translate not exactly in front of the plate. This effect is avoided by positioning the wheel center at the same height as the plate (as is depicted). Another discrepancy arises from the fact that the cylinder velocity is dependent on the radius r . Minimizing this effect is done by taking the radius as large as possible. This immediately limits the use of a rotating wheel wake generator in a Ludwig tube. The complete wheel must be incorporated in the test section (requirement 3), so the size of this section becomes very large.

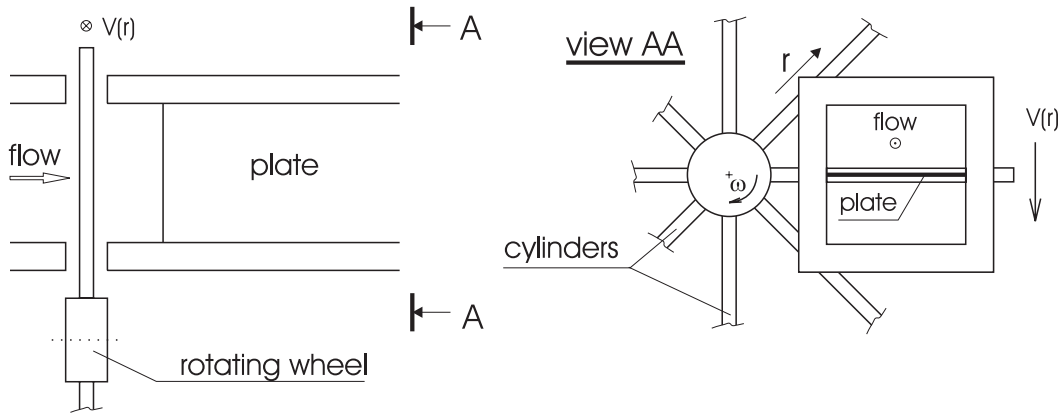


Figure 3.16: Rotating wheel wake generator.

3.6.3 Moving-belt wake generator

The third way to induce wakes is by means of a moving-belt wake generator. At each side wall, a belt is placed which runs along a number of discs. Between these belts the cylinders are attached. The main advantage is that the cylinder movement is ideal, i.e. the cylinders translate in front of the test plate. Cascade measurements, at low velocity ($V < 10$ m/s), are performed by *Dong and Cumpsty* [1990a,b] and *Schobeiri and Pappu* [1997].

Although a moving-belt wake generator is more complicated to manufacture than a rotating cylinder cascade wake generator, we decided to incorporate this generator in the Ludwig tube because of its ideal cylinder movement. Preliminary results of measurements in the modified set-up are described in *Schook et al.* [1999, 2000b] and *de Lange et al.* [2000].

The basis of the generator is the test section as used for the steady transition measurements. In figure 3.17 the modified section is shown schematically while photographs of the set-up are given in appendix B. At each side wall, a frame with four discs with a diameter of 160 mm is mounted. The opposite discs have a fixed position while they are connected by a shaft. One of the four shafts is driven by an electric motor placed outside the section.

Two belts with a length of 1500 mm run along a group of discs, so one belt on the left-hand side, and the other on the right-hand side of the test section. The belt width is 16 mm while the pitch is 5 mm, implying that 300 teeth are present on each belt. The number of teeth on a disc is 100, thus when a disc makes three rotations, the belt moves exactly one cycle. Four gaps, positioned every 90° , are present in a disc. This construction makes it possible to place the cylinders on the inner side of the belt. A maximum of twelve cylinders can be incorporated in the configuration as described above.

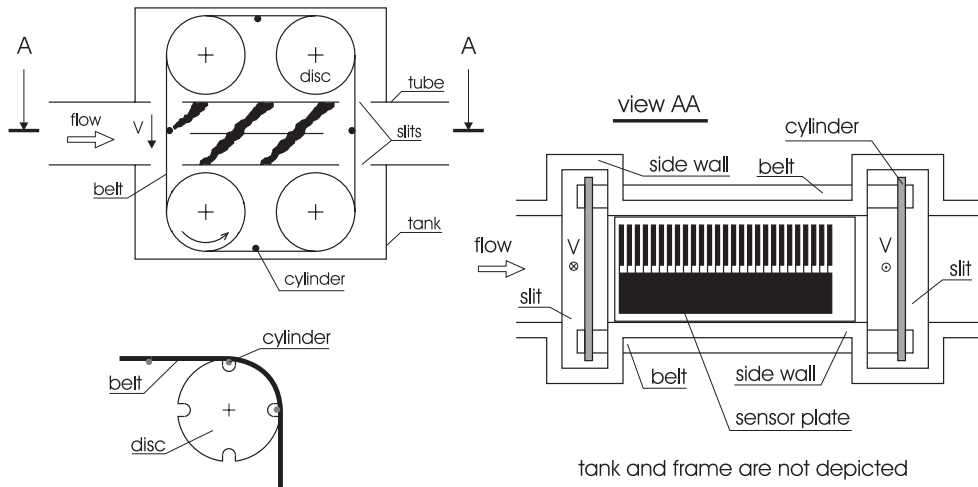


Figure 3.17: Moving-belt wake generator as used for the unsteady transition experiments. A schematic view of the disc-belt construction is also depicted; the cylinders are mounted on the inner side of the belt.

To make translation of the cylinder possible, slits are positioned in the upper and the lower section walls. The width of the slits most upstream is 20 mm while the width downstream is 60 mm. The leading edge of the plate is placed 40 mm behind the position where the center of the cylinders translates in front of this plate.

Velocities up to 35 m/s are required. Therefore, the disc diameter of 160 mm needs a rotational speed of 4200 rpm. The centrifugal acceleration due to the rotation ($\frac{V^2}{r}$) equals 15300 m/s². This high acceleration in combination with the relatively large span (180 mm), requires hollow cylinders which consist of carbon fibre. It appeared that cylinders with a diameter of 3 mm and 5 mm resist the high forces during rotation. To obtain wakes which are shed from 0.6 mm diameter cylinders, nylon wires are used. These wires also performed well at high velocities.

The complete wake generator is surrounded by a tank, with inner dimensions: 400 x 400 x 630 mm³. This tank is essential because the initial pressure should reach values below atmospheric as stated as one of the major requirements. A pressure difference of 0.5 bar results in a force of approximately 25000 N on the side walls. To handle this force, the tank is made of aluminium with a thickness of 30 mm. The driven shaft and the electrical wires for the hot-wire and the thin film gauges are led outwards by means of a special sealing.

Due to the tank and the slits in the upper and lower walls, the test section geometry is not ideal. In an ideal Ludwig tube the test section mainly consists of a tube in which the expansion wave can move without interacting with obstacles. However, incorporating the wake generator results in a secondary flow from the tank to the test section. This is explained as follows.

Prior to an experiment, the pressure in the tube, test section and wake generator are equal. When the experiment begins, the expansion wave starts travelling into the test section. As a result the pressure decreases, and air from the tank flows through the slits in the test section. Therefore, the according conditions in the unsteady-state test section, differ from the conditions obtained in a steady-state section. Minimizing the secondary flow effect can be achieved by reducing the free volume in the wake generator. This is realised by filling the tank with foam at places where no rotating parts are situated. It appeared that the volume reduces from about 0.15 m³ to 0.02 m³, which is 20% of the volume of the 10 m long tube itself.

To check the conditions in the new set-up pressure measurements are performed. A Viatran pressure gauge is mounted at the same position as was the case for the steady-state test section (20 mm behind and 25 mm above the leading edge). Figure 3.18 shows the pressure ratio, i.e. the pressure in the test section divided by the initial pressure. Two signals are shown, the first one is with the choking orifice, which is also used for the steady-state experiments ($D = 87.2$ mm), while the second signal is recorded for a choking orifice with a larger diameter ($D = 94.0$ mm). It is seen that not a (nearly) constant pressure ratio is obtained for the time which is supposed to be the test time for the steady experiments (between 0.02 s and 0.06 s). The ratio decreases during the measurement, implying that the Mach number is not constant either. It is assumed that the deviations obtained, are a result of the geometry in the test section, as described earlier. Mach number distributions for both choking orifices are depicted in fi-

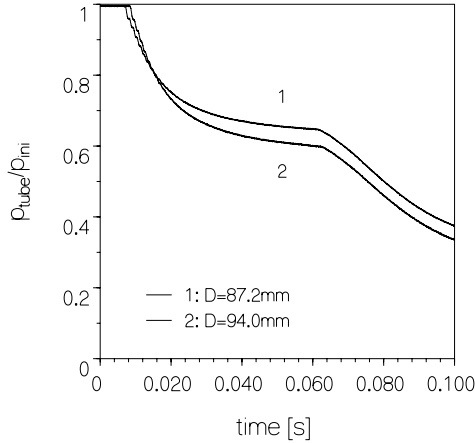


Figure 3.18: Pressure signal for the test section including the wake generator for two different choking orifices ($Re_u = 3.0 \cdot 10^6 \text{ m}^{-1}$).

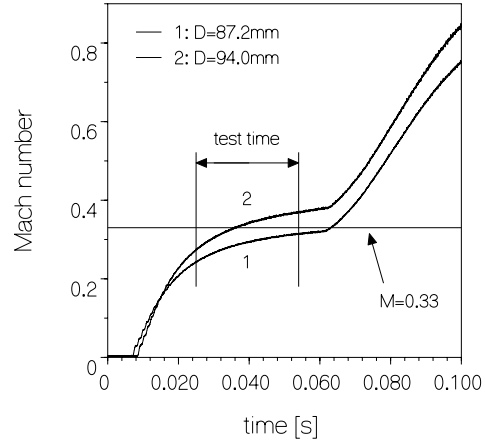


Figure 3.19: Mach number as a function of time for the section including the wake generator; test time is assumed to be 29 ms.

figure 3.19⁴. The test time for the new set-up is defined as the time during which the Mach number is almost constant as well as no reflections are visible in the hot-wire and flux measurements. It appeared that the test time duration is 29 ms, situated in the range: $0.025 \text{ s} < \text{test time} < 0.054 \text{ s}$. In case of the maximum cylinder velocity (35 m/s), within this definition exactly eight wake passings are present during the test time.

The mean Mach number is used for characterizing the flow velocity. This results in a Mach number of 0.29 when the same choking orifice as in the steady-state test section is used. For comparison, the Mach number in the steady-state test section is 0.35. To obtain a larger mean Mach number, the diameter of the orifice is increased ($D = 94.0 \text{ mm}$). All experiments with the unsteady-state test section are performed with this orifice, generating a mean Mach number of 0.33.

One remark should be made concerning the Mach number. It is found that the unsteady-test section shows a small Mach number dependence on the unit Reynolds number. Increasing Re_u from $1.5 \cdot 10^6 \text{ m}^{-1}$ to $3.0 \cdot 10^6 \text{ m}^{-1}$ results in an increase of the Mach number from 0.33 to 0.34. Probably this is due to the geometry which is not ideal. However, reproducibility of the flow conditions is found to be very good (within 0.08% concerning the mean Mach number).

Also it is checked whether it is possible to obtain a laminar boundary layer in

⁴For determining the Mach number equation (3.6) is used. However, due to reflections in the test section the calculation of the Mach number by use of this equation is not completely accurate.

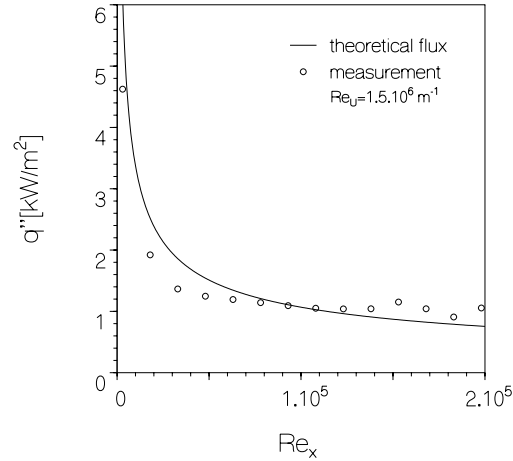


Figure 3.20: Laminar heat flux in the unsteady-test section ($Re_u = 1.5 \cdot 10^6 \text{ m}^{-1}$).

the new test section. Therefore, experiments are performed without a turbulence generating grid. It appeared that when the unit Reynolds number is less than $3.5 \cdot 10^5 \text{ m}^{-1}$, results are obtained which are comparable to those in the original set-up. Figure 3.20 shows the measurement for a unit Reynolds number of $1.5 \cdot 10^5 \text{ m}^{-1}$. Only, the even numbered sensors are connected in this experiment.

3.7 Conclusions

In this chapter the test sections for the steady as well as for the unsteady transition experiments are described. Steady-state experiments can be executed in an original Ludwig tube set-up, which has the advantage that the Mach number and the Reynolds number can be adjusted independently. Background turbulence is generated by means of static grids. Flow conditions are determined by hot-wire and pressure measurements and they show good reproducibility.

For performing unsteady transition experiments the test section is modified. Incorporation of a moving-belt wake generator is realised by making slits in the upper and lower walls of the section. The generator is able to translate cylinders with high velocity in front of the leading edge of the test plate. The wake characteristics can be altered by changing the cylinder diameter and/or their velocity.

Due to the geometry change, the flow conditions compared to the original Ludwig tube set-up are slightly different. The Mach number is not constant during the test time, but an increase of 20% is observed. Therefore, a mean

Mach number is used to determine the flow conditions. A small unit Reynolds number dependence is found; increasing this number gives a slight enlargement of the Mach number. However, reproducibility showed to be comparable with an original Ludwig tube. Therefore, it is concluded that well defined unsteady flows can be generated. Keeping in mind the restrictions as listed, the new section is suited for performing unsteady boundary layer transition experiments.

Chapter 4

Steady transition measurements

In this chapter the steady transition measurements are described. First the heat flux measurements in a transitional boundary layer are presented. From these measurements the intermittency distributions are calculated. It follows that for low turbulence levels very good agreement with literature is found. However, for intermediate and high turbulence levels, the existing models fail in describing the intermittency. A new model, based on the occurrence of turbulent spots which do not grow, is found to perform very well. A length scale analysis shows that the present measurements are done in a different parameter range compared to literature. Part of this chapter is published in *Schook et al.* [2000a].

4.1 Heat flux measurements

To determine the influence of the mainstream turbulence on boundary layer transition, heat flux measurements are done. These measurements are performed for the several turbulence generating grids at a Mach number of 0.34 (grid properties like the bar diameter, mesh size and turbulence level are discussed in chapter 3). The unit Reynolds number in the test section is adjusted such that the transition region covers a few centimetres of the plate. This implies that the number of sensors, situated in the transition zone, is sufficient to study the heat transfer in this region.

An example of the time dependent heat flux for several sensors is given in figure 4.1. It shows the heat flux for an experiment with the 1H grid at a unit Reynolds number of $3.0 \cdot 10^6 \text{ m}^{-1}$. The heat fluxes are plotted on the same y -scale but shifted vertically. The sensor positions are given in terms of the Reynolds number on the vertical axis on the right hand side. At $t = 0.01 \text{ s}$, the diaphragm is ruptured and the experiment starts.

It is seen that the sensor positioned at $Re_x = 0.36 \cdot 10^5$ has a nearly constant

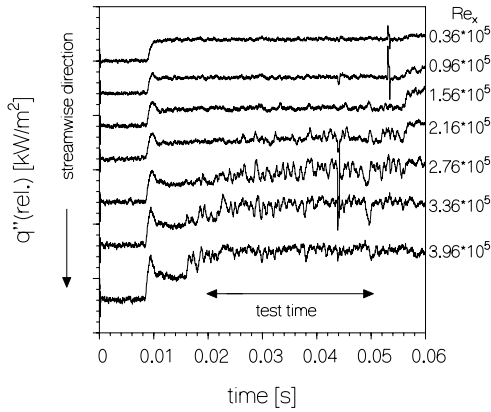


Figure 4.1: Measured heat flux for several sensors as a function of time for the 1H grid ($Re_u = 3 \cdot 10^6 \text{ m}^{-1}$).

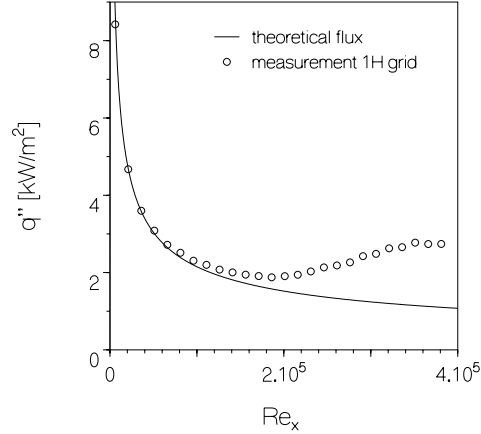


Figure 4.2: Time mean heat flux in streamwise direction for the 1H grid ($Re_u = 3 \cdot 10^6 \text{ m}^{-1}$).

output. In streamwise direction, spikes start to become visible in the signal. These spikes, which show an increase in heat flux, are the turbulent spots and will be treated further in section 4.3.2.

Also the test time is depicted in figure 4.1. For this experiment, the test time is assumed to be 30 ms instead of the 40 ms as described in chapter 3 (40 ms is the time the pressure in the test section is nearly constant). The reason for this is that after about 55 ms the heat flux at the first sensors starts to increase slightly. Therefore, the conditions in the set-up are not constant anymore, so the heat transfer experiment is assumed to end at this time.

There are twenty-seven sensors available on the sensor plate. However, the maximum number of channels which can be registered in one experiment is sixteen. For this reason the heat flux measurements have to be performed twice. The first experiment is taken with the odd numbered sensors connected, while the second experiment is taken with the even numbered sensors. Afterwards both measurements are combined.

The mean heat flux during the test time is depicted in figure 4.2. Also the theoretical heat flux, according to equation (3.21), is given. It is seen that the first sensors show a laminar flux level. At a Reynolds number of about $1.0 \cdot 10^5$ the flux starts to deviate from the theoretical flux. However, the absolute value still decreases in downstream direction. At a certain position the heat flux obtains a minimum ($Re_x = 1.6 \cdot 10^5$), after which the value of the mean flux level starts to increase. In the time dependent flux (figure 4.1) the spikes now can be observed clearly.

4.2 Intermittency calculation

The intermittency at a certain streamwise position is defined as the fraction of time the flow is turbulent on that position. However, based on the assumption that in a turbulent spot the heat flux has the turbulent value, another manner is used to define the intermittency. On basis of the time mean heat flux, $\overline{q''(x)}$, the intermittency can be written as the ratio:

$$\gamma(x) = \frac{\overline{q''(x)} - q_l''(x)}{q_t''(x) - q_l''(x)}. \quad (4.1)$$

In this equation $q_l''(x)$ and $q_t''(x)$ are the laminar and the turbulent heat flux, respectively.

When the intermittency is zero, the time mean flux has the laminar value, $q_l''(x)$, and when the intermittency is one the flux has the turbulent value, $q_t''(x)$. The mean heat flux is calculated by:

$$\overline{q''(x)} = \frac{1}{t_2 - t_1} \int_{t_1}^{t_2} q''(x, t) dt, \quad (4.2)$$

where the time interval $t_2 - t_1$ is the time in which the flow conditions in the Ludwig tube are constant (test time is 30 ms for the present experiments).

Determining the intermittency by means of the friction coefficient was already done by *Dhawan and Narasimha* [1958]. The heat flux analogy used here, was proposed by *Chen and Thyson* [1971]. This approach follows from the Reynolds analogy which describes that the friction coefficient and the heat flux are related. The Prandtl number determines this relation: $Pr = \frac{\nu}{\alpha}$, with ν the kinematic viscosity and α the thermal diffusivity. In the case that the Prandtl number is one the velocity and the temperature profiles in the boundary layer are similar.

For a non-accelerating flow, the heat fluxes in the boundary layer developing along a constant temperature surface are (*Schlichting* [1979], *Kays and Crawford* [1980]):

laminar:

$$q_l''(x) = 0.332 \frac{k}{x} (T_w - T_r) Re_x^{\frac{1}{2}} Pr^{\frac{1}{3}}, \quad (4.3)$$

turbulent:

$$q_t''(x) = 0.0287 \frac{k}{x} (T_w - T_r) Re_x^{0.8} Pr_t^{0.6}. \quad (4.4)$$

The equation for a turbulent boundary layer (equation(4.4)) is valid for: $0.5 < Pr_t < 1.0$ and $5 \cdot 10^5 < Re_x < 5 \cdot 10^6$. In both equations T_r is the recovery temperature which is a function of the Mach number:

$$T_r = T_\infty \left(1 + \frac{1}{2} (\kappa - 1) M^2 \sqrt{Pr}\right). \quad (4.5)$$

The ratio of the specific heats, κ , has the value 1.4 for air. The value of b is 2 for a laminar and 3 for a turbulent boundary layer (*Lin* [1959]). For a laminar boundary layer the Prandtl number is 0.72, while for a turbulent boundary layer an appropriate value is: $Pr_t = 0.9$. Both values are valid for ambient air in the temperature and pressure ranges as used in this thesis. Of course there is a difference in the validity of equations (4.3) and (4.4). Equation (4.3) follows from boundary layer analysis and is exact, while equation (4.4) is fitted to a data set. Therefore, the validity range of the latter equation is added to this equation.

A more common way to compare heat flux experiments is to present the fluxes in terms of the Stanton number:

$$St = \frac{q''(x, t)}{(T_w - T_r)kRe_u Pr}. \quad (4.6)$$

The intermittency also can be expressed in terms of the Stanton number:

$$\gamma(x) = \frac{\overline{St(x)} - St_l(x)}{St_t(x) - St_l(x)}. \quad (4.7)$$

The Stanton number distribution for the flow with a constant velocity along a semi-infinite plate with constant surface temperature follows by substitution of equations (4.3) and (4.4) in equation (4.6). For a laminar boundary layer this becomes:

$$St_l(x) = 0.322Pr^{-\frac{2}{3}}Re_x^{-\frac{1}{2}}, \quad (4.8)$$

and for a turbulent boundary layer (dividing by Pr_t instead of Pr):

$$St_t(x) = 0.0287Pr_t^{-0.4}Re_x^{-0.2}. \quad (4.9)$$

However, a problem occurs by applying equation (4.7) directly since St_t and St_l are based on different reference conditions, particularly via the recovery temperature. The reason for this is that Pr and b are different for laminar and turbulent boundary layers. Furthermore, the values for Pr and b are unknown in the transition zone. Therefore, St_t can not be calculated straightforward from equation (4.9).

To make the Stanton number applicable for determining the intermittency, the laminar values, i.e. $b = 2$ and $Pr_t = Pr = 0.72$, are taken as a reference in the complete boundary layer. Therefore, the resulting turbulent Stanton number becomes:

$$St_t(x) = C Re_{x-x_t}^{-0.2}, \quad (4.10)$$

with C a constant which will be determined for each experiment by a data fit.

4.3 Stanton number and intermittency distributions

To compare the fluxes for several heat transfer experiments the data are transformed to Stanton numbers (equation (4.6)). In this transformation the laminar values for b and Pr are taken ($b = 2$ and $Pr = 0.72$). Results of the measurements for the 2 and 3 mm grids are given in figure 4.3, while the 1 and 4 mm grid experiments are depicted in figure 4.4 (characterization of the grids is done in chapter 3). Also the theoretical laminar flux (equation(4.8)) is depicted. Clearly, it is seen that the turbulence generating grids have a large effect on the heat transfer distributions. Also note the significant difference on the streamwise positions of the points where the flux starts to deviate from the laminar value. There is a strong dependence of the turbulence level on the onset of transition.

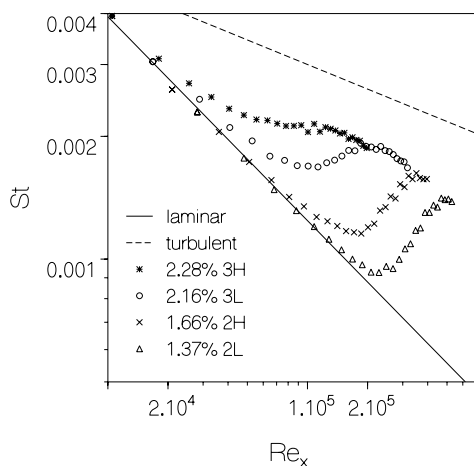


Figure 4.3: Stanton number distributions for various grids ($Re_u = 3 \cdot 10^6 \text{ m}^{-1}$, $M = 0.35$).

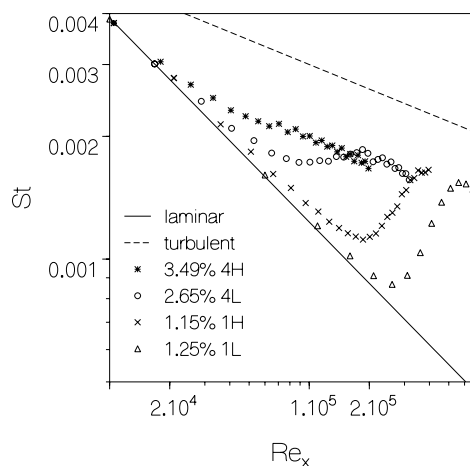


Figure 4.4: Stanton number distributions for various grids ($Re_u = 3 \cdot 10^6 \text{ m}^{-1}$, $M = 0.35$).

The heat flux distributions are comparable to those of *Blair* [1983a,b] obtained for low mainstream velocities (30 m/s, i.e. $M \sim 0.1$). However, the turbulence level giving a certain distribution is lower in our case (the results of a turbulence level of 1.25% are comparable to Blair's 2% distribution). This trend was also observed in earlier experiments (*Hogendoorn* [1997], *Hogendoorn et al.* [1997] and *Schook et al.* [1998]), where it was argued that increasing the Mach number results in a decrease of the turbulence level, while no influence on the transition was recognized (when the turbulence grid is unchanged). This indicates that the structure of turbulence has a more significant effect on transition than the turbulence level itself.

The turbulent heat transfer is approximately 60% of the expected turbulent

Table 4.1: Values of C and Re_{xt} .

grid	C	$Re_{xt} \cdot 10^{-4}$	—	grid	C	$Re_{xt} \cdot 10^{-4}$
4H	0.0197	1.11	—	3L	0.0209	0.99
4L	0.0196	1.31	—	2H	0.0206	4.97
3H	0.0224	1.21	—	1H	0.0215	6.03

flux as given by equation (4.4). In both figures the turbulent flux according to $Pr_t = 0.9$ is added. It also can be seen that the turbulent value is dependent on the turbulence generating grid, i.e. a non unique turbulent flux level is obtained for the different experiments. In chapter 5 the absolute values of the heat flux will be treated further. Now the attention is given to the intermittency distributions.

In order to obtain a useful definition of the intermittency, i.e. zero in the case of a laminar boundary layer and unity in a turbulent boundary layer, a data fit through the turbulent part according to equation (4.10) is used:

$$St_t = C Re_{x-x_t}^{-0.2}. \quad (4.11)$$

In this equation the transition start x_t is the point where the heat transfer starts to deviate from the laminar curve. This data fit is applied for each grid individually. In table 4.1 the values of C and Re_{xt} are given. The resulting intermittency distributions are shown in figure 4.5.

Characterization of the distributions can be done by means of the turbulence level. A distinction is made in terms of 'low', 'high' and 'intermediate'. It is not possible to give a sharp distinction for the designation of 'low', 'intermediate' and 'high' in terms of the turbulence level. The reason for this is that besides the turbulence level, length scales play an important role. However, a rough estimation for our case is: 'low': $Tu < 1.2\%$; 'intermediate': $1.2\% < Tu < 2\%$; 'high': $Tu > 2\%$. These are estimations for the mainstream turbulence levels at the transition start (see also section 4.6). Each subdivision will be part of a forthcoming section.

4.3.1 Low turbulence levels

Models which describe the intermittency are based on the assumption that turbulent spots develop after a certain Reynolds number based on the momentum thickness, Re_θ , has been reached. *Dhawan and Narasimha* [1958] assume that spots originate with a Gaussian distribution around the transition start x_t . Added to the assumption that the spots form at an infinitesimal size at one streamwise position with a rate of n per meter span per second, the Narasimha model is obtained (see also chapter 2). The Narasimha model assumes a constant spreading rate of the spot. This rate is characterized by a non-dimensional parameter

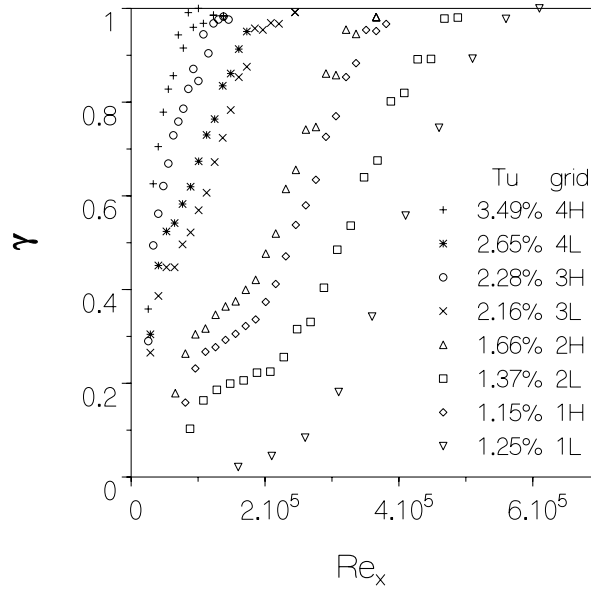


Figure 4.5: Intermittency distributions for all possible combinations of turbulence grids and grid positions. Turbulence level recorded at the streamwise position 27 mm upstream of leading edge (Tu_1 position).

σ , which depends on the spot growth angle α and the trailing and leading edge velocities of the turbulent spot (equation (2.3)). A more in depth discussion of the spot production rate is given in appendix A.

As given by equation (2.5), the Narasimha intermittency distributions in terms of the mainstream velocity is:

$$\gamma(x) = 1 - \exp\left[-\frac{\sigma n(x - x_t)^2}{U}\right]. \quad (4.12)$$

Johnson and Fashifar [1994] extended the model by taking $\frac{\sigma n}{U}$ not constant but a linear function of the streamwise distance. This results in the Johnson intermittency distribution (equation (2.19)):

$$\gamma(x) = 1 - \exp[-\mathcal{J}(x - x_t)^3]. \quad (4.13)$$

It should be noted that a similar distribution, i.e. third order dependence on the streamwise distance, was already proposed in the original paper of *Emmons* [1951] (see also chapter 2) by assuming not a point wise (at x_t) but a distributed (constant along x) breakdown of turbulent spots.

The start of boundary layer transition can be defined in several manners. The definition applied here is that the start of transition takes place when turbulent

spots are initiated. These spots influence the heat transfer as well as the friction coefficient. So, the point where the heat transfer and/or the friction coefficient starts to deviate from the expected value in the laminar case, is defined as the transition start ¹.

It should be noted that the here observed deviation from the measured heat flux compared to the laminar flux is not a result of a pressure gradient. The reason for this is that these effects, which are small in the present set-up (*Hogendoorn* [1997]), are cancelled out by sensor calibration and correction of the sensor output as described in chapter 3. This implies that the deviation is due to boundary layer transition.

To determine the start in accordance with the present definition applied, *Narasimha* [1957] transformed the intermittency by:

$$F(\gamma) = [-\ln(1 - \gamma)]^{1/s}. \quad (4.14)$$

Transforming a real *Narasimha* intermittency distribution with $s = 2$ results in a straight line. The start is obtained by taking $F(\gamma) = 0$, while the transition length depends on F by: $\sqrt{n\sigma\nu^2/U^3} = \text{slope } F$. Similarly, the transformation with $s = 3$ is used to see whether an intermittency follows the Johnson model.

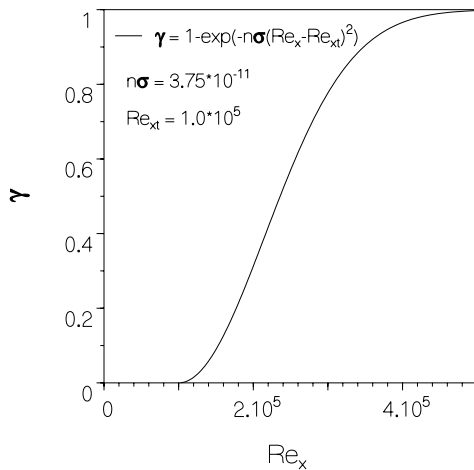


Figure 4.6: Theoretical *Narasimha* intermittency distribution, the chosen values are arbitrarily.

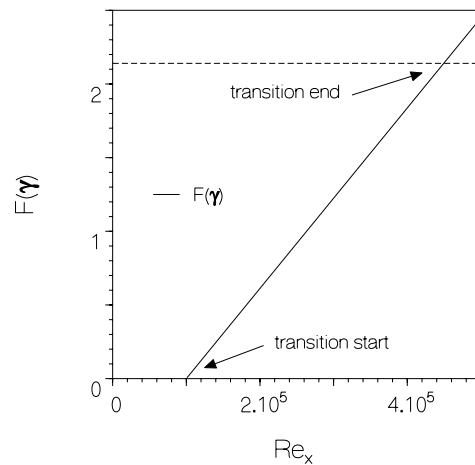


Figure 4.7: Transformed intermittency distribution of figure 4.6 for determining the transition start and the transition end.

¹Another definition is that the transition start takes place at the point where the heat flux and/or the friction coefficient obtains a local minimum. However, as can be seen in figures 4.3 and 4.4, this definition is not applicable for turbulence generating grids with large diameter bars because a local minimum can not be recognized.

An example of a typical Narasimha distribution is shown in figure 4.6 ($n\hat{\sigma} = 3.75 \cdot 10^{-11}$ and $Re_{xt} = 1.0 \cdot 10^5$). Figure 4.7 depicts the transformed intermittency distribution, in which it is assumed that the transition ends when $\gamma = 0.99$. This latter assumption corresponds to $F = 2.14$. The transition start and the transition end are marked in the figure.

In figure 4.8 the intermittency distribution for the 1L grid is shown. Figure 4.9 gives the function F for the experiment with the 1L grid. It is seen that the latter part of F indeed follows a line while the first part deviates. The discrepancy can be understood if turbulent spots do not originate at one fixed streamwise position but in a small area around this position. The Johnson model appears to give a better description of the intermittency distribution for the 1L grid, especially for the transition start.

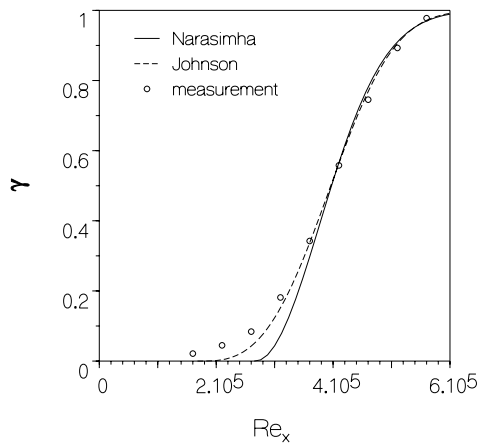


Figure 4.8: Intermittency distribution for the 1L grid.

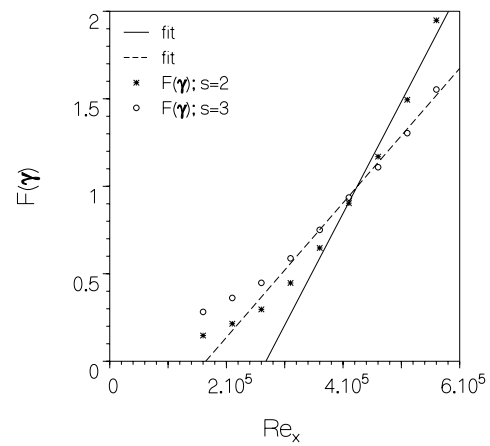


Figure 4.9: Transformed intermittency distribution for the 1L grid.

4.3.2 Turbulent spots

Individual turbulent spots can be recognized in the heat flux signals. The output for several sensors in the transition zone for the 2L grid and the 1H grid are given in figure 4.10 and figure 4.11, respectively (sampling frequency of the signals: 50 kHz). These fluxes are plotted on the same y -scale but shifted vertically. Note the difference in the Reynolds number based on the streamwise position, given on the right hand side of each picture.

In the output of the first sensors (most upstream of the plate) no spots are recognized in the signal. After a certain Reynolds number, spikes start to become clearly visible. These spikes, which are the turbulent spots, can be seen to grow

and convect in streamwise direction. An example of the spot growth and movement is indicated in figure 4.10 (the similarity of spots is discussed in *de Lange et al.* [1998]).

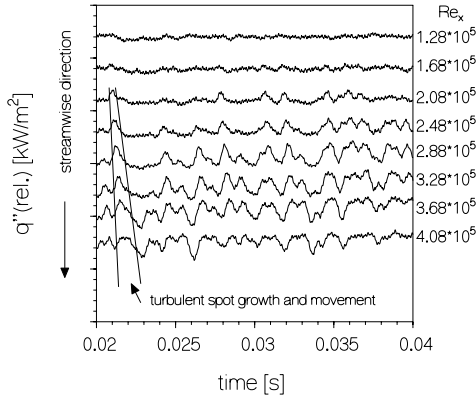


Figure 4.10: Heat flux signal for several streamwise sensors for the 2L grid ($Re_u = 4 \cdot 10^6 \text{ m}^{-1}$).

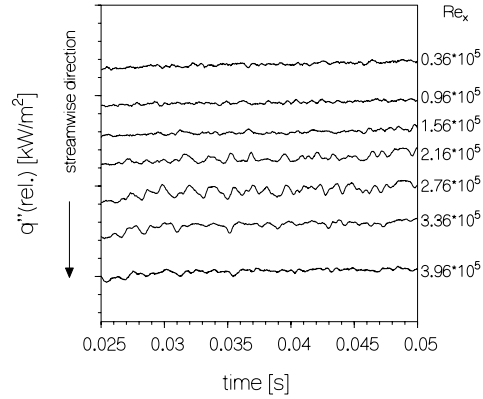


Figure 4.11: Heat flux signal for several streamwise sensors for the 1H grid ($Re_u = 3 \cdot 10^6 \text{ m}^{-1}$).

Cross-correlation of the output (sampling frequency 380 kHz) of two sensors, situated at $Re_x = 2.28 \cdot 10^5$ and $Re_x = 2.68 \cdot 10^5$, gives the mean velocity of the spots. The spot velocities, as related to the mainstream velocity, found for the several grids are given in table 4.2 (accuracy $\pm 2\%$). All the correlation experiments are performed at a unit Reynolds number of $4 \cdot 10^6 \text{ m}^{-1}$.

Table 4.2: Mean spot velocities.

grid	relative spot velocity [%]	Tu level [%]
2H	74	1.66
2L	64	1.37
1H	80	1.15
1L	75	1.25

From the table no distinct relation is observed between the grid size, the turbulence level and the spot mean velocity. The results found here can be compared to for example *Clark et al.* [1994] who performed measurements in an Isentropic Light Piston Tunnel (ILPT) to determine the velocity of natural occurring turbulent spots. They found that for a Mach number of 0.25 and 0.55 the mean velocity of the spots was 65% of the mainstream velocity. *Ching and LaGraff* [1995] did experiments at several unit Reynolds numbers in a Ludwig

tube with Isentropic Compression Heating (LICH). For a unit Reynolds number of $2.4 \cdot 10^6 \text{ m}^{-1}$ they found a mean spot velocity of 68% and for a unit Reynolds number of $4.2 \cdot 10^6 \text{ m}^{-1}$ they found a velocity of 63%. Therefore, the values listed in table 4.2 are slightly higher than the velocities which are found for naturally occurring spots. Due to the relatively low signal to noise ratio, no attempt has been made to distinguish between the leading- and trailing edge velocities of the turbulent spots.

4.3.3 High turbulence levels

The intermittency distributions for the 3H and 4H grids are depicted in figure 4.12. It is seen that the typical Narasimha shape is not found for these distributions. However, some kind of exponential growth can be recognized. The transition of the 4H grid seems to be completed earlier than the distribution for the 3H grid. Also, the intermittency at a certain streamwise position for the 4H grid is larger than for the 3H grid.

As the Narasimha and the Johnson models (equations (4.12) and (4.13)) do not describe the intermittency well, another model is developed. With this model it is aimed to describe the exponential growth of the intermittency. It is assumed that the turbulent spots are initiated not only at one streamwise position but along the whole distance in the transition zone. So, this hypothesis is identical to the one proposed by *Emmons* [1951]. Spots are assumed to enter the boundary layer at a rate of m per meter in streamwise direction per meter in spanwise direction (note that the dimension of m is different compared to that of n). A second assumption is that the spots enter the boundary layer, with an initial size w , in a boundary layer which is intrinsically stable. Therefore the spots do not grow. The resulting equation for the streamwise intermittency is:

$$\frac{d\gamma}{dx} = mw(1 - \gamma), \quad (4.15)$$

and the corresponding boundary condition is that $\gamma = 0$ for $x = x_t$. The solution is described by an exponential distribution:

$$\gamma(x) = 1 - \exp[-mw(x - x_t)]. \quad (4.16)$$

In figure 4.12 it is seen that a good agreement with the measured results is found for the exponential model. So, apparently the hypothesis of no spot growth in combination with a distributed spot production fits the measurements.

When an exponential intermittency distribution is transformed according to equation (4.14) with $s = 1$, a straight line is obtained ($F(\gamma) = 4.61$ corresponds to $\gamma = 0.99$). Figure 4.13 shows this transformation for the 4H and the 3H grid. Also the transformation for the Narasimha distribution ($s = 2$) is depicted. It is seen that the Narasimha distribution is not realistic to occur for these grids, because a virtual transition start would be situated too much in front of the

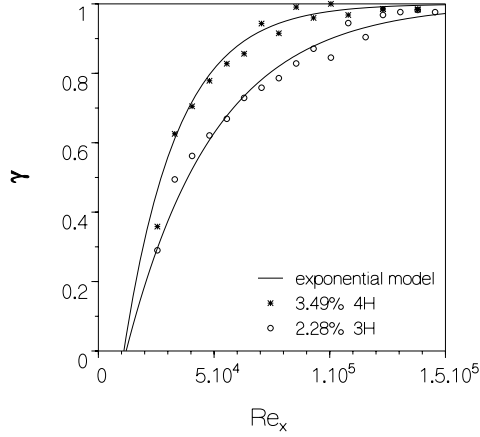


Figure 4.12: Intermittency distributions for the 4H and 3H grids compared to the exponential model. Lines are the best fits through the data points.

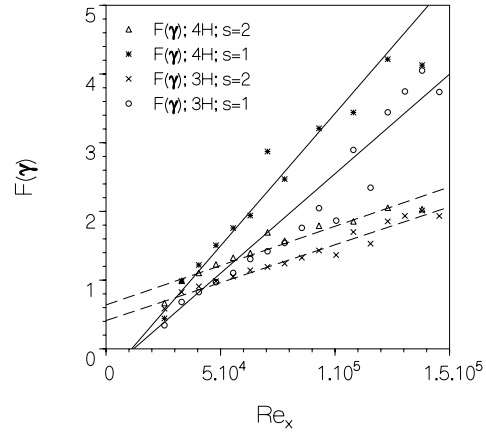


Figure 4.13: Transformed intermittency distributions for the 4H and 3H grids. Full lines: exponential model fit. Dashed lines: Narasimha model fit.

Table 4.3: Parameter values.

grid	mw	$Re_{xt} \cdot 10^{-4}$
[-]	$[m^{-1}]$	[-]
4H	65	1.1
3H	39	1.2

leading edge (dashed lines). This is in contradiction with the output of the first sensors which show a laminar heat flux.

The numerical values of the model parameters, i.e. the product mw and the Reynolds number at the transition start, are given in table 4.3.

4.3.4 Intermediate turbulence levels

The intermittency distributions for intermediate turbulence levels are shown in figure 4.14 and figure 4.15. It is seen that the intermittency can not be described well by either the Narasimha, Johnson or exponential model. The first part of the distribution shows an exponential growth towards a value not equal to one. After reaching a certain Reynolds number, the intermittency suddenly starts to increase and the typical Narasimha curve is followed during this stage. An attempt is made here to describe these distributions by coupling two mechanisms of the turbulent spot growth.

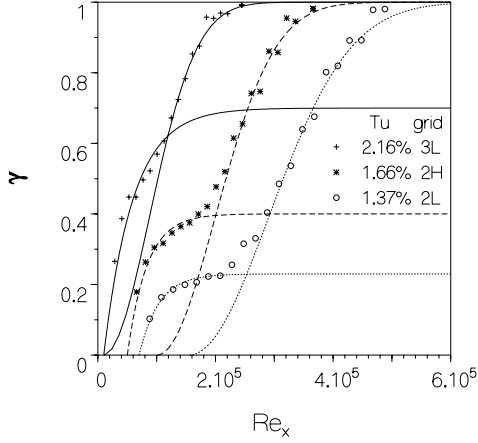


Figure 4.14: Intermittency distributions for the 2L, 2H and 3L grid compared to the pre-transition model.

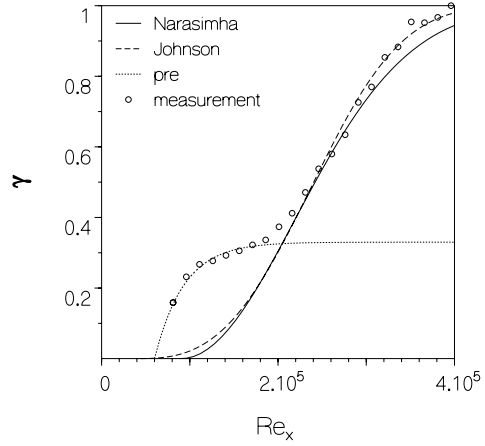


Figure 4.15: Intermittency distribution for the 1H grid compared to the several models.

Our hypothesis is that during the first part of transition, defined as the pre-transition part, spots are able to enter the boundary layer but decrease in size due to diffusion in the still stable boundary layer. After a certain Reynolds number the boundary layer will become unstable, spots start to grow and the conventional route to turbulence, according to the Narasimha model, is followed. It is likely that the spot growth parameter, or for present purpose: a spot decay parameter, is a function of the streamwise distance. However, for simplification this is not incorporated in the model. The equation describing the pre-transition zone with decreasing turbulent spot size is:

$$\frac{d\gamma}{dx} = -k\gamma + mw(1 - \gamma). \quad (4.17)$$

In this equation the first term on the right hand side describes the change in intermittency due to the decrease of spot size. For this purpose the parameter k , which is a measure for the 'spot decay rate', is introduced. The second term is the number of spots which enter the boundary layer. This term is the same as in the exponential model (equation (4.15)). The solution for the intermittency, using $\gamma = 0$ at $x = x_t$, is:

$$\gamma(x) = \frac{1}{1 + \frac{k}{mw}} [1 - \exp(-(mw + k)(x - x_t))]. \quad (4.18)$$

This pre-transition distribution has an exponential growth towards an intermittency which not equals one. In the limiting case of negligible spot decay, i.e.

Table 4.4: Parameter values.

grid	mw	k	$Re_{xc} \cdot 10^{-5}$
[-]	[m ⁻¹]	[m ⁻¹]	[-]
3L	34	82	1.2
2H	36	126	2.0
2L	28	92	2.5
1H	49	101	2.1

$k \ll mw$, equation (4.17) becomes equation (4.15) and the distribution (4.18) approaches equation (4.16).

For the intermittencies which can be described by the exponential and the pre-transition model, an estimate of the numerical values of the parameters involved is made by a least squares fitting method. The corresponding data fit gives the values of mw and k directly (table 4.4; estimated accuracy $\pm 10\%$).

Figure 4.14 shows the measurements together with the pre-transition model and the Narasimha model. It shows good agreement for the data obtained for the 2L, 2H and 3L grids. Therefore, the pre-transition model combined with the Narasimha model gives a good description of the intermittency distribution at these intermediate turbulence levels. It seems that until a critical Reynolds number, Re_{xc} , is reached, turbulent spots with a certain initial size enter the boundary layer and decrease in size. When this critical Reynolds number, which is dependent on the turbulence grid, has been surpassed, the boundary layer seems to be unstable enough to allow the spots to grow and the Narasimha intermittency curve is followed. The same trend can be found for the 1H grid (lower turbulence level). The only difference is that the latter part of the transition zone is described better by the Johnson model than by the Narasimha model. Both distributions are given in figure 4.15.

4.4 Transition start and length

The Narasimha model can be transformed to a dimensionless form (see also equation (2.31)):

$$\gamma(x) = 1 - \exp[-\hat{n}\sigma(Re_x - Re_{xt})^2]. \quad (4.19)$$

In this equation $\hat{n}\sigma$ is the dimensionless spot production parameter which describes the transition length. *Mayle* [1991] presented a correlation for the spot production parameter as a function of the turbulence level:

$$\hat{n}\sigma = 1.5 \cdot 10^{-11} Tu^{\frac{7}{4}}. \quad (4.20)$$

To check this relation, the production parameters are determined in the area in which the Narasimha model describes the intermittency best. Only for the 1L, 1H, 2L, 2H and 3L grids the data fit was possible, while for these grids at least the latter part of the intermittency distribution can be described by a Narasimha curve. Although the intermittency distribution of the 1H grid is described better by the Johnson curve, also the parameters for the Narasimha distribution can be determined by a data fit. This fit is used for determining the spot production parameter.

The spot production parameter as a function of the turbulence level resulting from the present measurements is given in figure 4.16². As is seen we find a $\hat{n}\sigma$ which agrees well with that of equation (4.20).

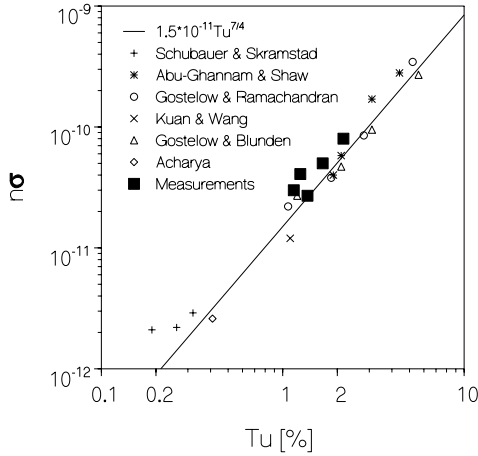


Figure 4.16: Dimensionless spot production parameter as function of the turbulence level.

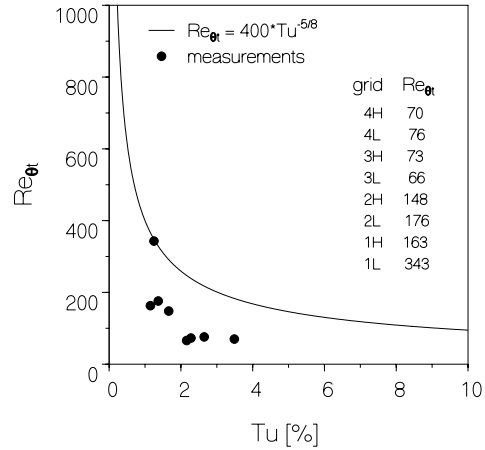


Figure 4.17: Momentum thickness Reynolds number at the transition start as function of the turbulence level.

Mayle [1991] also derived a correlation for the momentum thickness Reynolds number at the transition start. This relation is given by:

$$Re_{\theta t} = 400 Tu^{-\frac{5}{8}}. \quad (4.21)$$

The 1L grid is the only grid which does not show a pre-transition or exponential intermittency distribution. Determining the transition start by using equation (4.14) gives a $Re_{\theta t}$ of 343. Using Mayle's equation gives an expected start at $Re_{\theta t} = 348$, so good agreement is found for this turbulence grid. However, the transition start for the other grids is situated much more towards the leading edge.

²The turbulence levels depicted in this figure are measured 27 mm in front of the leading edge of the sensor plate. This implies that the turbulence level just above the leading edge is slightly lower due to the decay of turbulence in streamwise direction.

The results for the present measurements are depicted in figure 4.17 (estimated accuracy $\pm 10\%$).

So, in the experiments performed at intermediate turbulence levels, we find a transition start which is situated much further towards the leading edge than experiments listed in literature. However, the latter stage of the transition process is described well by the Narasimha (or Johnson) model with a growth parameter which is comparable to values found in literature.

4.5 Cross correlations

At low turbulence levels spots are recognized in the flux signal (e.g. figure 4.10). However, no spots are seen directly in the transition zone where the exponential models fits the measurements. The same is valid for the signals taken in the pre-transition zone for the several grids.

To check the occurrence of tiny spots in the flow, high frequency measurements are performed. The signals of two sensors are recorded at a sampling frequency of 380 kHz during one experiment. Cross-correlating the output of these sensors, which are situated with a streamwise distance of 10 mm, gives a correlation at a velocity of approximately 56% of the mainstream velocity. This indicates that in these areas in the transition zone disturbances are present which move at a velocity which is characteristic for turbulent spots. This leads us to the conclusion that very tiny spots, which are not directly visible in the heat flux signals, are present in both transition cases. For completeness, also cross-correlation measurements are performed in the laminar boundary layer. For these experiments no correlation at any velocity was found, indicating that no artifacts are present.

Examples of cross-correlations are given in figure 4.18. Both, the signals in a laminar and in a transitional boundary layer are depicted. It is seen that in the laminar region no correlation peak is obtained. However, in the transition zone a peak occurs at a time shift of 0.16 ms, which corresponds to a velocity of approximately 56% of the mainstream.

An estimate of the initial spot size for the exponential and pre-transition intermittency distributions can be made as follows. From the high frequency measured heat flux in the transition zone it is found that the (unfiltered) noise level is $\pm 1 \text{ kW/m}^2$. The sensor signal should raise from the laminar value to the turbulent value when the sensor (width 3 mm) is covered fully by a spot. In this case the sensor output increases with a flux level of the order of 1.5 kW/m^2 , depending on the unit Reynolds number and the streamwise position. To detect spots with size in the order of the sensor width, a minimum sampling frequency of 25 kHz is needed. For the correlation experiments the frequency was 380 kHz, so detection of that large spots should not be a problem.

Now suppose that the spot size is $\frac{1}{3}$ of the sensor width. This corresponds to

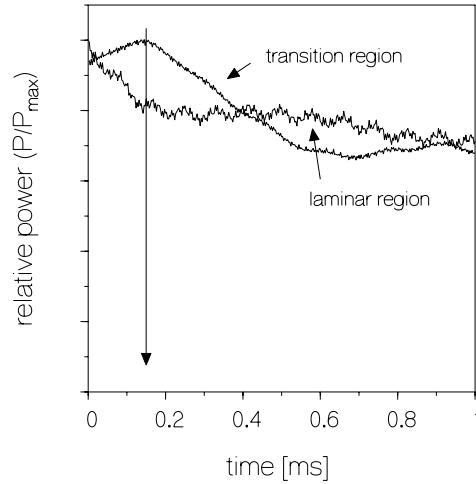


Figure 4.18: Cross correlation of two signals in the laminar region and the transition region.

a flux increase of 0.5 kW/m^2 and a frequency of 75 kHz . The noise level is too high for detecting these spots.

While no individual spots are recognisable in the flux signal but the cross-correlation indicates the appearance of spots, it is estimated that the sensor is covered for less than $\frac{1}{3}$. Therefore, this estimation gives a maximum size of 1 mm (approximately 3 times the boundary layer thickness at the transition start). Note that this argument also holds for clusters of spots.

4.6 Length scale analysis

As already mentioned in chapter 2, not only the turbulence level plays an important role in the transition process but also the length scales. Therefore, an attempt is made to calculate the length scales and to compare the results with literature (in appendix C an overview of length scales is given).

The length scales are not measured directly in the test section. However, from the decay of the mainstream turbulence in streamwise direction the dissipative scale can be estimated. The equation for the turbulent energy for decaying homogeneous turbulence is given by (*Simonich and Bradshaw [1978]*):

$$U \frac{\overline{du'^2}}{dx} = -\frac{\overline{(u'^2)^{3/2}}}{L_\epsilon}. \quad (4.22)$$

In this equation L_ϵ is the dissipative length scale and an overline denotes the time

mean value (other notations of the equation for turbulent energy can be found in *Bird et al.* [1960]). The velocity fluctuations u' are related with the turbulence level by:

$$\overline{u'^2} = Tu^2 \cdot U^2. \quad (4.23)$$

This is the definition for the turbulence level for an incompressible flow. In our case the mass fluctuations $(\rho U)'$ are used for determining the turbulence level (equation (3.12)). So, the density fluctuations are neglected by interchanging both definitions.

In the present experiments the turbulence level is determined at two streamwise positions, 27 mm upstream of the leading edge (position Tu_1) and 30 mm downstream of the leading edge (position Tu_2). From these measurements an estimate of the turbulence is made by assuming a linear decay between the two streamwise positions³. Also the turbulence level at the transition start, Tu_{tr} , is estimated from linear interpolation. By using equation (4.23) and this turbulence level, the term $\overline{u'^2}$ at the start is calculated. Now, all the required data are available to determine the dissipative length scale at the start of transition. The results are given in table 4.5, in which also the bar diameter and the mesh size of the turbulence generating grids are listed.

Table 4.5: Turbulence intensities and dissipative length scale for the turbulence generating grids.

grid	d	mesh	Tu_1	Tu_2	Tu_{tr}	L_ϵ
[-]	[mm]	[mm]	[%]	[%]	[%]	[mm]
4H	4	20	3.49	2.39	2.83	2.00
4L	4	20	2.65	2.42	2.52	7.82
3H	3	18	2.28	2.04	2.13	5.31
3L	3	18	2.16	1.93	2.03	5.07
2H	2	10	1.66	1.30	1.38	1.41
2L	2	10	1.37	1.22	1.25	2.87
1H	1	12.5	1.15	1.03	1.05	2.53
1L	1	12.5	1.25	0.95	0.83	0.49

It is seen that the dissipative length scale roughly scales with the bar diameter of the turbulence grid. This holds for all the grids except for the 4H, 1H and 1L grids. By comparing the turbulence levels, it seems that the value of 2.39 for the 4H grid is relatively low. A fast decay of the turbulence level is coupled to a small length scale (equation (4.22)). So, an underestimation of the turbulence

³An exponential decay of the turbulence level would be more realistic. However, we assume a linear decay because only two streamwise positions are available for measuring the turbulence level (Tu_1 and Tu_2).

level at the Tu₂ position results in an underestimation of the dissipative length scale.

It is also observed that the dissipative length scale for the 'L'-grids scales better with the bar diameter than those for the 'H'-grids. An explanation is that the 'H'-grids are situated much closer to the hot-wire than the 'L'-grids. Therefore, the turbulence generated by the 'H'-grids might not be completely homogeneous at the hot-wire position. This might introduce deviations in the measured turbulence level, and as a result in the dissipative length scale.

Another method of studying the length scale influence on transition was done by *Mayle et al.* [1998] and *Mayle and Schulz* [1997]. They found that the frequency of turbulence which is most effective in producing (pre-transitional) boundary layer fluctuations is equal to:

$$f_{eff} = \frac{0.3U}{2\pi\eta}, \quad (4.24)$$

with η Kolmogorov's length scale: $\eta = (\nu^3/\epsilon)^{1/4}$ in which ϵ is the dissipation of free-stream turbulent kinetic energy given by (*Simonich and Bradshaw* [1978]):

$$\epsilon = -\frac{3}{2}U \overline{\frac{du'^2}{dx}}. \quad (4.25)$$

A length scale which plays an important role in the transition process therefore is likely to be:

$$l_{eff} = \frac{U}{f_{eff}} = 21\eta. \quad (4.26)$$

Bypass transition experiments performed by several researchers were evaluated by *Mayle* [1999]. He formed a dimensionless frequency, $\hat{f} = f_{eff}\nu/U^2$, and found for bypass transition that: $1.7 \cdot 10^{-4} < \hat{f} < 5.6 \cdot 10^{-4}$. These values are all larger than the characteristic value of Tollmien-Schlichting instabilities for which the dimensionless frequency equals $0.5 \cdot 10^{-4}$ (*Mayle* [1999]). Thus, bypass transition is situated in a different frequency range compared to 'natural' transition.

Also the ratio of the effective length scale and the boundary layer thickness at the transition start, δ_{xt} , were calculated by *Mayle* [1999] (the boundary layer thickness is defined as the height where the local velocity reaches 0.99 times the mainstream velocity). For the evaluated bypass transition measurements he found that $0.9 < l_{eff}/\delta_{xt} < 1.7$. As the effective length scale is approximately the boundary layer thickness, it was deduced that the initial size of a turbulent spot is about the same. Unfortunately, it is not possible to detect spots with a size in the order of the boundary layer thickness. As discussed in section 4.5, the minimum detectable spot size is about 1 mm.

For the present measurements the parameters as proposed above, are calculated and shown in table 4.6. The values of the effective length scale, l_{eff} , and the dissipative length scale, L_ϵ , appear to have the same order of magnitude. For

all the grids, except the 1L grid, the dimensionless frequency \hat{f} is situated in the range where bypass transition is found in literature.

It is also seen that the ratio of the effective length scale (l_{eff}) and the boundary layer thickness at the transition start (δ_{xt}), is significantly larger than the values given by *Mayle* [1999]. This holds for all the turbulence generating grids except the 1L grid. Only this grid has a value comparable to those calculated by *Mayle* [1999]. It is worthwhile to mention that in our experiments, only with this grid, a complete Narasimha intermittency distribution is obtained, while in literature in general the experiments are described by this distribution.

Table 4.6: Effective frequencies and length scales for the turbulence generating grids.

grid	f_{eff}	\hat{f}	η	l_{eff}	δ_{xt}	l_{eff}/δ_{xt}
[-]	[kHz]	[-]	[mm]	[mm]	[mm]	[-]
4H	81	$4.90 \cdot 10^{-4}$	0.0645	1.35	0.35	3.86
4L	75	$2.84 \cdot 10^{-4}$	0.0696	1.46	0.24	6.08
3H	51	$3.09 \cdot 10^{-4}$	0.1021	2.14	0.37	5.78
3L	71	$2.69 \cdot 10^{-4}$	0.0735	1.54	0.21	7.33
2H	87	$2.64 \cdot 10^{-4}$	0.0603	1.27	0.37	3.43
2L	84	$1.91 \cdot 10^{-4}$	0.0625	1.31	0.33	3.97
1H	61	$1.85 \cdot 10^{-4}$	0.0857	1.80	0.41	4.39
1L	113	$0.20 \cdot 10^{-4}$	0.0463	0.97	0.52	1.87

Our findings now can be summarised as follows. When the ratio of the effective length scale and the boundary layer thickness at the transition start is comparable to values in literature, transition indeed can be described well by the Narasimha (or Johnson) intermittency curve. However, when this ratio enlarges, other distributions must be used. A general overview of the distributions is given in the next section.

4.7 Overview of intermittency distributions

It is found that several stages in the transition process can be recognized, depending on the turbulence generating grid. These stages can be well described by assuming some new sources of the initiation and growth of turbulent spots. Figure 4.19 shows a schematic overview of the three different intermittency distributions obtained in the present experiments. The observations in the heat flux signals as a function of the turbulence grid, can be summarised in five regions which are given below.

1. Laminar boundary layer. In this region no turbulent spots are recognized. Cross-correlation at high frequency does not give any indication of spots.

2. Transition zone for the 4H and 3H grids (high turbulence levels). No turbulent spots can be recognized in the heat flux signals directly. However, cross-correlation of high frequency flux signals indicates that small spots are present. The exponential model describes the intermittency well.
3. Pre-transition zone for the 1H, 2L, 2H and 3L grids (intermediate turbulence levels). No turbulent spots are recognized in the heat flux signals directly. However, cross-correlation of high frequency signals indicates that small spots are present. The first part of the intermittency curve is described by an intermittency distribution which follows from the assumption that spots decrease in size.
4. Transition zone for the 2L, 2H and 3L grids. Turbulent spots can clearly be recognized in the heat flux signals. This zone is described well by the Narasimha intermittency distribution.
5. Transition zone for the 1L grid. Turbulent spots can clearly be recognized in the heat flux signals. This zone is described well by the Johnson intermittency distribution.

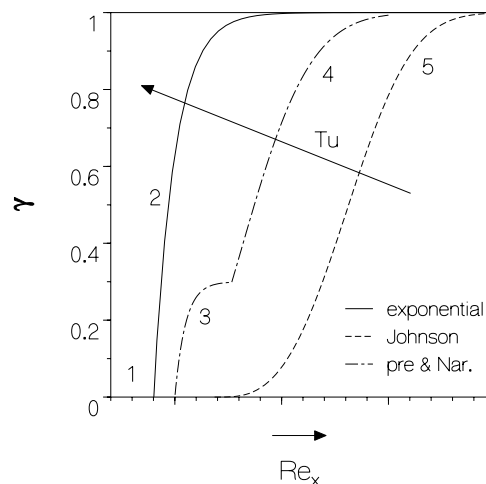


Figure 4.19: Intermittency distributions for different turbulence levels. *Low turbulence level*: Johnson distribution, *intermediate turbulence level*: pre-transition and Narasimha distribution combined, *high turbulence level*: exponential distribution.

4.8 Mach number influence

The Ludwig tube is suitable for studying the effect of compressibility on transition. In the past, steady transition experiments are performed in the set-up as is discussed in this thesis (*Schook et al.* [1998]). These measurements are done with the Mach number ranging from 0.13 to 0.56, making sure that choking does not occur at the turbulence generating grids. The preliminary results will be discussed in this section.

When the turbulence grid is unchanged and the Mach number is increased, it appeared that the intermittency distributions remain unchanged. This suggests that the Mach number has not a significant influence on the transition. However, the hot-wire measurements show that the turbulence level decreases considerably when the Mach number is increased from 0.13 to 0.56 (turbulence level decrease is about 40% (relatively) for all the grids). From this it can be concluded that the turbulence level alone, is not an appropriate parameter for characterizing the transition process. Besides the turbulence level, the turbulence length scale seems to play an important role. From the length scale analysis described in section 4.6, it follows that this is indeed a plausible supposition.

It appeared that the sensor plate, used for the measurements described in this section, was not manufactured according to the high standards applied later on. Therefore, the results presented here should be used with care. However, the reproducibility of the measurements is found to be very good.

Due to the uncertainties concerning the sensor plate, the results are not accurate enough to compare them with observations described in literature (see section 2.2.3). Due to the small number of measurements available in literature, it is interesting to study the effect of compressibility more accurately in future experiments.

4.9 Conclusions

In this chapter the steady state heat flux measurements are presented. From these experiments intermittency distributions are determined. It is found that for low turbulence levels, these distributions can be described well by the Narasimha distribution. However, for large values of the turbulence level, an exponential intermittency curve fits the measurements. This behaviour is explained by the occurrence of non-growing turbulent spots.

For intermediate turbulence levels a combination of a pre-transition model and the Narasimha model fits the measurements. The pre-transition model is based on turbulent spots which decrease in size. Describing the latter part of the transition zone can be done by the Narasimha model. In this region the spot production parameter is found to agree with literature.

Also agreement of intermittency distributions with literature is found for measurements in which the ratio of the effective length scale and the boundary layer

thickness at the transition start do match. When this ratio is significantly larger, i.e. in our intermediate and high turbulence level experiments, the new distributions are found.

Correlating the heat flux signals indicates that the turbulent spot velocities are slightly higher than velocities found by other researchers. However, determination of individual spot properties and measurements in the range of the initial spot size, can not be done with our set-up. The signal to noise ratio and the sampling frequency are not sufficient. Only, an estimation of the maximum initial turbulent spot size can be made. The thus determined upper limit is a few times the boundary layer thickness which is a plausible value.

Chapter 5

Unsteady transition measurements

This chapter deals with the unsteady transition measurements. The influence of wakes on the heat transfer is studied by means of a system of translating cylinders in front of the test plate. Wake induced transition experiments are performed for different wake strengths. Also, measurements with both a turbulence generating grid and moving cylinders are presented. With these measurements the combination of wake induced transition and bypass transition is studied. This latter series of measurements makes it possible to validate the superposition criterion as used in literature. Also attention will be given to the absolute value of the heat flux in the turbulent part of the flow. It appears that the heat flux is dependent on the strength of the wake. This means that the flux based intermittency, as used for the steady transition measurements, can not be extended to the unsteady case in a straightforward manner. Finally, the resulting difference in the time based intermittency and the flux based intermittency is discussed. In *Schook et al.* [2000c] a part of this chapter is published.

5.1 Wake induced heat transfer measurements

The first series of measurements is performed without the presence of a turbulence grid included in the test section. As a result, the background turbulence in the main flow is approximately 0.25%. This implies that a complete laminar boundary layer is obtained in the case of non-moving cylinders.

As discussed in chapter 3, the mean Mach number is supposed to be 0.33 (corresponding mainstream velocity: $U = 107$ m/s). This Mach number is based on the test time which is in the range: 0.025 s $<$ test time $<$ 0.054 s. The unit Reynolds number is adjusted to $3.0 \cdot 10^6$ m⁻¹, and is based on the mean Mach number. All the heat flux experiments are performed at a sampling frequency of 50 kHz with the odd numbered sensors connected. Triggering is done by means

of the pressure signal (similarly as for the steady transition measurements).

The translation speed V of the cylinders varies between 0 and 35.2 m/s. In the latter case eight cylinder passings are occurring in the test time of 29 ms. The distance between the leading edge of the test plate and the center of the cylinders is adjusted to a value of 40 mm. This is the case for all the experiments as described in this chapter.

5.1.1 Unsteady transition initiated by strong wakes

Figure 5.1 shows the output (reconstructed flux) for several sensors in streamwise direction for an unsteady experiment. These fluxes are plotted on the same vertical ordinate but shifted vertically (for getting some idea of the peak heights: one division in vertical direction equals 0.2 kW/m²). There are twelve cylinders, made of carbon fibre with a diameter of 5 mm, mounted between the belts. Figure 5.1(a) shows the output for a laminar boundary layer. This latter case is denoted by: $V = 0$ m/s, i.e. non-moving cylinders¹. The remaining three figures show the sensor output for increasing cylinder speed: figure 5.1(b): 17.7 m/s, figure 5.1(c): 26.7 m/s and figure 5.1(d): 35.2 m/s, respectively. Peaks are observed in the heat transfer, with the frequency of the passing cylinders. The increase in heat transfer is due to the wake which is shed behind the cylinders.

Peaks are already recognizable at very low Reynolds number (streamwise position just behind the leading edge). This implies that the strength of the wake is large enough to initiate transition which starts at the leading edge. The wakes² also are seen to convect in streamwise direction. It is seen that the shape of the wake remains nearly unchanged. This is in accordance with individually occurring turbulent spots. Their shape is also supposed to remain unchanged throughout the complete transition process (*Emmons [1951]*). By comparing the figures 5.1(b), 5.1(c) and 5.1(d), it is clearly seen that the width of the wake decreases when the speed V enlarges.

Sometimes, a small decrease of heat transfer is visible just before the large increase due to transition (see e.g. figure 5.1(c)). This can be explained by the so called 'negative jet' effect (*Meyer [1958]* and *Hodson and Dawes [1998]*). Behind the cylinder a velocity deficit occurs, sometimes resulting in a 'negative jet'. This jet removes fluid from the surface, which results in a local decrease of heat transfer.

Figure 5.2 shows the flux for the case of twelve 3 mm carbon fibre cylinders mounted between the belts. In figure 5.2(a) the laminar signals are depicted

¹Note that in this experiment the cylinders are positioned such that they do not influence the flow along the plate, i.e. the cylinders are positioned in the upper and lower slits of the test section. Otherwise, steady bypass transition might occur due to turbulence generated by the non-moving cylinder.

²Although the wake is not visible in the signals, but the increase in heat flux due to the passing wakes, the peaks in the signals will be mentioned as the 'wakes'.

(identical to figure 5.1(a)). The remaining figures show the sensor output for an increasing cylinder speed: figure 5.2(b): 17.7 m/s, figure 5.2(c): 26.7 m/s and figure 5.2(d): 35.2 m/s, respectively.

The same phenomena as for the 5 mm cylinders are visible in the experiment for the 3 mm cylinders. Transition seems to start at the leading edge and the wake shape is conserved reasonably. The only difference is that the wake width is smaller than in the 5 mm case.

It is observed that for both the 5 mm and the 3 mm diameter cylinders, sometimes spikes occur between the wakes (e.g. figures 5.1(d) and 5.2(c)). This is recognizable for sensors positioned at a Reynolds number of $2.8 \cdot 10^5$ and more. The background turbulence level is only 0.25%, so it is unlikely that these spikes are 'naturally' occurring spots. An estimation of the transition start in the case of 0.25% background turbulence can be made by using equation (4.21). This results in: $Re_{\theta t} = 951$, which corresponds for a Blasius boundary layer to $Re_x = 9.6 \cdot 10^5$. As can be seen this value is much larger than the streamwise position where the spikes occur. Therefore, it is plausible that the spikes are initiated by disturbances caused by the passing wakes.

5.1.2 Unsteady transition initiated by weak wakes

The experiments described thus far, i.e. with cylinder diameters of 5 mm and 3 mm, all cause unsteady transition starting at the leading edge of the sensor plate. To obtain unsteady transition for which the start is situated further downstream, experiments are conducted with cylinders having a diameter of 0.6 mm. Nylon instead of carbon fibre is used for manufacturing these cylinders.

In figure 5.3 the sensor output in streamwise direction is given for 5 mm and 0.6 mm cylinders, and 3 mm and 0.6 mm cylinders combined in one experiment. For both cylinder combinations an alternating pattern of cylinders is used. This means that in one measurement six 0.6 mm cylinders are present in combination with six 5 mm or 3 mm cylinders. Figure 5.3(a) shows the laminar sensor output which is identical to those given in figures 5.1(a) and 5.2(a). The unsteady experiments performed at a velocity of 35.2 m/s, 17.7 m/s and 26.7 m/s are depicted in figures 5.3(b), 5.3(c) and 5.3(d), respectively. Note that the diameter of the carbon cylinders is not identical for all the experiments.

It is observed that the transition of the 5 mm and the 3 mm cylinders begins at the leading edge of the plate. However, the wakes shed by the 0.6 mm cylinders cause transition which indeed is situated further downstream. For example, in figure 5.3(b) it is seen that at $Re_x = 0.36 \cdot 10^5$ four spikes are visible in the signal. These spikes are caused by the wakes shed behind the 3 mm cylinders. At a Reynolds number of $0.96 \cdot 10^5$, new spikes become visible in between already existing spikes. These are the wakes shed behind the 0.6 mm cylinders. The same phenomena are observed for smaller cylinder velocities (figures 5.3(c) and 5.3(d), in which $V = 17.7$ m/s and $V = 26.7$ m/s). Therefore, it is concluded that the

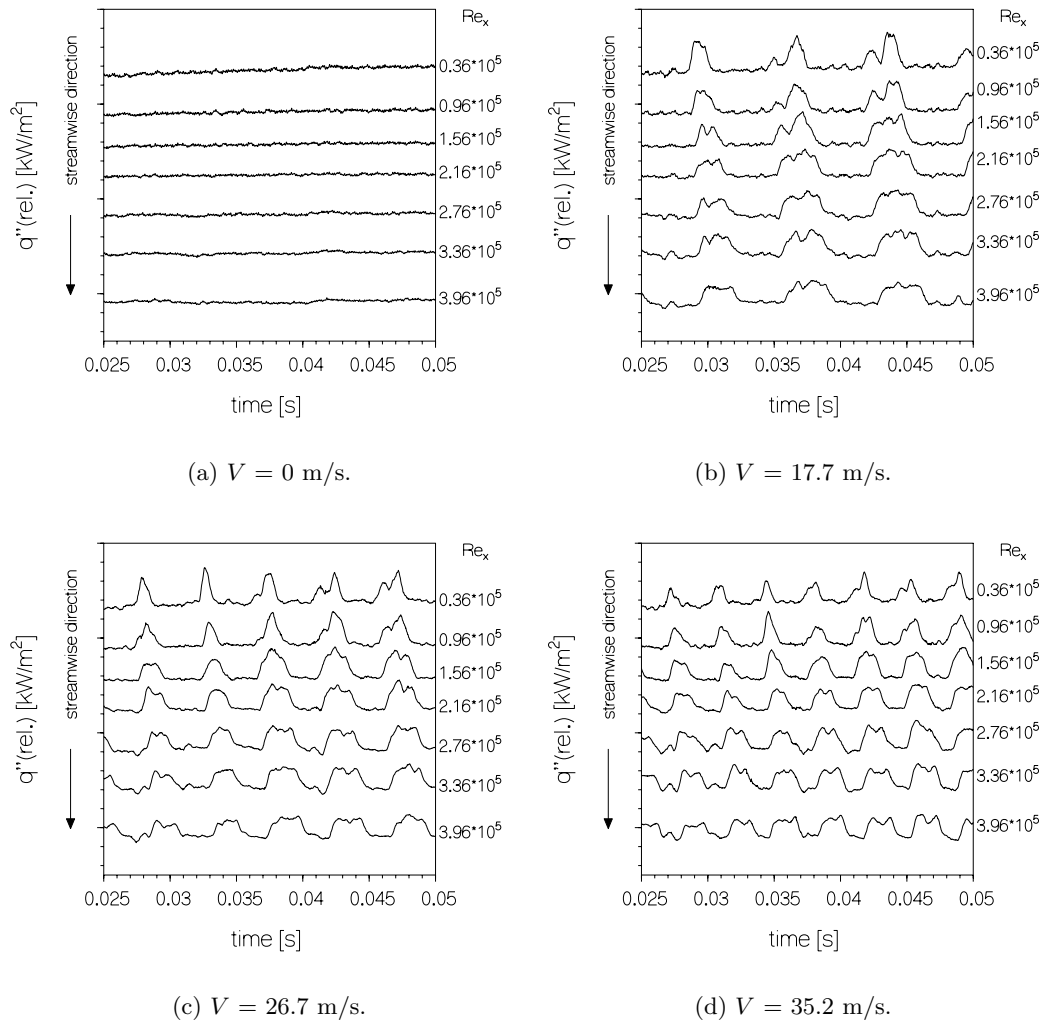


Figure 5.1: Heat fluxes for several sensors in streamwise direction. No turbulence grid included. Cylinder diameter is 5 mm; $Re_u = 3.0 \cdot 10^6 \text{ m}^{-1}$.

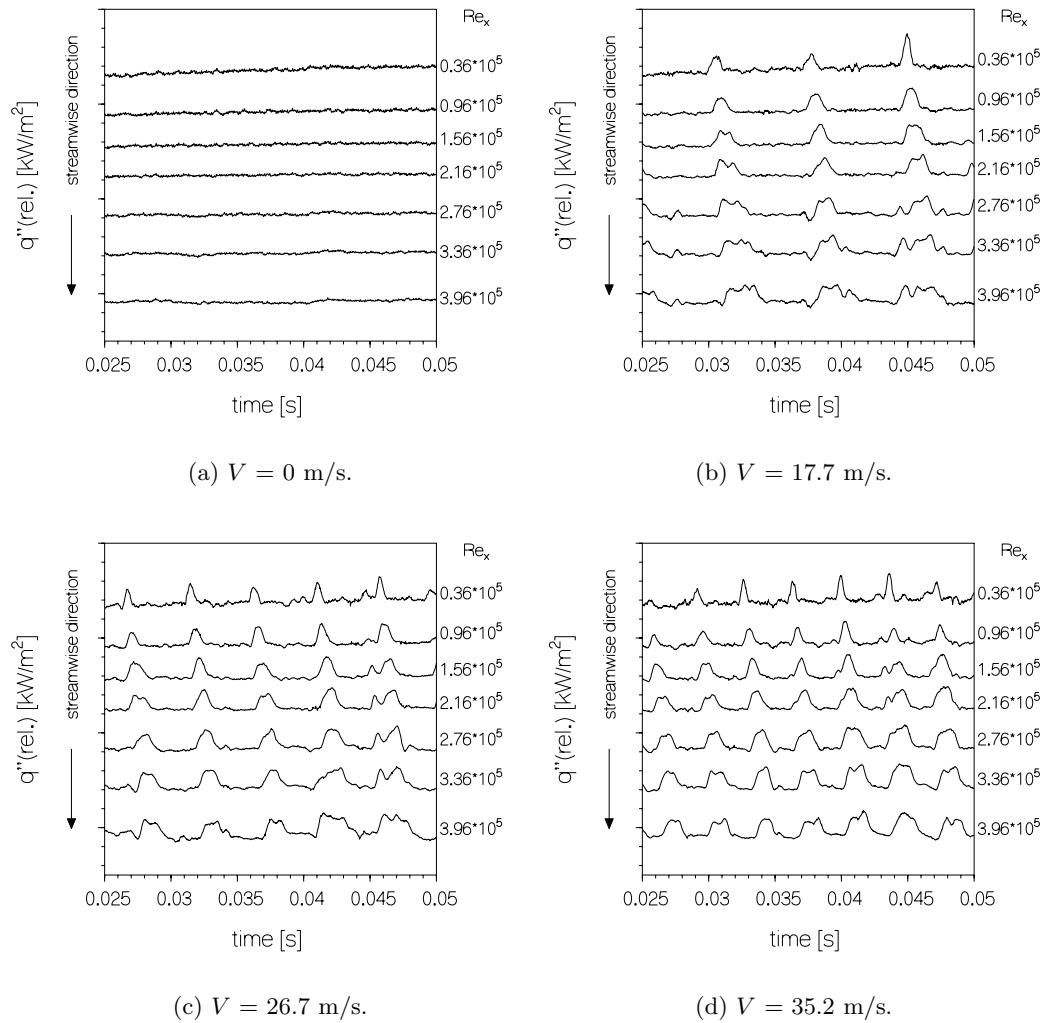


Figure 5.2: Heat fluxes for several sensors in streamwise direction. No turbulence grid included. Cylinder diameter is 3 mm; $Re_u = 3.0 \cdot 10^6 \text{ m}^{-1}$.

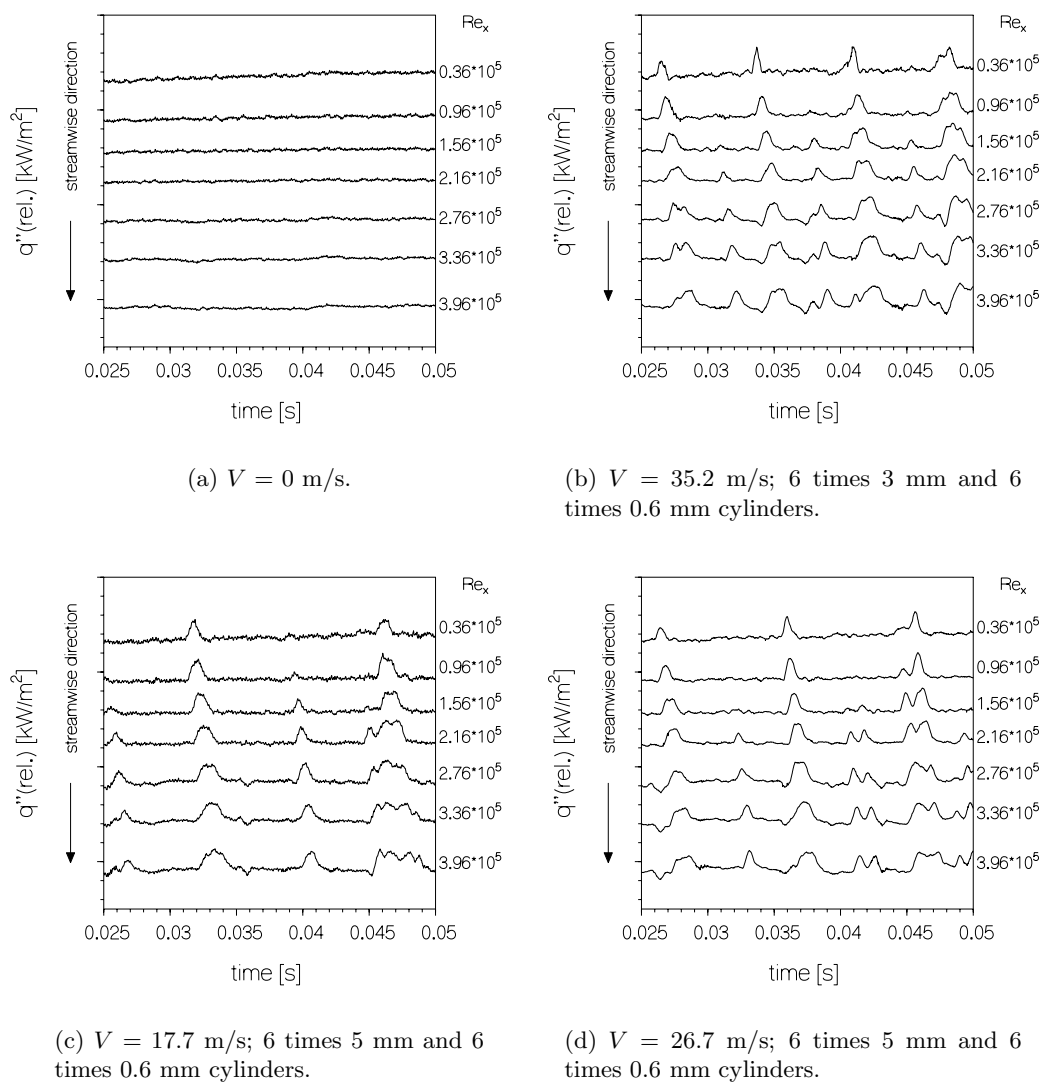


Figure 5.3: Heat fluxes for several sensors in streamwise direction. No turbulence grid included; $Re_u = 3.0 \cdot 10^6 \text{ m}^{-1}$.

wakes behind the 0.6 mm cylinders disturb the boundary layer as is the case for the 3 mm and the 5 mm cylinders. However, these disturbances are such small that transition to turbulent flow occurs at a streamwise Reynolds number which is situated between zero (leading edge) and the value for natural (or bypass) transition. Also for the 0.6 mm cylinders it is seen that the shape of the wake keeps its initial shape in downstream direction. Sometimes, it is seen that two peaks occur in the wakes. It is supposed that this is caused by vibration of the cylinders. Due to these vibrations, it might be possible that two successive wakes are shed behind the cylinder.

5.2 Combined heat transfer measurement

The background turbulence intensity can be varied by altering the turbulence generating grid. Non-moving cylinders in combination with a turbulence generating grid cause steady transition as discussed in chapter 4 of this thesis. However, the influence of both wakes and the background turbulence also can be studied in the Ludwig tube set-up. This simply is done by using translating cylinders and a turbulence grid during one experiment. These measurements will be referred to as combined experiments.

Figure 5.4 shows the sensor output for non-moving cylinders and the 1H grid. This grid causes a background turbulence intensity of 1.15% (see also table 3.2). The steady transition can be recognised by the occurrence of turbulent spots which are visible as the growing spikes in streamwise direction.

In figure 5.5 the combined transition experiment is shown. For this experiment the 1H grid is used in combination with twelve 5 mm cylinders moving at a speed of 35.2 m/s. It is seen that turbulent spots are initiated between two passing wakes. These spots merge with each other and with the turbulence generated by the wakes. This process proceeds until a fully turbulent boundary layer is obtained at approximately $Re_x = 3.4 \cdot 10^5$.

Although not shown here, the same kind of measurements are performed for several cylinder velocities, cylinder diameters and turbulence generating grids. For all these experiments the same phenomena as described above are observed.

5.3 Hot-wire measurements

To obtain insight in the wake turbulence, hot-wire measurements are performed. The position of the hot-wire is equal to the streamwise position for the steady transition measurements performed in front of the leading edge of the plate, i.e. 27 mm. As the distance from the center of the cylinders is 40 mm, the hot-wire is situated 13 mm downstream of the cylinder center. The sampling frequency of all the experiments is 400 kHz (the same as for the steady transition measurements).

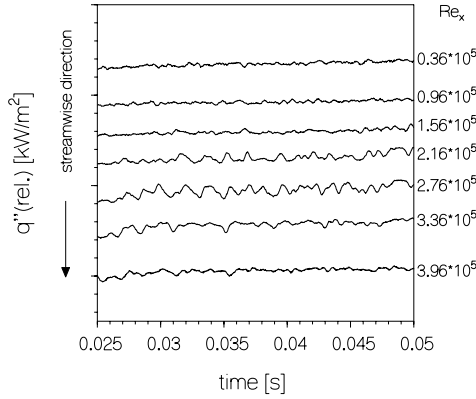


Figure 5.4: Heat fluxes for several sensors in streamwise direction. Turbulence grid 1H included; $V = 0$ m/s; $Re_u = 3.0 \cdot 10^6$ m⁻¹.

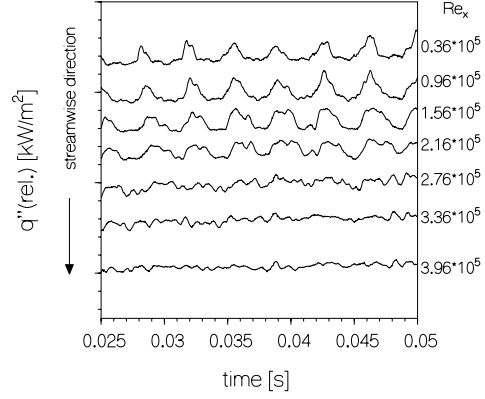


Figure 5.5: Heat fluxes for several sensors in streamwise direction. Turbulence grid 1H included. $V = 35.2$ m/s; Cylinder diameter = 5 mm; $Re_u = 3.0 \cdot 10^6$ m⁻¹.

It appeared that hot-wires, with a diameter of $2.5 \mu\text{m}$, are damaged very fast due to vibrations of the wake-generator (when accelerated to the required cylinder velocity). Therefore, hot-wires with a diameter of $5 \mu\text{m}$ are used for the measurements described in this section. In spite of the larger diameter, the lifetime of the wires appeared to be only a few experiments. For this reason, calibration of the hot-wire is almost impossible and a few assumptions are made to obtain a useful signal. The procedure to obtain the velocity as a function of time is explained as follows.

King's law (equation (3.10)) describes the relation between the recorded hot-wire voltage and the Reynolds number (the length which is incorporated in the Reynolds number is lumped into the constant B):

$$V_0^2 = A + B \sqrt{\frac{U \rho}{\mu}}. \quad (5.1)$$

Normally, the constants A and B are determined by performing measurements at different Reynolds number. Deviations in the hot-wire resistances of different wires mainly occur by a non-unique length and the change in contact resistance (wire-prong contact). There is no particular reason to place these deviations in A or B . Here, it is supposed that B has the same value for all the hot-wires used for the unsteady experiments (so B is kept constant). When performing steady transition experiments it was found that B has a value which is situated in the range: $0.75 < B/\sqrt{\mu} < 0.95$. As a result, $B/\sqrt{\mu}$ is set to 0.85 for the unsteady experiments.

The Mach number is found to be 0.33 for all the experiments (see section 3.6.3). The according mainstream velocity is approximately 107 m/s. The constant A is determined such that the hot-wire reading corresponds with the experimental mainstream velocity. This implies that for every new hot-wire A has a different value. Another assumption is that the density during the experiment is constant, i.e. there are no density fluctuations. Now, the constant A is calculated by rearranging King's law:

$$A = V_0^2 - B \sqrt{\frac{U_\infty \rho}{\mu}}, \text{ with } U_\infty = 107 \text{ m/s.} \quad (5.2)$$

Velocity signals for an unsteady transition experiment in which only moving cylinders are present, are given in figure 5.6. This figure shows the velocities for twelve cylinders with a diameter of 3 mm. Note that the three signals (different cylinder velocity) are shifted vertically. The mean velocity of each signal is 107 m/s as is imposed by the calibration procedure. For getting an idea of the velocity deficit behind the cylinder: five divisions correspond with a velocity difference of 100 m/s (as indicated in the figure). It is seen that in the case of $V = 17.7$ m/s, four cylinder (thus wake) passings are present during the test time, while eight wake passings are present when $V = 35.2$ m/s. This is in agreement with the number of wake passings which are counted in the heat flux measurements.

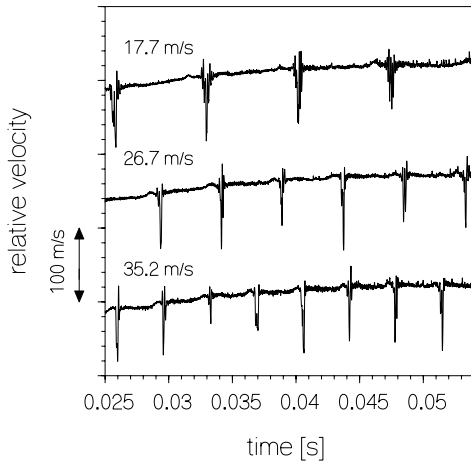


Figure 5.6: Relative velocity for twelve cylinders with a diameter of 3 mm. Velocities V are: 17.7 m/s, 26.7 m/s and 35.2 m/s; no turbulence generating grid.

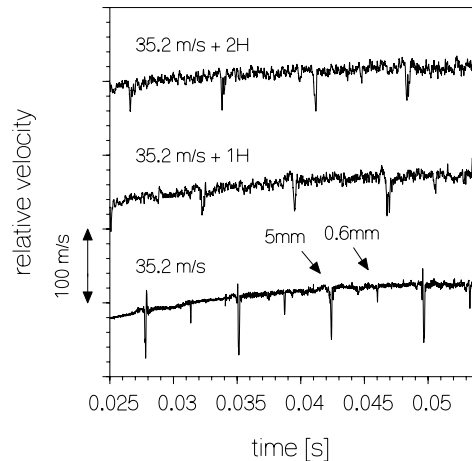


Figure 5.7: Relative velocity for six cylinders with a diameter of 5 mm and six with a diameter of 0.6 mm (alternating pattern) no grid, 1H grid or 2H grid included.

In between the wake passages, the background turbulence is visible as small velocity fluctuations. Although the inaccuracy of the absolute velocity behind the cylinder is not high due to the calibration, it is seen that an enormous velocity deficit appears when a cylinder passes. Unfortunately, it is not possible to determine the turbulence intensity in the wakes.

In literature, the velocity deficits behind moving cylinders are measured for low speed experiments (*Funazaki* [1996a,b] and *Han et al.* [1993]). It appeared that the maximum turbulence intensity in the wake has roughly a value (in percentages) of the relative velocity deficit. For example, when the mainstream velocity is 20 m/s and the velocity deficit is 5 m/s, the turbulence level is approximately 25%. If an analogous assumption is applied to the present measurements, it is seen that the wake turbulence level in the case of 3 mm cylinders has a value of about 50%. It must be mentioned that the total inaccuracy is large. The constant B has an inaccuracy of about 13%. This results in a relative inaccuracy of 26% for the velocity-difference $U - U_\infty$, as the velocity is proportional to $1/B^2$.

In figure 5.7 the velocity signals are shown for unsteady and combined experiments performed at a cylinder velocity of 35.2 m/s. Again, the sensor signals are shifted vertically. An alternating pattern of cylinders is used in which six cylinders with a diameter of 5 mm and six cylinders with a diameter of 0.6 mm are used. In the case of the combined experiments the same cylinder configuration together with the 1H or the 2H grid is used (denoted by: 35 m/s + 1H and 35 m/s + 2H).

For the experiment without a turbulence grid it is seen that large and small velocity deficits are present. These velocity deficits are initiated by the 5 mm and 0.6 mm cylinders, respectively. In between the wake passages the background turbulence is visible (as in figure 5.6). The velocity deficits of the 3 mm and the 5 mm wake passages are found to have approximately the same absolute value.

When the turbulence generating grids are included, the background turbulence level increases significantly. In both cases (35.2 m/s + 1H and 35.2 m/s + 2H) the wake passages of the 5 mm cylinders are observed. However, wakes originating from the 0.6 mm cylinders are not recognizable in the signal. This indicates that the disturbance level of these cylinders (in terms of the velocity deficit) coincide, or is smaller, than the background turbulence generated by the 1H and 2H grids.

The heat flux signals as depicted in figure 5.3, already showed that the unsteady transition caused by the 0.6 mm cylinders starts at a streamwise Reynolds number of about $1 \cdot 10^5$. In terms of a Reynolds number based on the momentum thickness this becomes: $Re_{\theta_t} \sim 200$. In chapter 3 it is described that the transition start for the 1H grid is situated at $Re_{\theta_t} = 163$ and for the 2H grid at $Re_{\theta_t} = 148$. As the velocity deficit, and thus the turbulence level, for the 0.6 mm cylinders is slightly lower than those for the 1H and 2H grid, a wake induced transition start at $Re_\theta = 200$ for the 0.6 mm cylinders seems to be reasonable.

5.4 Comparison of observations with literature

The important parameters for the unsteady transition process are shown schematically in figure 5.8. There are the mainstream velocity U and the cylinder translating velocity V . The ratio of these velocities determines the unsteadiness of the flow, i.e. the flow coefficient: $\Phi = \frac{V}{U}$.

The diameter of the cylinders is d and the distance between different cylinders is the mesh size M . Parameter a is the distance between the center of the cylinders and the leading edge of the test plate (length L) which is adjusted to 40 mm for all the experiments described. The strength of the wakes is determined by d (for the present measurements the diameter is 5 mm, 3 mm or 0.6 mm). Large diameters result in strong wakes and an early transition start. The ratio of length scales which determine this process is: $\frac{d}{a}$. When this ratio becomes small the transition start will shift downstream. Then the transition process will be governed by 'weak' wakes. In this case a more important ratio is probably $\frac{d}{\delta}$, with δ the local boundary layer thickness determined by the local position x . So, independent characterizing parameters are $\frac{d}{x}$ and Re_x .

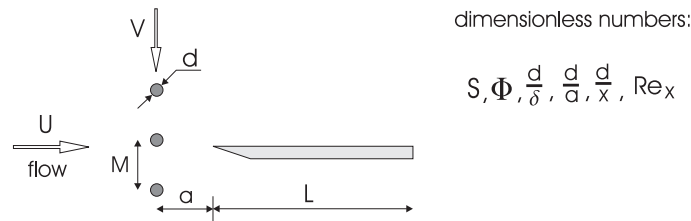


Figure 5.8: Important parameters for unsteady transition.

The mesh in combination with the velocity V characterizes a frequency f . When the wake passing frequency is large enough, wake-wake interaction will take place. In the present set-up, it is not possible to study the effects of this phenomena (due to the limited number of cylinders in combination with the maximum of the velocity V). From the wake passing frequency f , the Strouhal number, which is a measure for the unsteadiness, is introduced:

$$S = \frac{\ell f}{U}. \quad (5.3)$$

In this equation ℓ is an involved length, e.g. the length of the test plate. However, it is not convenient to incorporate the length of the plate. The physics of the problem might suggest another length scale, for example the cylinder diameter or the boundary layer thickness. To make an unambiguous comparison with

literature possible, the length scale is disregarded in the Strouhal number. This results in the so-called *unit* Strouhal number (dimension m^{-1}):

$$S_u = \frac{f}{U}. \quad (5.4)$$

In a wind tunnel set-up, *Funazaki* [1996a,b] performed wake induced heat transfer measurements along a flat plate. Generation of wakes was done by means of a rotating disk wake generator (as discussed in chapter 3). In this generator cylinders with a diameter between 2 and 10 mm were mounted. For these experiments he used a mainstream velocity of 30 m/s and a wake passing frequency of 50 Hz. Therefore, the according unit Strouhal number had a value of: $S_u = 1.67 \text{ m}^{-1}$.

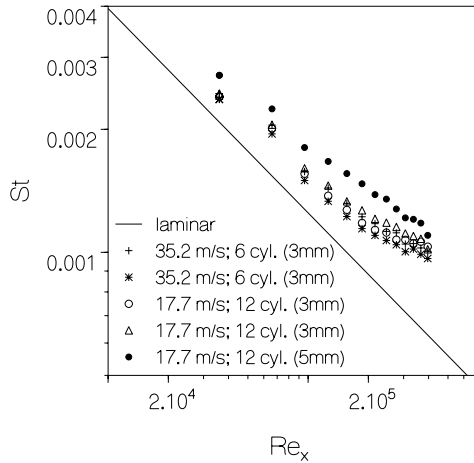


Figure 5.9: Mean heat flux for unsteady experiments; $V = 35.2 \text{ m/s}$: six 3 mm cylinders, $V = 17.7 \text{ m/s}$: twelve 3 mm and 5 mm cylinders; $S_u = 1.29 \text{ m}^{-1}$.

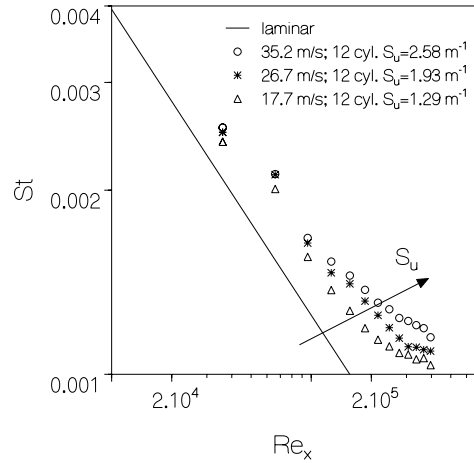


Figure 5.10: Mean heat flux for unsteady experiments with twelve 3 mm cylinders; $V = 35.2 \text{ m/s}$, $V = 26.7 \text{ m/s}$ and $V = 17.7 \text{ m/s}$; $Re_u = 3.0 \cdot 10^6 \text{ m}^{-1}$.

When the disk rotational speed and the number of cylinders are changed such that the frequency (and thus the unit Strouhal number) remained the same, identical mean heat flux distributions are obtained (*Funazaki* [1996a,b]). This means that the flow coefficient Φ has a minor effect on wake induced transition. Also, it appeared that when the cylinder diameter is enlarged the heat flux increases.

The mean heat transfer in terms of the Stanton number for our experiments is shown in figure 5.9. Stanton number distributions are given for a constant Strouhal number. For the 3 mm cylinders two combinations of cylinder velocities and wake passing frequencies are studied. For the first experiment six cylinders moving at a velocity of 35.2 m/s are used. The second experiment is conducted

with twelve cylinders and a velocity of 17.7 m/s (implying that the number of cylinders is doubled and the velocity is two times less). Four wake passings are present during the test time which ranges from 0.025 s to 0.054 s. For a Mach number of 0.33 the mainstream velocity is approximately 107 m/s, so the unit Strouhal number for the present experiments is 1.29 m^{-1} .

To check the reproducibility each experiment is done twice. It is seen that within the reproducibility range both Stanton number distributions for the 3 mm cylinders coincide. This finding is in agreement with the observations of *Funazaki* [1996a,b], who stated that the Strouhal number is a significant parameter in the wake induced transition process.

Also, the distribution for twelve 5 mm cylinders moving at a velocity of 17.7 m/s is shown ($S_u = 1.29 \text{ m}^{-1}$). Clearly, this distribution is situated above the 3 mm case. This implies that when the cylinder diameter is enlarged, and as a result the wakes in the flow become stronger, the heat transfer increases. These findings are in agreement with literature too.

In figure 5.10 the Stanton number distributions are given for the case of twelve 3 mm cylinders moving at a velocity of 17.7 m/s, 26.7 m/s and 35.2 m/s (the corresponding unit Strouhal numbers are 1.29 m^{-1} , 1.93 m^{-1} and 2.58 m^{-1} , respectively). It is observed that when the unit Strouhal number increases the heat transfer becomes larger. This finding is explained as follows. When the wake passing frequency increases, and thus the Strouhal number, the number of wakes per time unit becomes larger. As a result the duration of turbulent flow increases and so does the mean heat flux.

A remark should be made on the Strouhal number effect on unsteady transition by considering the present measurements compared to those found in literature. *Funazaki* [1996a,b] argued that the Strouhal number is a significant parameter in describing unsteady boundary layer transition. He found that when the Strouhal number is increased, the heat transfer also increases. When the Strouhal number is kept constant no influence of the cylinder speed is measured in the heat flux. This finding is in agreement with the observations derived from figure 5.9. However, the present measurements show that when the moving cylinder velocity becomes larger the wake width decreases (e.g. see figure 5.1). In combination with the observation that the cylinder velocity has no effect on the maximum turbulent heat flux, it must be concluded that for a wide wake (small velocity) the mean heat flux is larger than for a narrow wake (large velocity). So, the mean heat flux scales with the wake width. This implies that not only the Strouhal number, but also the cylinder velocity is an important parameter (i.e. Φ). This is in contrast to the finding of *Funazaki* [1996a,b]. Although the velocity had to have an effect on the Stanton number distributions measured, we did not find it experimentally in a convincing manner.

5.5 Heat flux levels

5.5.1 Mean heat flux

As already discussed in chapter 4, the heat flux in terms of the Stanton number for a laminar Blasius boundary layer is:

$$St_l = 0.322Pr^{-\frac{2}{3}}Re_x^{-\frac{1}{2}}. \quad (5.5)$$

The Stanton number relation for a turbulent boundary layer, which starts at the leading edge, equals (*Kays and Crawford* [1980]):

$$St_t = 0.0287Pr_t^{-0.4}Re_x^{-0.2} = C Re_x^{-0.2}. \quad (5.6)$$

For a turbulent Prandtl number of 0.9 the constant C becomes 0.030.

Another relation for the turbulent Stanton number is the relation as used for the grid induced turbulence (chapter 4):

$$St_t = C Re_{x-x_t}^{-0.2}. \quad (5.7)$$

The constant C is obtained by applying a data fit through the turbulent part of the heat flux distribution. Furthermore, it is supposed that this curve begins at the transition start ($x = x_t$).

The mean Stanton number distributions for different experiments are given in figure 5.11. The steady, unsteady and combined measurements of 5 mm and 3 mm cylinders in combination with the 1H, 2H and 3H turbulence generating grids are shown. As already mentioned, the 5 mm distributions are situated above the 3 mm distributions. This holds for the unsteady and the combined experiments in the transition zone (e.g. figures 5.11(a) and 5.11(b)). It also is seen that the combined experiments have a higher heat flux than the steady and unsteady measurements alone (e.g. figure 5.11(c)). The latter part of the transition for the combined experiments of the 1H grid shows the classical shape which also occurs for steady transition. For the combined experiments with the 3H grid, this is not the case; as is visible in figure 5.11(d) (this is also observed for the steady transition for the 3H grid; chapter 4). *Mayle and Dullenkopf* [1990] argued that the combined transition process occurs by the formation of turbulent spots too. The two sources of spot production (natural or bypass occurring spots and wake induced turbulent spots) can be supposed to behave independently. The superposition which results from this assumption will be treated in a forthcoming section. First, attention is given to the absolute value of the 'turbulent' heat flux.

Equation (5.6) results in a serious over-prediction of the mean heat flux for a turbulent boundary layer. This is clearly visible in figure 5.11. Also the curve which is used for determining the intermittency for the 1H grid is shown ($St = 0.0215 Re_{x-x_t}^{-0.2}$; this is the curve as used in chapter 4). It is seen that the turbulent part of the Stanton curve for the combined experiments reasonably fits this curve.

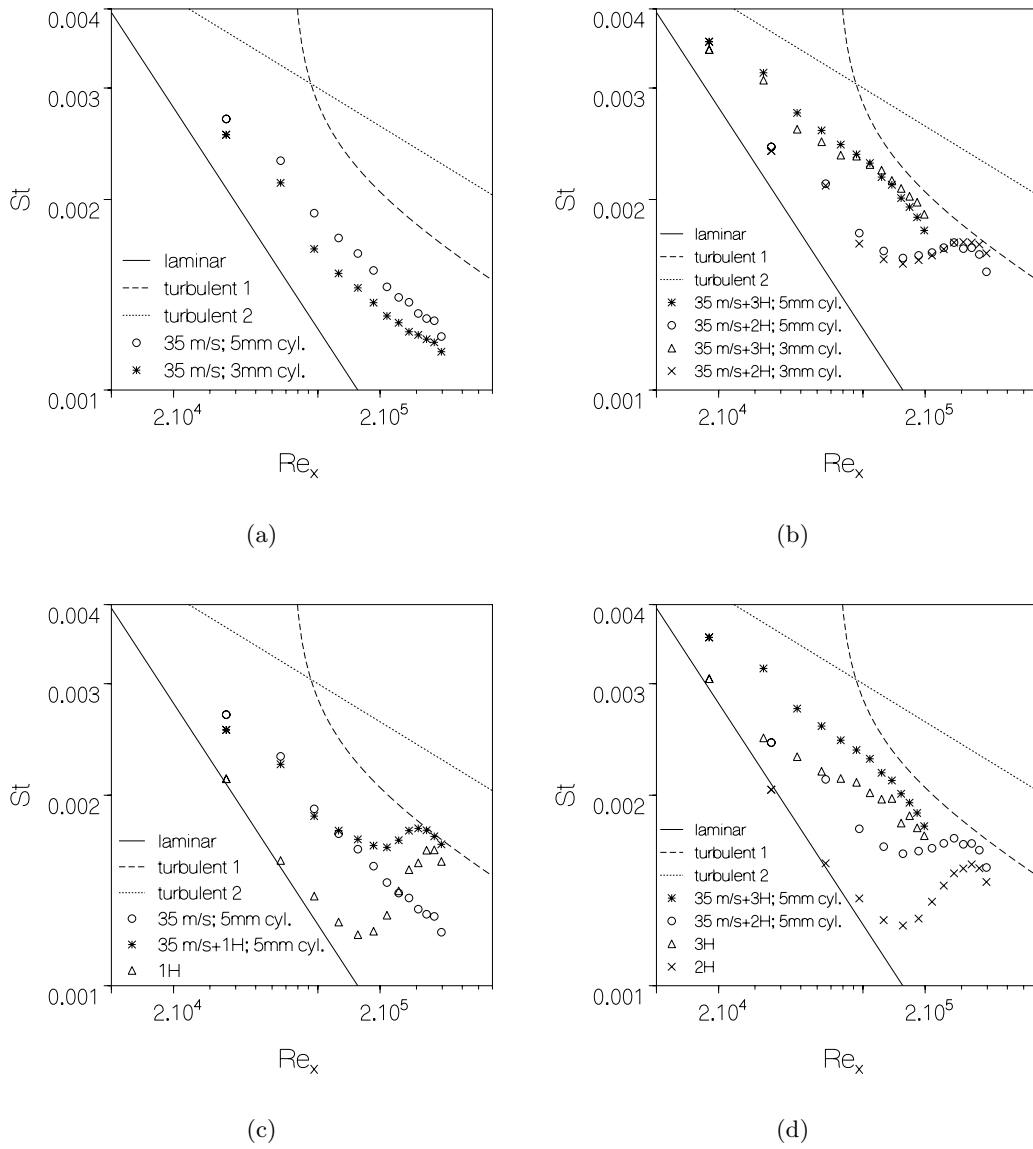


Figure 5.11: Mean heat flux for unsteady experiments at a velocity of 35 m/s (twelve 5 mm and 3 mm cylinders); combined experiments with the 1H, 2H and 3H turbulence grid; steady experiments with the 1H, 2H and 3H turbulence grid; all experiments: $M = 0.33$; laminar curve: Blasius eq. (5.5); 'turbulent 1'-curve: eq. (5.7) with $C = 0.0215$; 'turbulent 2'-curve: eq. (5.6).

5.5.2 Heat flux extrema

To determine the influence of the wake strength on the heat transfer, the flux signal as a function of time is investigated. The minimum and the maximum heat fluxes during the test time are calculated. For this, the maximum flux is determined by taking the mean heat flux of the highest flux levels during 7% of the test time. The minimum heat flux is determined in an analogous manner (the mean heat flux of the minimum flux levels during 7% of the test time). To avoid an under-prediction of the minimum flux and an over-prediction of the maximum flux due to the noise band in the signals, a correction is taken into account. This correction is estimated as follows. The minimum and maximum heat fluxes are calculated for an experiment in which no transition occurs. The mean heat flux for this experiments exactly has the value according to equation (5.5) (due to the calibration, see section 3.5). While no transition occurs, the minimum and maximum heat fluxes should coincide. However, due to the noise in the flux signals, the minimum heat flux and the maximum heat flux are not the same. The correction now is estimated as half the difference between the minima and the maxima obtained for the laminar experiment, and is added to the minimum and subtracted to the maximum values.

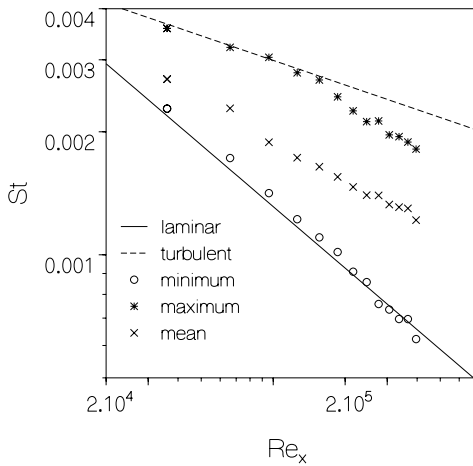


Figure 5.12: Minimum, maximum and mean heat fluxes for the unsteady experiments with 5 mm cylinders at a velocity of 35 m/s; $Re_u = 3.0 \cdot 10^6 \text{ m}^{-1}$; laminar curve: Blasius; turbulent curve: $St = 0.03Re_x^{-0.2}$, i.e. $Pr_t = 0.9$.

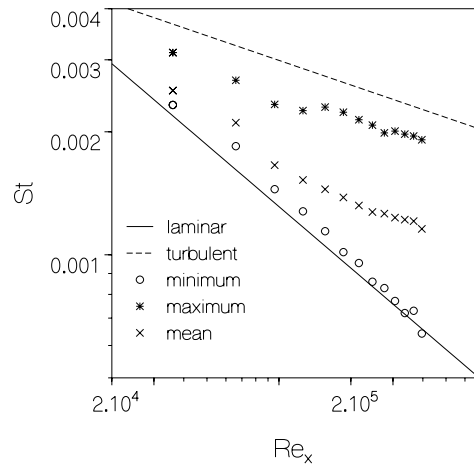


Figure 5.13: Minimum, maximum and mean heat fluxes for the unsteady experiments with 3 mm cylinders at a velocity of 35 m/s; $Re_u = 3.0 \cdot 10^6 \text{ m}^{-1}$; laminar curve: Blasius; turbulent curve: $St = 0.03Re_x^{-0.2}$, i.e. $Pr_t = 0.9$.

The thus determined results for the unsteady experiments are depicted in figures 5.12 and 5.13 (the according time dependent flux signals are depicted in figures

5.1(d) and 5.2(d)). Also the laminar (equation (5.5)) and the turbulent (equation (5.6)) curves are shown. It follows that for the 5 mm cylinders and the 3 mm cylinders, the minimum heat flux agrees with the value for a laminar boundary layer. This means that in between two wake passages the flow relaminarizes. The maximum heat flux (which occurs during a wake passage) is seen to differ for both cases. For the 5 mm cylinders the 'turbulent' heat flux follows equation (5.6) with $C = 0.03$ accurately, until a Reynolds number of $1.5 \cdot 10^5$ is reached. After this streamwise position, the turbulent flux starts to become smaller than the flux according to equation (5.6).

Also the minimum and maximum heat fluxes are determined for unsteady experiments performed at cylinder velocities of 26.7 m/s and 17.7 m/s. Within the reproducibility range of the measurements, no velocity influence is found on the maximum and minimum heat fluxes. The same holds for the Strouhal number.

In the case of 3 mm cylinders the maximum heat flux values are all found to be less than those for the 5 mm cylinders. The slope of the turbulent fluxes is found to be approximately -0.2 for the complete sensor plate. In this situation, a reasonable value for C appeared to be 0.024. So, the turbulent flux for the 3 mm cylinders is about 80% of the flux for the 5 mm cylinders (where $C = 0.03$). This is valid for a Reynolds number less than $1.5 \cdot 10^5$. For larger Reynolds number the difference between the turbulent fluxes of the 5 mm and 3 mm cylinders becomes smaller. It seems that after this critical Reynolds number, the turbulent heat flux level obtains a value which is not dependent on the cylinder diameter.

This might be explained as follows. In downstream direction the difference in wake strength between the 5 mm and 3 mm cylinders becomes less due to diffusion of turbulence in the boundary layer. If the difference in turbulence diminishes, i.e. the turbulence level of both situations becomes the same, it is plausible that the 'turbulent' heat flux level of both cases starts to coincide.

The steady transition experiments showed a 'turbulent' heat flux of about 60% (chapter 4) of equation (5.6), and the unsteady transition experiment show a 'turbulent' flux level of approximately 80%. Therefore, an important conclusion is that there does not exist a unique 'turbulent' heat flux, as it is dependent on the mainstream turbulence and the wake turbulence. This finding is in agreement with *Simonich and Bradshaw* [1978], who studied the effect of turbulence on the heat transfer in a turbulent boundary layer. They found that the free stream turbulence level has a significant effect on the heat transfer. Increasing the disturbance level resulted in an enlargement of the flux. In terms of the Stanton number the following relation is proposed:

$$\frac{St}{St_{Tu=0\%}} = 1.0 + 0.05 Tu. \quad (5.8)$$

In this equation the turbulence level in terms of percentages must be used. Due to the scatter in the measurements, the factor 0.05 has an uncertainty of about 20%

(*Simonich and Bradshaw* [1978]). Equation (5.8) shows that when the free stream turbulence level increases, the heat transfer rises significantly. If the turbulence level is 5%, it follows that the heat transfer is 25% higher compared to a turbulent boundary layer with zero percent free stream turbulence. However, the turbulence level in the strong wakes is 50%, as suggested by the hot-wire measurements. Then equation (5.8) would predict a Stanton number distribution which is 3.5 times the undisturbed distribution. This is not the case for our experiments (the constant C increases with only 25% from $C = 0.024$ to $C = 0.03$).

5.6 Intermittency distributions

The original definition of the intermittency is that it is the fraction of time the flow is turbulent at a certain streamwise position. If turbulent events can be recognized in for example a hot-wire or heat flux signal, the intermittency can be determined by taking the time period of these turbulent events. In this chapter, the intermittency calculated by this method will be referred to as the time based intermittency.

A method of calculating the flux based intermittency is already treated in chapter 4. When the actual, the laminar and turbulent heat fluxes are known, the intermittency is determined by:

$$\gamma_f(x) = \frac{\overline{St(x)} - St_l(x)}{St_t(x) - St_l(x)}. \quad (5.9)$$

The subscript 'f' is added to distinguish between the time based and the flux based intermittency.

First the intermittency distributions for the unsteady transition measurements are treated. A threshold value for determining the time based intermittency is applied. This threshold is set to:

$$St_* = \frac{St_{max} + St_{lam}}{2}. \quad (5.10)$$

If the heat flux has a higher value than St_* , the flow is assumed to be turbulent. Now, the time based intermittency is determined by using the time this is the case. The flux based intermittency is determined by using equation (5.9), in which equation (5.5) is applied for the laminar heat flux. The maximum heat flux, i.e. $St_t(x) = St_{max}(x)$, is used for the turbulent heat flux.

5.6.1 Wake induced transition (no grid included)

Both, the time- and the flux based intermittencies for twelve 5 mm and 3 mm cylinders moving at a velocity of 35.2 m/s, are shown in figure 5.14. It is seen that already at very low Reynolds numbers the intermittency has a non-zero value.

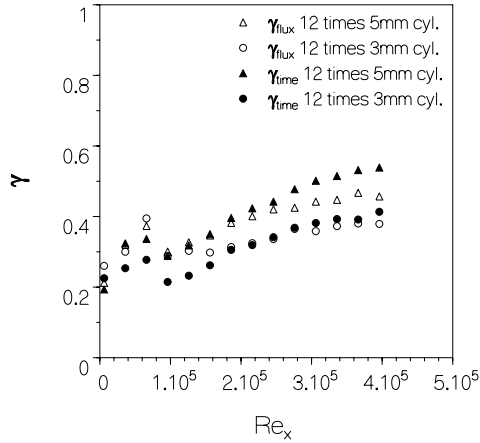


Figure 5.14: Flux based intermittencies (open symbols) and time based (closed symbols) intermittencies for twelve 5 mm and 3 mm cylinders; $V = 35.2$ m/s; no turbulence grid included.

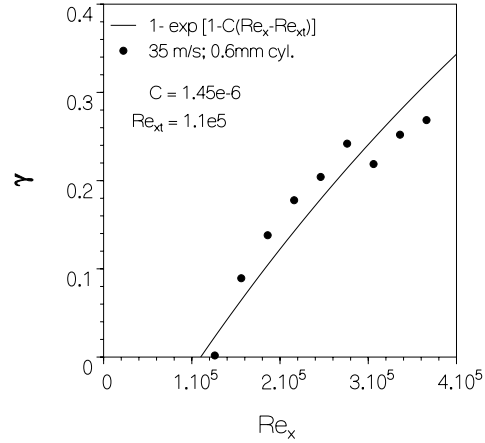


Figure 5.15: Flux based intermittency for 0.6 mm cylinders moving at a velocity of 35.2 m/s; also the model developed by *Mayle and Dullenkopf* [1990] is shown (data fit).

The reason for this is that the wakes initiate transition which begins at the leading edge. This holds for the 5 mm cylinders and the 3 mm cylinders. Disregarding the first part of the intermittency (until $Re_x = 1 \cdot 10^5$), the intermittency increases in streamwise direction. The intermittency curve for the 5 mm cylinders is situated above the 3 mm curve. This is in agreement with the heat flux distributions, which indicate that for a certain Strouhal number the heat flux (and thus the intermittency) increases with the cylinder diameter (see figures 5.1 and 5.2).

The transition process occurs by the initiation and growth of turbulent spots. If a turbulent spot is supposed to behave as a local area of fully turbulent flow, the heat flux in the spot should have the 'turbulent' value. In the case of a non-unique 'turbulent' heat flux, the time based intermittency and the flux based intermittency should be the same. Figure 5.14 shows that there is a reasonable agreement for both intermittencies. This especially holds when one realizes that the time based intermittency can be manipulated easily by defining another threshold value for the heat flux.

The heat flux signals already showed that wake induced transition generated by the 5 mm and 3 mm cylinders already starts at the leading edge of the sensor plate. However, the experiments with 0.6 mm cylinders indicated that transition starts somewhere between the leading edge and the point where natural transition takes place (see e.g. figure 5.3(b)). The measurements with the 0.6 mm cylinders are done in combination with the 5 mm or 3 mm cylinders, i.e. an alternating pattern of cylinders is used. Therefore, the mean heat flux for the 0.6 mm

cylinders can not be calculated in a straightforward manner. An estimate of the mean heat flux for these cylinders is made as follows. In the experiment with the 3 mm and the 0.6 mm cylinders, eight wake passages are present during the test time. For determining the mean flux, only the four passages of the 0.6 mm cylinders are taken into account (implying that the test time becomes 29/2 ms instead of 29 ms). An estimate of the shape of the flux based intermittency curve is obtained by using equation (5.6) with $C = 0.030$. The thus obtained intermittency is given in figure 5.15. It is seen that the intermittency is zero until a Reynolds number of approximately $1.1 \cdot 10^5$. After this, the intermittency starts to increase. A data fit shows that the curve can be described reasonably well by an exponential distribution. This can be explained as follows.

Suppose that the spot production originates from two sources. The first one is initiation due to natural (or bypass) transition, while the second source originates from wake induced transition. When both contributions are independent, it is shown by *Mayle and Dullenkopf* [1990] that the intermittency can be written as:

$$\tilde{\gamma}(x) = 1 - [1 - \gamma_n(x)][1 - \tilde{\gamma}_w(x)]. \quad (5.11)$$

In this equation $\gamma_n(x)$ is the intermittency for natural (or bypass) transition, while the contribution of the wakes is incorporated in the term $\tilde{\gamma}_w(x)$. Equation (5.11) shows that steady and unsteady transition can be superposed to obtain the intermittency distribution for the case of combined transition. The contribution for unsteady transition is found to be (see chapter 2):

$$\tilde{\gamma}_w(x) = 1 - \exp[-1.9(\frac{x - x_{tw}}{UT})], \quad (5.12)$$

with T the wake period. In the case of low background turbulence, the steady term ($\tilde{\gamma}_n(x)$) becomes negligible because transition is completed before natural (or bypass) spots start to occur. So for this situation the total intermittency becomes:

$$\tilde{\gamma}(x) = \tilde{\gamma}_w(x), \quad (5.13)$$

which is an exponential distribution.

No attempt is made to quantify the distribution of the present measurements (figure 5.15) in terms of the mainstream velocity or wake period. The first reason for this is that only four wake passages are available for determining the mean heat flux. Another reason is that the absolute value of the intermittency can not be quantified unequivocal, as a unique 'turbulent' heat flux does not exist. However, the according intermittency distribution agrees (at least qualitatively) with the model proposed by *Mayle and Dullenkopf* [1990] (equation (5.12)). Finally, it is worthwhile to notice that for steady transition also an exponential intermittency distribution is found when large disturbances are present in the main flow. However, for wake induced transition the transition start is situated more downstream (see chapter 4).

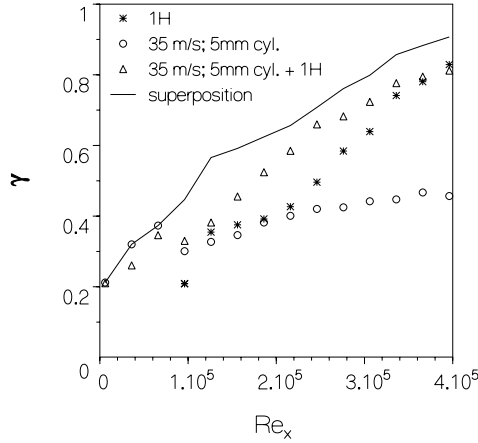


Figure 5.16: Time based intermittencies for steady, unsteady and combined transition; also the superposition of turbulent spots is shown.

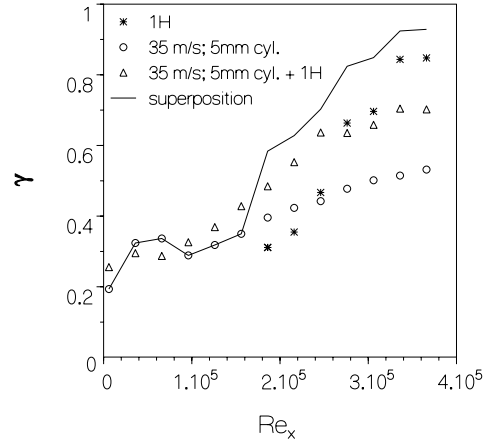


Figure 5.17: Flux based intermittencies for steady, unsteady and combined transition; also the superposition of turbulent spots is shown.

5.6.2 Combined transition

Time based and flux based intermittencies for steady, unsteady and combined transition experiments are compared in figures 5.16 and 5.17. Also the intermittency which follows from the superposition principle applied to the steady and unsteady measurements (equation (5.11)) are shown. The curves depicted in figure 5.16 are roughly as expected. The combined experiment gives an intermittency which is situated above the steady and unsteady experiments. At least the trend of the intermittency according to the superposition, follows the measurements (compare the full line to the triangles).

However, the superposition applied to the flux based intermittencies fails. It is seen (figure 5.17) that for higher Re_x -values the intermittency of the steady experiment is larger than the intermittency of the combined experiment. For combined transition the number of spots, and thus the intermittency, must be larger. It is obvious that this contradicts with reality. The reason for this discrepancy is the difference in the applied turbulent heat flux levels. As the maximum turbulent heat flux of the steady experiment is less than the maximum heat flux of unsteady experiment, the superposition can not be applied unequivocally. Therefore, a flux based intermittency must be used with care. The only possibility to obtain an unambiguous flux based intermittency, is to report the flux level(s) on which the intermittency is based. However, with this restriction the advantage of the intermittency, i.e. describing the state of the boundary layer in a unique manner, disappears.

5.7 Conclusions

The unsteady transition experiments are treated in this chapter. It is shown that strong wakes and weak wakes can be generated in the Ludwig tube set-up. The strong wakes initiate transition which starts at the leading edge of the test plate, and the weak wakes cause transition further downstream. For both situations, the initial shape of the wake remains recognizable in the heat flux signals. Increasing the flow coefficient ($\frac{V}{U}$), i.e. increasing the cylinder velocity, results in a decrease of the width of the wake. Combined transition experiments show that the turbulent spots originating from steady and unsteady transition merge with each other until a complete turbulent boundary layer is obtained. As a result, the mean heat flux of a combined experiment is larger than the flux of a steady or unsteady experiment alone.

It is concluded that the Strouhal number has an effect on wake induced transition. Increasing the Strouhal number results in an increase of the heat flux. However, the Strouhal number is determined by the mainstream velocity and the wake passing frequency; it does not contain information about the flow coefficient. As the cylinder velocity (together with the cylinder diameter) determine the width of the wake, it is the combination of the Strouhal number and the flow coefficient which is important here. The latter determines the shape of the wake, but its effect is not convincingly visible in the mean heat flux.

For the unsteady transition resulting from strong wakes, it is found that the time based intermittency and the flux based intermittency roughly coincide. For the weak wakes, it is not possible to determine the time based intermittency. However, it is possible to determine the flux based intermittency. It follows that for this situation the relation between the flux based intermittency and the streamwise position can be described by an exponential curve. Qualitatively, this agrees with the turbulent spot based model found in literature.

The minimum heat flux for unsteady experiments has the value which belongs to a laminar boundary layer. From this, it is derived that in between two wake passages the flow relaminarizes. The maximum (turbulent) heat flux is seen to depend on the cylinder diameter. When this diameter is enlarged the maximum heat flux increases. From this it follows that a unique 'turbulent' heat flux does not exist. Therefore, it is not possible to define the flux based intermittency, and thus the state of the boundary layer, without taking into account the effect of wake passages on the turbulent heat flux. A modified superposition model for a time based intermittency (which includes separate turbulent heat flux levels) seems then to be more appropriate.

Chapter 6

Conclusions

This thesis deals with boundary layer transition representative for turbines. It describes steady and unsteady transition measurements performed at high velocities.

Bypass transition models presented in literature are based on the point-wise initiation of turbulent spots. These spots grow and merge throughout the complete transition region. For steady transition the generation of spots at one streamwise position in an unstable boundary layer results in the Narasimha intermittency distribution. A spatial uniform spot production gives the Johnson model. The same approach is followed for unsteady transition. It is supposed that the wakes also generate turbulent spots. The resulting intermittency distribution is different from that of steady transition. This is due to the wake induced spot production which is very large. If spots are supposed to be initiated at one streamwise position, an exponential intermittency distribution is obtained. However, in literature it is found that this model does not always agree with the measurements.

The experiments in this thesis are done in a Ludwig tube. In the past it has been shown that with this set-up well defined high velocity flows are generated. A main advantage is that the Reynolds number and the Mach number can be varied independently. Also, the turbulence characteristics of the main flow can be changed easily. For performing unsteady transition experiments, the original Ludwig tube set-up is modified. A special wake generator makes it possible to translate cylinders at high velocity in front of a test plate. Due to this generator, the flow conditions in the test section differ compared to the section used for the steady transition experiments. However, the reproducibility of the unsteady experiments is found to be sufficient.

Steady transition experiments are performed at different turbulence levels. Heat flux measurements show that low background turbulence initiates similar boundary layer transition as found in literature. The transition start and the transition length show good agreement with models based on the growth of tur-

bulent spots initiated in an unstable boundary layer. The intermittency distributions can be described well by the Narasimha or the Johnson model. However, for large turbulence levels these models fail while an exponential curve fits the measurements more accurately. This behaviour is explained by the occurrence of non-growing turbulent spots which enter the stable boundary layer with a certain initial size. It also is observed that for these experiments the transition start is situated closer to the leading edge compared to literature. For intermediate values of the background turbulence, a combination of two models is applicable. The first part of the transition zone, denoted by the pre-transition region, can be described by turbulent spots which decrease in size due to a still stable boundary layer. The resulting intermittency has an exponential distribution. After a critical Reynolds number which depends on the structure of the turbulence, the boundary layer becomes unstable and the conventional route to a complete turbulent boundary layer is followed.

A length scale analysis shows that when the ratio of an effective length scale and the boundary layer thickness at the transition start equals a value found in literature, the Narasimha intermittency distribution is obtained. For larger turbulence levels it is found that this ratio is significantly larger. These are the measurements in which the new intermittency distributions are found.

Unsteady experiments are performed for different wake strengths and cylinder velocities in case of a low background turbulence level. Parameters which have a significant effect on unsteady transition are the Strouhal number and the flow coefficient. Increasing these parameters results in an increase of the mean heat flux. The influence of strong and weak wakes on boundary layer transition is studied. Strong wakes cause transition which starts at the leading edge of the test plate. It is observed that the initial shape of the wake remains nearly unchanged when moving in downstream direction. For unsteady experiments, the time based intermittency and the flux based intermittency (when the maximum value of the heat flux is well defined) are seen to coincide roughly. Weak wakes cause transition which starts somewhere between the point of bypass transition and the leading edge. The flux based intermittency as a function of the streamwise Reynolds number is seen to follow an exponential curve. Qualitatively, this agrees with wake induced transition models found in literature.

It appears that the strength of the wake, and thus the wake turbulence, has a significant effect on the maximum heat transfer. This implies that a 'unique' turbulent heat flux does not exist. As a result, the intermittency based on the heat flux cannot be used when no information is given about this turbulent heat flux. Therefore, the intermittency concept must be applied with care, as it does not describe the state of the boundary layer in a unique manner. More difficulties concerning the intermittency arise for the experiments in which unsteady and steady transition together occurs. These combined measurements show that the spots initiated by both processes merge until a fully turbulent boundary layer is obtained. The according heat flux has a larger value than unsteady- or steady

experiments alone. Describing the transition zone by a flux based intermittency fails due to the direct effect of the passing wakes to the maximum heat flux. A time based intermittency model seems then to be more appropriate.

In future experiments attention should be given to a few topics. The first one is to improve the signal to noise ratio in the electronic device for measuring the thin film resistance. It is found that for an increasing number of channels, this ratio significantly decreases. This implies that for the present measurements it is difficult to study the time evolution of the turbulent spots in streamwise direction. With this improvement the structure of an individual turbulent spot can be studied more accurately. In combination with smaller sensors, it becomes possible to visualize the turbulent spots in the region where the intermittency as a function of the streamwise Reynolds number is described by the exponential model.

Also the sample frequency should be increased. It is seen that the 'effective' frequency for bypass transition, as proposed in literature, is higher than the sample frequency in the present experiments. Only if this frequency increases, more attention can be given to the influence of the various length scales.

The influence of the structure of the wake on the turbulent heat flux is a subject of interest too. If one is able to predict this heat flux, the flux based intermittency becomes more appropriate to describe unsteady transition.

To approach the flow conditions in turbines more closely, the flow coefficient should increase. This can only be done by increasing the translating cylinder velocity, as decreasing the mainstream velocity results in a decrease of the signal to noise ratio.

Another subject of interest is to study the effect of wake-wake interaction. This can be realized by increasing the cylinder speed, or by using more cylinders in the wake generator, i.e decreasing the cylinder mesh.

Bibliography

- Abu-Ghannam, B. J. and Shaw, R. (1980). Natural transition of boundary layers - The effects of turbulence, pressure gradient, and flow history. *J. Mech. Eng. Sci.*, 22:213–228.
- Addison, J. S. and Hodson, H. P. (1990a). Unsteady transition in an axial-flow turbine: Part I - Measurements on the turbine rotor. *Journal of Turbomachinery*, 112:206–214.
- Addison, J. S. and Hodson, H. P. (1990b). Unsteady transition in an axial-flow turbine: Part II - Cascade measurements and modeling. *Journal of Turbomachinery*, 112:215–221.
- Bird, R. B., Stewart, W. E., and Lightfoot, E. N. (1960). *Transport Phenomena*. John Wiley and Sons.
- Blair, M. F. (1983a). Influence of free-stream turbulence on turbulent boundary layer heat transfer and mean profile development, part I - Experimental data. *Journal of Heat Transfer*, 105:33–40.
- Blair, M. F. (1983b). Influence of free-stream turbulence on turbulent boundary layer heat transfer and mean profile development, part II - Analysis of results. *Journal of Heat Transfer*, 105:41–47.
- Bruun, H. H. (1995). *Hot-wire Anemometry*. Oxford University Press.
- Cebeci, T. and Smith, A. M. O. (1974). *Analysis of Turbulent Boundary Layers*. Academic Press, New York.
- Chen, K. K. and Thyson, N. A. (1971). Extension of Emmons' spot theory to flows on blunt bodies. *AIAA Journal*, 9:821–825.
- Ching, C. Y. and LaGraff, J. E. (1995). Measurement of turbulent spot convection rates in a transitional boundary layer. *Experimental Thermal and Fluid Science*, 1995:52–60.
- Clark, J. P., Jones, T. V., and LaGraff, J. E. (1994). On the propagation of naturally-occurring turbulent spots. *Journal of Engineering Mathematics*, 28:1–19.
- Cohen, H., Rogers, G. F. C., and Saravanamuttoo, H. I. H. (1996). *Gas Turbine Theory*. Longman Group Limited, fourth edition.
- Consigny, H. and Richards, B. E. (1982). Short duration measurements of heat-transfer rate to a gas turbine rotor blade. *Journal of Engineering for Power*, 104:542–551.

- Dhawan, S. and Narasimha, R. (1958). Some properties of boundary layer flow during the transition from laminar to turbulent motion. *J. Fluid Mech.*, 3:418–436.
- Diller, T. E. (1993). Advances in heat flux measurements. In *Advances in heat transfer*. Academic Press Inc.
- Dong, Y. and Cumpsty, N. A. (1990a). Compressor blade boundary layers: Part I - Test facility and measurements with no incident wakes. *Journal of Turbomachinery*, 112:222–230.
- Dong, Y. and Cumpsty, N. A. (1990b). Compressor blade boundary layers: Part II - Measurements with incident wakes. *Journal of Turbomachinery*, 112:231–240.
- Doorly, D. J. (1987). Modelling the unsteady flow in a turbine rotor passage. ASME-Paper 87-GT-197.
- Emmons, H. W. (1951). The laminar-turbulent transition in a boundary layer; part I. *J. Aero. Sci.*, 18:490–498.
- Esch van, B. P. M. (1997). *Simulation of three-dimensional unsteady flow in hydraulic pumps*. PhD thesis, University of Twente.
- Funazaki, K. (1993). Studies on the unsteady boundary layer on a flat plate subjected to incident wakes. *JSME International Journal*, 36:532–539.
- Funazaki, K. (1996a). Unsteady boundary layers on a flat plate disturbed by periodic wakes; part I: Measurement of wake-affected heat transfer and wake-induced transition model. *Journal of Turbomachinery*, 118:327–336.
- Funazaki, K. (1996b). Unsteady boundary layers on a flat plate disturbed by periodic wakes; part II: Measurements of unsteady boundary layers and discussion. *Journal of Turbomachinery*, 118:337–346.
- Funazaki, K., Meguro, T., and Yamawaki, S. (1993). Studies on the unsteady boundary layer on a flat plate subjected to incident wakes (Forced transition models of the boundary layer). *JSME Int. Journal, Series B*, 36:532–539.
- Gostelow, J. P. (1989). Adverse pressure gradient effects on boundary layer transition in a turbulent free-stream. In *Proc. 9th Int. Symp. Air Breathing Engines*, pages 1299–1306.
- Gostelow, J. P. and Blunden, A. R. (1989). Investigations of boundary layer transition in an adverse pressure gradient. *Journal of Turbomachinery*, 111:366–375.
- Gostelow, J. P., Blunden, A. R., and Walker, G. J. (1994). Effects of free-stream turbulence and adverse pressure gradients on boundary layer transition. *Journal of Turbomachinery*, 116:392–404.
- Gostelow, J. P. and Dey, J. (1991). Spot formation rates in transitional boundary layers under zero and adverse pressure gradients. In *Proc. Boundary Layer Transition and Control Conference*, pages 29:1–29:7.
- Gostelow, J. P., Walker, G. J., Solomon, W. J., Hong, H., and Melwani, N. (1997). Investigation of the calmed region behind a turbulent spot. *Journal of Turbomachinery*, 119:802–809.

- Hall, D. J. and Gibbings, J. C. (1972). Influence of stream turbulence and pressure gradient upon boundary layer transition. *Journal Mechanical Engineering Science*, 14:134–146.
- Han, J. C., Zhang, L., and Ou, S. (1993). Influence of unsteady wake on heat transfer coefficient from a gas turbine blade. *Journal of heat Transfer*, 115:904–911.
- Hinze, J. O. (1975). *Turbulence*. McGraw-Hill Book Company, second edition.
- Hodson, H. P., Addison, J. S., and Shepherdson, C. A. (1992). Models for unsteady wake-induced transition in axial turbomachines. *J. Phys. III France*, 2:545–574.
- Hodson, H. P. and Dawes, W. N. (1998). On the interpretation of measured profile losses in unsteady wake-turbine blade interaction studies. *Journal of Turbomachinery*, 120:276–284.
- Hogendoorn, C. J. (1997). *Heat transfer measurements in subsonic transitional boundary layers*. PhD thesis, Eindhoven University of Technology.
- Hogendoorn, C. J., Lange de, H. C., Dongen van, M. E. H., and Steenhoven van, A. A. (1997). Influence of turbulence intensity on intermittency model in by-pass transition. ASME-Paper 97-GT-473.
- Hogendoorn, C. J., Lange de, H. C., and Steenhoven van, A. A. (1998). Design optimisation for fast heat-transfer gauges. *Measurement Science and Technology*, 9:428–434.
- James, C. J. (1958). Observations of turbulent burst geometry and growth in supersonic flow. NACA Tech. Note 4235.
- Johnson, M. W. (1994). A bypass transition model for boundary layers. *Journal of Turbomachinery*, 116:759–764.
- Johnson, M. W. and Ercan, A. H. (1999). A physical model for bypass transition. *Int. J. Heat and Fluid Flow*, 20:95–104.
- Johnson, M. W. and Fashifar, A. (1994). Statistical properties of turbulent bursts in transitional boundary layers. *Int. J. Heat and Fluid Flow*, 15:283–290.
- Kays, W. M. and Crawford, M. E. (1980). *Convective Heat and Mass Transfer*. McGraw-Hill.
- Lange de, H. C., Hogendoorn, C. J., and Steenhoven van, A. A. (1998). The similarity of turbulent spots. *Int. Comm. Heat and Mass Transfer*, 25:331–337.
- Lange de, H. C., Schook, R., and Steenhoven van, A. A. (2000). Instationary heat transfer measurements in a ludwig tube. 3rd Thermal Sciences Conference, Heidelberg, accepted for publication.
- Lin, C. C. (1959). *Turbulent Flows and Heat Transfer*. Princeton University Press.
- Liu, X. and Rodi, W. (1991). Experiments on transitional boundary layers with wake-induced unsteadiness. *J. Fluid Mech.*, 231:229–256.
- Mayle, R. E. (1991). The role of laminar-turbulent transition in gas turbine engines. *Journal of Turbomachinery*, 113:509–537.
- Mayle, R. E. (1999). A theory for predicting the turbulent-spot production rate. *Journal of Turbomachinery*, 121:588–593.

- Mayle, R. E. and Dullenkopf, K. (1990). A theory for wake-induced transition. *Journal of Turbomachinery*, 112:188–195.
- Mayle, R. E. and Dullenkopf, K. (1991). More on the turbulent strip theory for wake-induced transition. *Journal of Turbomachinery*, 113:428–432.
- Mayle, R. E., Dullenkopf, K., and Schulz, A. (1998). The turbulence that matters. *Journal of Turbomachinery*, 120:402–409.
- Mayle, R. E. and Schulz, A. (1997). The path to predicting bypass transition. *Journal of Turbomachinery*, 119:405–411.
- Meyer, R. X. (1958). The effect of wakes on the transient pressure and velocity distributions in turbomachines. *Transactions of the ASME*, 80:1544–1552.
- Miller, J. A. and Fejer, A. A. (1964). Transition phenomena in oscillating boundary layer flows. *J. Fluid Mech.*, 18:438–485.
- Narasimha, R. (1957). On the distribution of intermittency in the transition region of a boundary layer. *J. Aero. Sci.*, 24:711–712.
- Narasimha, R. (1985). The laminar-turbulent transition zone in the boundary layer. *Prog. Aerospace Sci.*, 22:29–80.
- Nieuwstadt, F. T. M. (1992). *Turbulentie*. Epsilon Uitgaven.
- Obrenski, H. J. and Fejer, A. A. (1967). Transition in oscillating boundary layer flows. *J. Fluid Mech.*, 29:93–111.
- Obrenski, H. J., Morkovin, M. V., and Landahl, M. (1969). A portfolio of stability characteristics of incompressible boundary layers. AGARDograph 134.
- O’Brien, J. E. and Capp, S. P. (1989). Two-component phase-averaged turbulence statistics downstream of a rotating spoked-wheel wake generator. *Journal of Turbomachinery*, 111:475–482.
- Orth, U. (1993). Unsteady boundary-layer transition in flow periodically disturbed by wakes. *Journal of Turbomachinery*, 115:707–713.
- Owczarek, J. A. (1964). *Gas Dynamics*. International Textbook Company.
- Owen, F. K. and Hortsman, C. C. (1972). Hypersonic transitional boundary layers. *AIAA Journal*, 10:769–775.
- Pfeil, H. and Herbst, R. (1979). Transition procedure of instationary boundary layers. ASME-Paper 79-GT-128.
- Pfeil, H., Herbst, R., and Schröder, T. (1983). Investigation of the laminar-turbulent transition of boundary layers disturbed by wakes. *Journal of Engineering for Power*, 105:130–137.
- Schlichting, H. (1979). *Boundary Layer Theory*. McGraw-Hill Book Company, seventh edition.
- Schobeiri, M. T. and Pappu, K. (1997). Experimental study on the effect of unsteadiness on boundary layer development on a linear turbine cascade. *Experiments in Fluids*, 23:306–316.

- Schook, R., Lange de, H. C., and Steenhoven van, A. A. (1998). Effects of compressibility and turbulence level on bypass transition. ASME-Paper 98-GT-286.
- Schook, R., Lange de, H. C., and Steenhoven van, A. A. (1999). Unsteady transition measurements using a ludwig tube. In *Turbomachinery: Fluid Dynamics and Thermodynamics, volume A*, pages 147–155.
- Schook, R., Lange de, H. C., and Steenhoven van, A. A. (2000a). Heat transfer measurements in transitional boundary layers. accepted for: *Int. J. Heat and Mass Transfer*.
- Schook, R., Lange de, H. C., and Steenhoven van, A. A. (2000b). Unsteady heat transfer in subsonic boundary layers. In *Turbulence Heat and Mass Transfer 3*, pages 331–338.
- Schook, R., Lange de, H. C., and Steenhoven van, A. A. (2000c). Unsteady heat transfer in subsonic boundary layers. submitted for publication in: *Int. J. Heat and Fluid Flow*.
- Schubauer, G. B. and Klebanoff, P. S. (1955). Contributions on the mechanics of boundary-layer transition. NACA Tech. Note TN 3489.
- Schubauer, G. B. and Skramstad, H. K. (1947). Laminar boundary layer oscillations and stability of laminar flow. *J. Aero. Sci.*
- Schultz, D. L., Oldfield, M. L. G., and Jones, T. V. (1980). Heat transfer rate and film cooling effectiveness measurements in a transient cascade. *AGARD-CP*, 281:8,1–8,9.
- Simoneau, R. J. and Simon, F. F. (1993). Progress towards understanding and predicting heat transfer in the turbine gas path. *Int. J. Heat and Fluid Flow*, 14:106–128.
- Simonich, J. C. and Bradshaw, P. (1978). Effect of free-stream turbulence on heat transfer through a turbulent boundary layer. *Journal of Heat Transfer*, 100:672–677.
- Steketee, J. A. (1955). Note on a formula of H.W. Emmons. *J. Aero. Sci.*, 22:578–579.
- Tennekes, H. and Lumley, J. L. (1972). *A First Course in Turbulence*. MIT Press.
- Walker, G. J. (1989). Transitional flow on axial turbomachine blading. *AIAA Journal*, 27:595–602.
- Walker, G. J. (1993). The role of laminar-turbulent transition in gas turbine engines: a discussion. *Journal of Turbomachinery*, 115:207–217.
- Zhang, M. Y., Tsou, F. K., Chen, Z. J., and Chen, S. J. (1993). Film cooling experimental technique using a ludwig tube wind tunnel. *Experimental Thermal and Fluid Science*, 6:186–195.
- Zysina-Molozhen, L. M. and Kuznetsova, V. M. (1969). Investigation of transition conditions in a boundary layer. *Teploenergetika*, 16:16–20.

Appendix A

Derivation of intermittency

In this appendix the derivation of the intermittency with a constant spot production rate g along a flat plate, according to *Emmons* [1951], is given.

The fraction of time during which a certain point P is turbulent, i.e. the intermittency, can be expressed by:

$$\gamma(P) = 1 - \exp\left[-\int_R g(P_0)dV_0\right], \quad (\text{A.1})$$

with g the spot production rate and R the cone of dependence (figures A.1 and A.2). This relation can be derived by assuming a random spot generation and by taking into account overlap of turbulent spots (*Emmons* [1951] and *Steketee* [1955]).

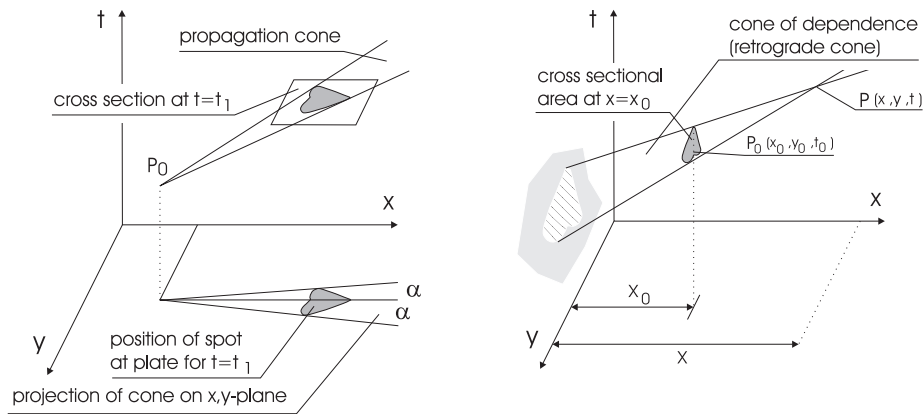


Figure A.1: Spot propagation in (x, y, t) -space. Figure A.2: Dependence volume of P (cone of dependence).

If the propagation cone is a cone with straight generators, the dependence volume R is also a straight cone. Therefore, the integral becomes:

$$\int_R g dV = gV, \quad (\text{A.2})$$

with V the volume of dependence (in the x, y, t -space).

The volume of a cone is the area of the base multiplied by the altitude divided by three. Introduce A_1 as the cross section at unit distance from the top of the cone ($x_{A_1} - x_0 = 1$):

$$A_1 = \frac{1}{(x_{A_1} - x_0)^2} \int_{x=\text{constant}} dy_1 dt_1. \quad (\text{A.3})$$

In this equation, the integral is taken at the section where x is constant. A cross section of the dependence cone is called the 'time-width shape' of a turbulent spot. This cone is depicted in figure A.3. The volume V at any position x can be written as:

$$V = \frac{A_1(x - x_0)^3}{3}. \quad (\text{A.4})$$

Now, the dimensionless spot propagation parameter is defined as (U is the main-stream velocity):

$$\sigma = A_1 U. \quad (\text{A.5})$$

By use of equations (A.2), (A.4) and (A.5) and assuming that $g = \text{constant} = a$, the intermittency (equation (A.1)) can be written as:

$$\gamma(x) = 1 - \exp\left[-\frac{\sigma a x^3}{3U}\right], \quad (\text{A.6})$$

which gives the desired result.

It is possible to rewrite σ in terms of the geometrical spot dimensions. Therefore, the relation between the 'time-width shape', given in the $x = \text{constant}$ -plane (vertical-plane), must be transformed to the $t = \text{constant}$ -plane (horizontal-plane).

Consider a cone, as depicted in figure A.4, in the ξ, η, y -space, which is symmetrical with respect to the ξ, η -plane ($y = 0$). The relations between elements of area on a horizontal cross section at $\eta = \eta_2$ and a vertical section at $\xi = \xi_1$ are:

$$dy_1 = \frac{\xi_1}{\xi_2} dy_2, \quad (\text{A.7})$$

$$d\eta_1 = \frac{\xi_1}{\xi_2} d\eta_2 \quad (\text{A.8})$$

and

$$d\eta_2 = \frac{\eta_2}{\xi_2} d\xi_2. \quad (\text{A.9})$$

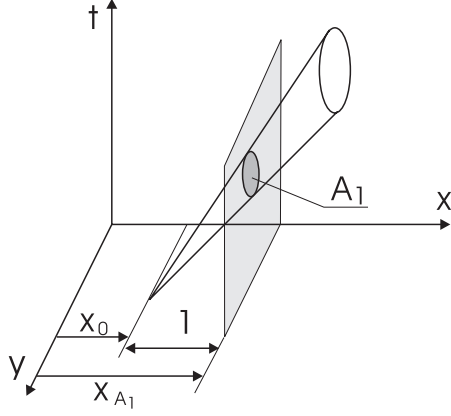


Figure A.3: 'Time-width shape' of a cone at unit distance from the top.

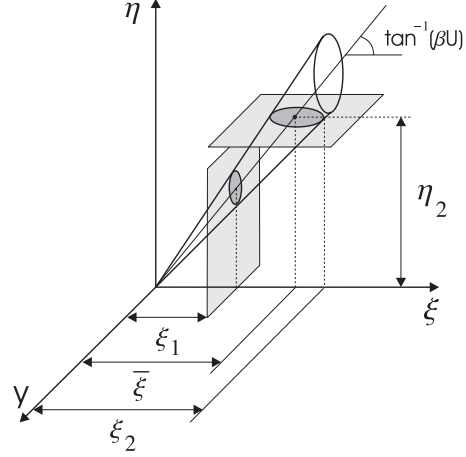


Figure A.4: Cone in the ξ, η, y -space (symmetrical in ξ, η -plane).

Combining equations (A.8) and (A.9) gives:

$$d\eta_1 = \frac{\xi_1}{\xi_2} \left(\frac{\eta_2}{\xi_2} d\xi_2 \right). \quad (\text{A.10})$$

The dimensionless area A_1 in the ξ, η, y -space, then follows by substitution of equations (A.7) and (A.10) in equation (A.3), where t_1 is replaced by η_1 and $(x_{A_1} - x_0)$ by ξ_1 :

$$A_1 = \frac{1}{\xi_1^2} \int dy_1 dt_1 = \eta_2 \int \frac{dy_2 d\xi_2}{\xi_2^3}. \quad (\text{A.11})$$

The parameter η_2 is taken arbitrarily by using the center of the geometrical spot:

$$\eta_2 = \frac{\bar{\xi}}{\beta U}, \quad (\text{A.12})$$

with $\bar{\xi}$ the distance from the top of the cone to the center of the spot, and βU the propagation rate of this center. Incorporation in equation (A.11) gives (α is the spot half spreading angle):

$$A_1 = \frac{\bar{\xi}}{\beta U} \frac{\tan^3(\alpha)}{\tan^3(\alpha)} \int \frac{dy d\xi}{\xi^3}. \quad (\text{A.13})$$

This equation is valid for every arbitrarily position '2', and can be rewritten in:

$$A_1 = \frac{\tan^2(\alpha)\lambda}{\beta U}, \quad (\text{A.14})$$

with

$$\lambda = \tan(\alpha) \bar{\xi} \int \frac{dy d\xi}{[\tan(\alpha)\xi]^3}. \quad (\text{A.15})$$

When the spot is assumed to be small compared to its distance where it was initiated (top of the cone), λ can be simplified by taking $\xi = \bar{\xi}$, which results in:

$$\lambda = \frac{A}{[\tan(\alpha)\bar{\xi}]^2}. \quad (\text{A.16})$$

Now, λ represents a dimensionless area of the turbulent spot which is determined by the actual area A divided by the square of the half width of the spot.

It follows from equations (A.5) and (A.14) that the dimensionless spot propagation parameter σ can be written as:

$$\sigma = \frac{\tan^2(\alpha)\lambda}{\beta}. \quad (\text{A.17})$$

Thus, the parameters for determining σ are:

- α , the spot half spreading angle.
- β , the spot center velocity divided by the free stream velocity.
- λ , the area of the spot divided by the square of the half width.

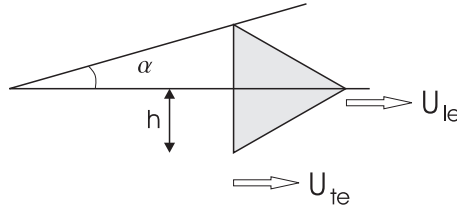


Figure A.5: Triangular turbulent spot.

A turbulent spot can be modelled as having a triangular shape (figure A.5). The leading edge velocity of the spot is U_{le} and the trailing edge velocity U_{te} . The spot half spreading angle is α . Assume a spot at a time t after its initiation. Now, the area of the spot equals:

$$A = \frac{1}{2}(U_{le} t - U_{te} t) 2h. \quad (\text{A.18})$$

The half width h is:

$$h = \tan(\alpha) U_{te} t. \quad (\text{A.19})$$

The parameter λ can be written as:

$$\lambda = \frac{1/2 t (U_{le} - U_{te}) 2h}{h^2} = \frac{U_{le} - U_{te}}{U_{te} \tan(\alpha)}. \quad (\text{A.20})$$

The spot propagation parameter (equation (A.17)) now becomes:

$$\sigma = \tan(\alpha) \left[\frac{U_{le} - U_{te}}{U_{te}} \right] \frac{U}{U_s}. \quad (\text{A.21})$$

By ignoring the difference between the leading edge velocity of the spot and the center velocity of the spot, i.e. assuming that $U_s = U_{le}$, it follows that:

$$\sigma = \tan(\alpha) \left[\frac{U}{U_{te}} - \frac{U}{U_{le}} \right]. \quad (\text{A.22})$$

Appendix B

Ludwig tube set-up



Figure B.1: Overview of the tube, test section and dump tank.

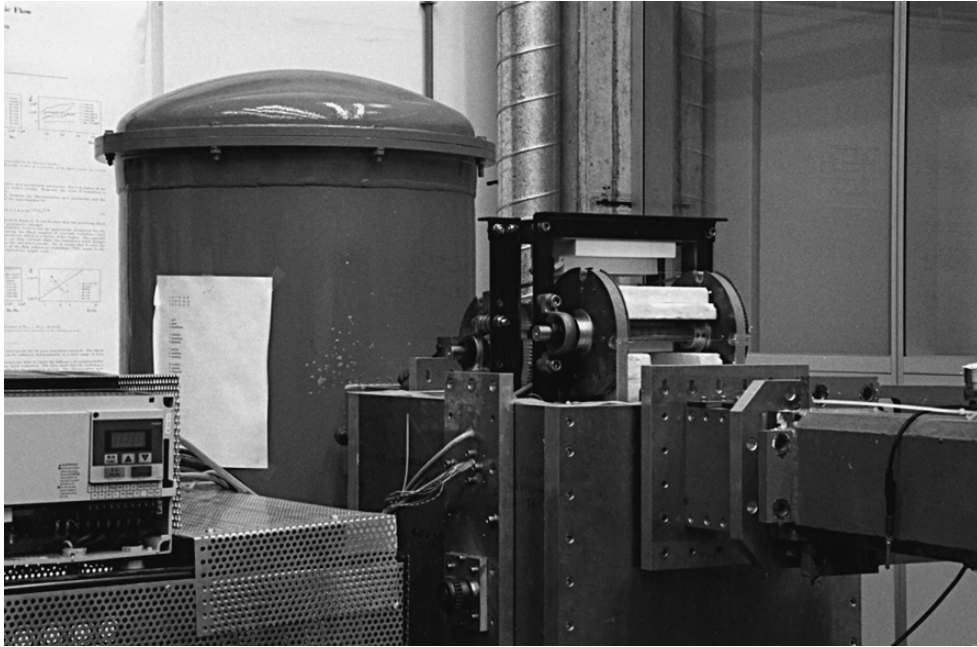


Figure B.2: Close-up of the test section.

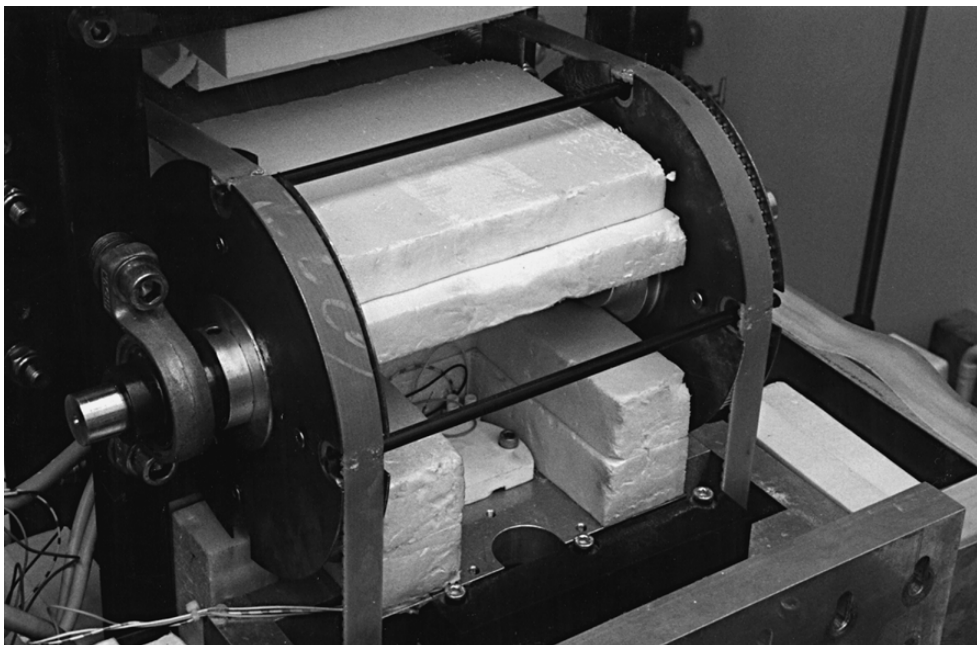


Figure B.3: Wake generator.

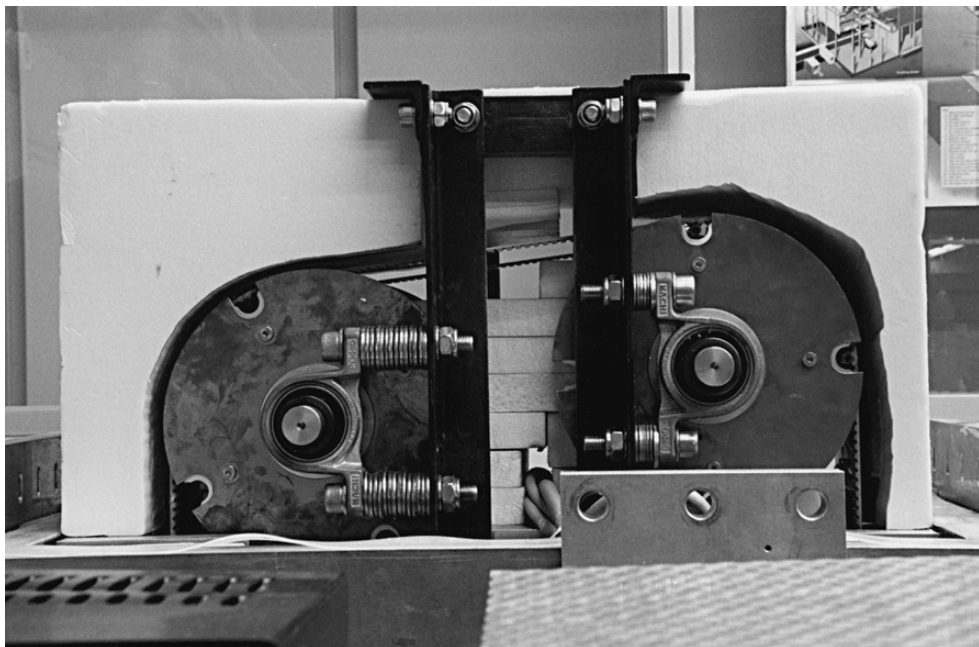


Figure B.4: Wake generator: side view.

Appendix C

Length scales

In this appendix different length scales are summarized briefly. Details can be found in *Tennekes and Lumley* [1972], *Hinze* [1975] and *Nieuwstadt* [1992].

A length scale which plays an important role is the boundary layer thickness. At the leading edge of the plate it has zero thickness. In streamwise direction it grows with the square-root of the distance. For our conditions, the boundary layer thickness at the transition start (δ_{xt}) ranges from 0.2 mm to 0.5 mm.

Suppose that \mathcal{U} and \mathcal{L} are the velocity and the length scale of the macroscopic structure of the flow. Examples of macroscopic scales are velocity fluctuations of the main stream and the dimensions of the turbulence generating grids (mesh size, ranging from 10 mm to 20 mm).

The smallest important length scale in a flow is the Kolmogorov length scale. It represents the size of the smallest eddies and is defined as:

$$\eta = \left(\frac{\nu^3}{\epsilon}\right)^{\frac{1}{4}}, \quad (\text{C.1})$$

in which ν is the kinematic viscosity and ϵ the dissipation. The dissipation of turbulent energy in a flow with decaying homogeneous turbulence can be determined experimentally by (*Simonich and Bradshaw* [1978]):

$$\epsilon = -\frac{3}{2}U \frac{\overline{du'^2}}{dx}. \quad (\text{C.2})$$

For the measurements described in this thesis the Kolmogorov scale ranges from approximately 0.05 mm to 0.1 mm.

For decaying homogeneous turbulence, the dissipative length scale L_ϵ can be derived by (*Simonich and Bradshaw* [1978]):

$$U \frac{\overline{du'^2}}{dx} = -\frac{\overline{(u'^2)^{3/2}}}{L_\epsilon}. \quad (\text{C.3})$$

As can be seen, this scale is directly related to equation (C.2). The dissipative scale ranges from 0.5 mm to 8 mm, depending on the turbulence generating grid.

In literature an effective length scale l_{eff} is assumed to be responsible for bypass transition (*Mayle* [1999]). This scale is found to be 21 times the Kolmogorov length scale. It is found that for the present measurements l_{eff} has the same order of magnitude as the dissipative length scale (1 mm to 2 mm). Table C.1 shows all the length scales as treated above.

Table C.1: Length scales.

length scale	minimum [mm]	maximum [mm]
η	0.05	0.1
δ_{xt}	0.2	0.5
L_ϵ	0.5	8
l_{eff}	1	2
\mathcal{L}	10	20

Nomenclature

a	spot formation rate	$[\text{m}^{-2} \text{s}^{-1}]$
a	turbulent strip production strength	$[\text{s}^{-1}]$
A	area	$[\text{m}^2]$
A	calibration constant	$[\text{V}^2]$
A_1	calibration constant	$[-]$
b	constant	$[-]$
b	constant	$[\text{s}^{-1}]$
B	calibration constant	$[\text{V}^2]$
B_1	calibration constant	$[-]$
c	specific heat capacity	$[\text{J kg}^{-1} \text{K}^{-1}]$
c	speed of sound	$[\text{m s}^{-1}]$
d	diameter	$[\text{m}]$
C, \mathcal{C}	constant	$[-]$
C_r	Tollmien-Schlichting phase velocity	$[\text{m s}^{-1}]$
f	frequency	$[\text{Hz}]$
\hat{f}	dimensionless frequency	$[-]$
$F(\gamma)$	transformation function	$[-]$
\mathcal{F}	correction factor	$[-]$
g	spot production parameter	$[\text{m}^{-2} \text{s}^{-1}]$
H	Heaviside function	$[-]$
i	electrical current	$[\text{C s}^{-1}]$
\mathcal{J}	constant	$[\text{m}^{-3}]$
k	thermal conductivity	$[\text{W m}^{-1} \text{K}^{-1}]$
k	reduced frequency	$[-]$
k	spot decay rate	$[\text{m}^{-1}]$
l	integral wavelength	$[\text{m}]$
ℓ	length	$[\text{m}]$
L	integral length scale, plate length	$[\text{m}]$
L_ϵ	dissipative length scale	$[\text{m}]$
L_t	transition length ($0.01 < \gamma < 0.99$)	$[\text{m}]$
m	spot formation rate	$[\text{m}^{-2}]$
M	Mach number	$[-]$
M	cylinder mesh	$[\text{m}]$
n	King's law constant	$[-]$
n	spot formation rate	$[\text{m}^{-1} \text{s}^{-1}]$
\hat{n}	dimensionless spot formation rate	$[-]$
N	number of spots	$[-]$
\hat{N}	modified spot production rate	$[-]$
Nu	Nusselt number	$[-]$
p	pressure	$[\text{Pa}]$
P	total pressure	$[\text{Pa}]$

P	fraction of velocity minima	[-]
P	power	[W]
Pr	Prandtl number	[-]
Pr_t	turbulent Prandtl number	[-]
q''	heat flux	[W m ⁻²]
q_l	laminar heat flux	[W m ⁻²]
q_t	turbulent heat flux	[W m ⁻²]
\bar{q}	averaged measured heat flux	[W m ⁻²]
r	number of cylinders	[-]
R	electrical resistance	[Ω]
R	cone of dependence	[m ² s]
R	gas constant	[J kg ⁻¹ K ⁻¹]
Re	Reynolds number	[-]
Re_{ns}	unsteady Reynolds number	[-]
Re_u	unit Reynolds number	[m ⁻¹]
Re_x	local Reynolds number	[-]
Re_{xt}	transition start Reynolds number	[-]
Re_θ	momentum thickness Reynolds number	[-]
s	transformation coefficient	[-]
S	Strouhal number	[-]
St	Stanton number	[-]
t	time	[s]
T	temperature	[K]
T	disturbance period, wake period	[s]
T_r	recovery temperature	[K]
Tu	turbulence level	[%]
u	local streamwise velocity	[m s ⁻¹]
U	mainstream velocity	[m s ⁻¹]
U_s	mean spot velocity	[m s ⁻¹]
V	cylinder speed	[m s ⁻¹]
V_0	bridge voltage	[V]
w	spot size	[m]
x	streamwise direction	[m]
x_t	transition start	[m]
y	spanwise direction	[m]
z	coordinate perpendicular to surface	[m]
Z	dimensionless coordinate perpendicular to surface	[-]

Greek symbols

α	temperature resistance coefficient	[K ⁻¹]
α	spot half spreading angle	[°]
α	strip half propagation angle	[°]
β	proportionality factor	[-]

β_E, β_F	velocity fraction	[-]
γ	intermittency	[-]
δ	boundary layer thickness	[m]
δ	Dirac delta function	[-]
δ^*	boundary layer displacement thickness	[m]
ϵ	dissipation	[m ² s ⁻³]
ζ	constant	[m ⁻³]
η	Kolmogorov length scale	[m]
θ	boundary layer momentum thickness	[m]
κ	specific heat ratio	[-]
λ	transition length ($0.25 < \gamma < 0.75$)	[m]
λ_θ	pressure gradient parameter	[-]
Λ	number of spots generated upstream	[-]
μ	dynamic viscosity	[N s m ⁻²]
ν	kinematic viscosity	[m ² s ⁻¹]
ξ	non-dimensional streamwise coordinate	[-]
Φ	flow coefficient	[-]
ρ	density	[kg m ⁻³]
σ	turbulent spot propagation parameter	[-]
τ_w	wake duration	[s]
v	number of spots per integral wavelength	[-]
ω	circular frequency	[Hz]

Subscripts

c	critical
eff	effective
f	flux
i	initial
g	gauge
l	laminar
la	lateral
le	leading edge
lo	longitudinal
m	minimum
n	natural
rms	root mean square
t, tr	transition
t	test section
t	turbulent
te	trailing edge
w	wake

Summary

The heat transfer in a boundary layer increases significantly when laminar to turbulent transition occurs. Especially in the field of turbomachinery design, knowledge of the heat transfer and thus the transition is of major importance since a large part of the turbine blade is covered by the transition zone.

Two kinds of transition can be distinguished in a turbomachine. The first one is steady bypass transition which is a result of large disturbances in the main flow. These disturbances are present in the flow continuously and therefore this type of transition is assumed to be steady in time. In contrast, there exist unsteady transition which finds its origin in rotor-stator interaction. Wakes are shed behind the stator blades and flow along the rotor blades. The high turbulence in the wakes cause transition which starts more upstream compared to steady transition.

The aim of this thesis is to investigate the influence of the turbulence level, the turbulence structure and the Reynolds number on both steady and unsteady transition. All experiments are done at turbine-like conditions, i.e. at high velocities and large disturbance levels.

The flow is initiated by a Ludwieg tube set-up. A major advantage of this transient facility is that the Reynolds number and the Mach number can be adjusted independently. Determination of the flow conditions is done by hot-wire and pressure measurements. These measurements show that a good reproducibility of the conditions is obtained.

Steady transition experiments are performed for several disturbance levels at a constant Mach number. A thin-film technique is used to determine the heat flux. For comparison the data are transformed to intermittency distributions which describe the transition in streamwise direction. Agreement with literature is found for small turbulence levels. However, for large and intermediate values significant deviations are observed. A new model based on the occurrence of turbulent spots, is able to fit the data. The resulting intermittency curve has an exponential distribution which is also applicable in the pre-transition zone.

For obtaining an unsteady flow, the test section is modified. A wake generator which translates cylinders in front of the test plate is developed. The modification results in a slight deviation in flow conditions compared to the original set-up.

Wake induced transition experiments are performed for several wake strengths and wake velocities. It is found that the streamwise position of the transition start depends on the wake strength. Also the turbulent heat flux level is strongly dependent on the wake.

Measurements are done to study the combined effect of background turbulence and wakes. Both, a turbulence generating grid and moving cylinders are used together in these experiments. It is shown that a superposition of intermittencies as is proposed in literature, is not valid in all cases. The reason for this is the non-unique turbulent flux level. Therefore, attention must be paid when using the intermittency based on the heat flux.

Samenvatting

De warmte-overdracht in een grenslaag verandert sterk als grenslaagtransitie optreedt. Vooral voor het ontwerpen van gasturbines is kennis van de warmte-overdracht, en dus van grenslaagtransitie, van groot belang.

Er kan onderscheid gemaakt worden tussen twee, voor turbines belangrijke, soorten transitie. De eerste is stationaire bypass transitie, welke geïnitieerd wordt door grote verstoringen in de hoofdstroom. Doordat deze verstoringen continu in de stroming aanwezig zijn, is de optredende transitie stationair. Een tweede vorm van transitie is een gevolg van rotor-stator interactie, welke instationair is. Achter de statorbladen worden zoggen gevormd die vroegtijdige transitie op de stroomafwaarts geïntegreerde rotorbladen veroorzaken. Vooral de hoge turbulentiegraad in de zoggen is verantwoordelijk voor deze vorm van transitie.

Het doel van dit proefschrift is om de invloed van turbulentiegraad, turbulentiestructuur en het Reynoldsgetal op zowel stationaire als instationaire transitie te bestuderen. De stromingscondities moeten in de buurt komen van de condities die optreden in echte gasturbines. Dit betekent dat de metingen uitgevoerd dienen te worden bij hoge snelheden en bij grote verstoringen. Een groot voordeel van de Ludwig buis is dat het Reynolds- en het Mach getal onafhankelijk van elkaar ingesteld kunnen worden. Verificatie van de stromingscondities is gedaan met behulp van hittedraads- en drukmetingen, waarbij een goede reproduceerbaarheid van de condities is gevonden.

Stationaire transitie metingen zijn gedaan voor verschillende verstoringen bij een constant Mach getal. Uit de warmteoverdrachtsmetingen, uitgevoerd door middel van een dunne film methode, zijn intermittency verdelingen bepaald. Voor kleine verstoringen komen de gevonden verdelingen goed overeen met de literatuur. Echter, voor grote verstoringen in de hoofdstroom treden aanzienlijke afwijkingen op. Een nieuw model dat gebaseerd is op het ontstaansproces van turbulent spots is in staat deze afwijkingen te verklaren. Dit model resulteert in een exponentiële intermittency verdeling die ook in het pre-transitie gebied toepasbaar is.

De instationaire stroming wordt opgewekt door middel van een speciaal ontwikkelde zoggenerator. Deze generator transleert cylinders met grote snelheid voor de meetplaat. Door de benodigde aanpassingen aan de Ludwig buis, wijken de stromingscondities af van het ideale geval.

Instationaire metingen zijn uitgevoerd voor verschillende translatie-snelheden en zogsterktes. Het blijkt dat de positie waar transitie optreedt en het maximale (turbulente) flux niveau afhankelijk zijn van het zog.

Ook zijn metingen gedaan waarbij zowel stationaire als instationaire transitie gelijktijdig plaatsvinden. Hieruit volgt dat een superpositie die vaak in de literatuur wordt toegepast, niet zonder meer geldig is. De reden hiervoor is dat er niet een eenduidig 'turbulente' flux niveau bestaat, maar dat deze sterk afhankelijk is van de zogsterkte.

Nawoord

Het is zover, vier jaar van werk aan de universiteit van Eindhoven zit erop. De mensen die een bijdrage hebben geleverd aan mijn promotie-onderzoek wil ik van harte bedanken.

In de eerste plaats noem ik Anton, Rini en Rick, mijn directe begeleiders die allen op hun eigen manier een grote invloed hebben gehad op het eindresultaat.

De beginperiode bij het lab. van W&S is vlot verlopen mede door de inbreng van Jan, Harm en Eep. Na ongeveer anderhalf jaar zijn we met de hele opstelling verhuisd naar ons eigen gebouw, waar ik kon rekenen op steun in het lab. van Frits en Frank, en in de werkplaats(en) van Peter, Lambert en Rob.

Voor computerondersteuning kon ik altijd terecht bij Jan en Roy. Ook noem ik bij het opbouwen en het doen van de eerste proefmetingen het werk van mijn stagiairs Ernst-Jan en David.

Buiten het lab. heb ik veel tijd doorgebracht op de gang in W-hoog. De vele discussies met mijn kamergenoten Jankees, Jakob en Corine waren altijd leuk en gevarieerd. Hierbij vergeet ik zeker niet Douwe en Rob, vanwege hun humor en behulpzaamheid.

Zonder de hulp en gezelligheid van Marjan en Rian op het secretariaat zou het maar een saaie boel zijn. Ook jullie wil ik hier speciaal noemen.

Buiten mijn directe collega's waren er natuurlijk ook nog de mensen van iets verder weg, namelijk het eind van de gang. Ik wil dan ook Marco en René apart bedanken voor de vele gesprekken, ook buiten het werk om. Ook bedank ik Erik, het bewijs dat de opstelling echt werkt hebben we geleverd om zo'n drie uur 's nachts.

Verder bedank ik een ieder van onze vakgroep die ik hier niet bij naam heb genoemd. De sfeer die er de afgelopen jaren heerste was meestal zeer goed en ontspannen.

Ik wil apart mijn ouders vermelden. Zij hebben mij altijd gesteund met de dingen die ik gedaan heb (en nog steeds doe). Tot slot, Rien en Marcel, ontzettend leuk dat jullie mij willen helpen met de laatste loodjes op de 26^e.

Rob

Curriculum vitae

- 1971, October 2nd Born in Rotterdam, The Netherlands.
- 1984-1988 Education: HAVO 1-4,
"Christelijke Scholengemeenschap" (CSG) in Emmeloord.
- 1988-1990 Education: VWO 5-6,
"Christelijke Scholengemeenschap" (CSG) in Emmeloord.
- 1990-1996 Study Mechanical Engineering,
University of Twente.
- 1996-2000 Ph.D.-research, faculty of Mechanical Engineering,
Eindhoven University of Technology.

St e

behorende bij het proefschrift van Rob Schook

T r t o E e r e t S b o c o r e r

1. De Ludwig buis is een geschikt instrument voor het onderzoek aan instationaire grenslaag transitie (dit proefschrift, hoofdstuk 3).
2. De Narasimha intermittency verdeling voldoet niet bij hoge turbulentiegraden (dit proefschrift, hoofdstuk 4).
3. Flux-gebaseerde intermittency is niet geschikt om er zog-geïnduceerde transitie eenduidig mee te beschrijven (dit proefschrift, hoofdstuk 5).
4. The production of thin film gauges in the laboratory has always been an art rather than a method of manufacture.
Jessen, C. and Grönig, H. *Shock Waves* (1991) 1:161-164.
5. De complexiteit van stromingsleer wordt regelmatig onderstreept door een foute weersvoorspelling.
6. Indien promoveren gelijkwaardig zou zijn aan voetbal, is het raadzaam de spelregels te veranderen. Er wordt veel te vaak in de verlenging doorgespeeld.
7. Na 2002 is de eerste klap geen daalder meer waard.
8. Nomaden kunnen niet thuiswerken.
9. Oeverloos zeiken kan alleen vanaf een boot.
10. Gezien de enorme hoeveelheid papier die een promovendus verbruikt tijdens het schrijven van een proefschrift, kan promoveren bestempeld worden als milieu-onvriendelijk.